Title
Development of Stimuli-Responsive Elastin-like Polypeptide-based Nanocomposite Biomaterials

Author
Wang, Eddie Eugene

Publication Date
2012

Peer reviewed|Thesis/dissertation

Development of Stimuli-Responsive Elastin-like Polypeptide-based Nanocomposite Biomaterials

by

Eddie Eugene Wang

A dissertation submitted in partial satisfaction of the

requirements for the degree of

Joint Doctor of Philosophy
with the University of California, San Francisco

in

Bioengineering

in the

Graduate Division

of the

University of California, Berkeley

Committee in charge:

Professor Seung-Wuk Lee, Chair
Professor Stefan Habelitz
Professor Matthew Francis

Fall 2012

Development of Stimuli-Responsive Elastin-like Polypeptide-based Nanocomposite Biomaterials

by

Eddie Eugene Wang

Abstract

Development of Stimuli-Responsive Elastin-like Polypeptide-based Nanocomposite Biomaterials

by

Eddie Eugene Wang

Joint Doctor of Philosophy with the University of California, San Francisco

in Bioengineering

University of California, Berkeley

Professor Seung-Wuk Lee, Chair

Smart biomaterials that can actively respond to and interact with their environment are sought after for regenerative medicine, therapeutic delivery, sensing, and actuation. Polymer-nanoparticle hybrids are a promising class of smart materials, but thus far the choice of polymers has predominantly been chemically synthesized ones. In contrast, natural tissues commonly utilize proteins to interface with nanoparticles and provide smart functionalities. Inspired by nature, this dissertation describes the development of genetically engineered, protein-based polymers (PBPs) for use as components of smart, polymer-nanoparticle hybrids. Specifically, elastin-like polypeptides (ELPs), a class of thermoresponsive PBPs, were utilized to functionalize two nanoparticles.

First, an improved method for synthesizing PBP genes was developed. Crafting new PBPs is limited by the ease with which their genes can be engineered. The new method utilizes a specific architecture of restriction enzymes to address some of the drawbacks of previous methods and was used to efficiently and accurately produce ELP genes.

Next, ELPs were engineered to display biomimetic, bone mineral-binding peptides and their effect on therapeutic bone cements was investigated. Bones are mechanically robust, composites composed predominantly of proteins and nanocrystalline mineral. In contrast, bone cements are brittle and do not contain organic materials. Composites of mineral-binding ELPs and cement had significantly improved strength. Furthermore, the injectability and washout resistance of cements were improved as a result of the ELP's thermoresponsive behavior.

Finally, photoresponsive composites were created by engineering ELPs to display graphene-binding peptides. Graphene-derived nanoparticles (GNs) exhibit unique mechanical, electrical, and optical properties but are difficult to integrate into biological systems due to their hydrophobic nature. The engineered ELPs non-covalently bound to GNs and the resulting ELP-GN hybrids exhibited increased colloidal stability and a reversible temperature-controlled aggregation behavior. The ability of GNs to convert near-infrared light to heat was exploited in order to remotely induce aggregation of ELP-GN hybrids in solution and to induce rapid, site-specific actuation of ELP-GN composite hydrogels.

Finally, cell adhesion on ELP-functionalized graphene was enhanced by genetic addition of integrin-binding peptide motifs.

These studies demonstrate that PBPs can be tailored to interact with nanoparticles of choice and can provide stimuli-responsive and bioactive properties to biologically relevant nanoparticles. Hybrid materials of PBPs and nanoparticles are, therefore, well suited for biotechnological applications which require smart behavior.

Dedicated to Lorraine

Acknowledgements

I have had the privilege of being advised by Professor Seung-Wuk Lee. He has been exceptionally supportive of my work while also showing great consideration for my overall well-being. Working with him has inspired me to think bigger, to not fear the pursuit of "crazy" ideas, and to strive to constantly learn new techniques. I hope to bring his passion and creativity to the next stages of my career.

In my time in the Lee lab I have been consistently graced by the presence of great labmates. Being in the trenches with them definitely made the tough times easier. I want to thank Justyn, Chris, Sean, and Anna for their friendship and advice. Justyn in particular has my gratitude for introducing me to the lab and being a model for someone who grabs life by the proverbial horns. I am also indebted to Ki-Young for allowing me to work with him, teaching me, and bringing his special brand of humor to the lab. I am ever grateful and will likely never repay Woo-Jae for his friendship, his patience for answering my questions, allowing me to take part in his research, and for being an awesome tennis opponent. Special appreciation also goes to Sang and Malav for working so hard with me even if it didn't seem like I knew what I was doing. My thanks go to Jin-Woo and Byung Yang for allowing me to help in my small way on their projects and for demonstrating how to dedicate oneself to research. I also want to thank So Young, Keisuke, and Masae for displaying the type of constant optimism and politeness that makes me have greater faith in mankind. To the rest of my Korean labmate crew past and present: Dong Shin, Jin, Joseph, Tae-Hyun, Kwang, Hyo Eon, and Sung Ho, my thanks for your help and advice, but mostly for teaching me Korean words, drinking games, and card games. Kamsahamnida!

I would also like to thank Professors Francis, Habelitz, Healy, and Kumar for their time and advice while serving on my dissertation and qualifying exam committees. In addition, I am grateful to Rebecca Pauling for her hard work in making sure that I stayed on the path to graduation.

I would also like to acknowledge my support system outside of the university. First, I am grateful to my girlfriend's family for helping to provide a home away from home. Finally, I want to acknowledge my parents, sister, sister-in-law and Lorraine for putting up with me all these years and doing fairly well at not asking when I was going to graduate too often. Their seemingly unending love and support means everything to me.

Table of Contents

Chapter One: Introduction

1.1 Overview

The overarching goal of the studies described in this text is to demonstrate the utility of combining genetically engineered protein-based polymers with nanoparticles for the creation of "smart" biomaterials. This chapter provides an introduction to and motivation for the work by reviewing the topic of nanoparticle-polymer hybrid materials and then describing the role that protein-based polymers could play in their development.

1.2 "Smart" Hybrids of Polymers and Nanoparticles

A central challenge of modern biomaterials engineering is to create "smart" materials: multifunctional materials that can respond to stimuli from their surroundings, interact with cells and biomolecules, and satisfy more traditional requirements like biocompatibility and physical stability (*1-4*). As a hypothetical example, we can envision a material that self-assembles when injected into the body, releases chemoattractants in response to light, and then promotes the proliferation of attracted cells by binding to cell surface receptors. Including so many functions into a single component material is a formidable task. Therefore, one strategy for developing smart biomaterials is to combine complementary components together to form hybrid materials. These materials can perform multiple functions that neither component could achieve individually. In particular, I and others are interested in merging the chemical functionality of polymers with the unique properties of inorganic and carbon-based nanoparticles to create nanoparticle-polymer hybrids (NPHs).

Three factors motivate the development of NPHs. First, there is a large diversity of synthetic techniques and chemical building blocks now available to chemists with which stimuli-responsive and bioactive polymers can be created. Second, advances in nanotechnology research now allow us to synthesize a variety of nanoparticles with exceptional mechanical, electrical, and optical properties in tunable and reproducible manners (*5-7*). Many of these properties cannot be achieved with polymeric materials. Third, nanoparticles are almost never suitable for biological applications without first being combined with other components. This is because most unmodified nanoparticles in solution are inherently prone to colliding and aggregating due to their high energy surfaces, large surface area to volume ratios, and rapid Brownian motion (*8*). Furthermore, nanoparticles are relatively bioinert. They have little to no specific affinity to cells or biomolecules. Considering these factors, polymers and nanoparticles are well-suited to complement each other.

1.2.1 Polymer Design Factors

A hypothetical nanoparticle-polymer interface is shown in Figure 1-1. As the schematic indicates, several design questions must be considered when choosing or designing a polymer for NPHs. First, what physical and stimuli-responsive properties should the polymer backbone have? Second, how should smart behavior in regards to cell and biomolecule interactions be introduced? Third, how should the polymer become interfaced with the nanoparticle?

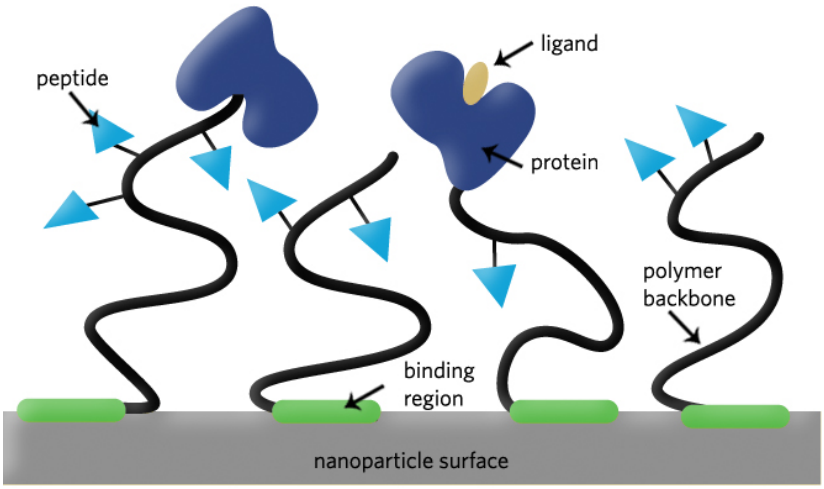

Figure 1-1. Schematic of a hypothetical polymer-nanoparticle interface. The polymer chains control how the nanoparticles are presented to their surroundings. Peptides and proteins are conjugated to the polymers to add bioactivity. The polymers are interfaced to the nanoparticle surface by various binding interactions.

Properties of polymers for NPHs

There are two main classes of polymers currently utilized for NPHs: chemically synthesized and naturally-derived (i.e., proteins, and polysaccharides). Regardless of source, the polymer's most critical role in an NPH is to make nanoparticles compatible with the environment in which they will be utilized. In the case of bulk scale materials (nanocomposites), this means that the polymer and nanoparticles should not phase separate (described further in section 1.2.3) (*9*). In the case of NPH-based sensors, it means that the polymer should prevent non-specific interactions with the nanoparticles (*10*). For most other applications, it means that the polymer should prevent aggregation of the nanoparticles in whatever solutions will be encountered (e.g., buffers, cell culture media, or bodily fluids). Aggregation can be prevented by coating or encapsulating the nanoparticle in polymers that can provide a source of steric or electrostatic repulsive forces. Polyethylene glycol (PEG) chains are commonly utilized in this capacity due to their biocompatibility and ability to prevent non-specific adsorption, though other synthetic and natural polymers can also serve the same purpose (*11*). In addition to preventing aggregation, shielding nanoparticles with polymers can improve in vivo circulation times and biocompatibility (*12, 13*).

Stimuli-responsive polymers can add further functionality to NPHs. Polymers engineered to respond to stimuli, such as pH, temperature, light, and ions, undergo dynamic and often reversible changes in hydrophobicity, solubility, and chain conformation (*14-18*). These changes can lead to nanoscale self-assembly or to changes in the size and shape of materials at larger scales (*16, 19*). For biological applications, pH-responsive polymers and thermoresponsive polymers that exhibit a lower critical solution temperature (LCST) are often exploited as smart materials and will, therefore, be highlighted.

Most weak polyelectrolytes, such as those bearing carboxylic acid or amino groups (e.g., polyacrylic acid and polyallylamine, respectively), can be reversibly protonated or deprotonated by changes in pH. The same is true of certain naturally derived polyelectrolytes like chitosan and proteins.

The changes in physical properties that accompany a change in pH can be utilized to introduce smart behaviors. For example, Bellomo et al. chemically synthesized amphiphilic, lysine-containing block copolymers that self-assembled into nanoscale vesicles when the lysine blocks became protonated by a decrease in pH (*20*). Other pH-responsive polymers allowed for smart drug delivery by exploiting pH variations that exist in different parts of the body, near tumors, and in cellular organelles (*21, 22*).

Polymers that exhibit an LCST behavior are useful as thermoresponsive elements in NPHs. Below their LCST, these polymers are hydrophilic and water soluble. Above their LCST, the polymers become desolvated and phase separate from water. When these polymers are crosslinked into hydrogels, raising or lowering the temperature across the LCST manifests as a reversible change in swelling (deswelling when heating to above the LCST and swelling when cooling to below the LCST). Although several polymers and copolymers have an LCST, poly(*N*-isopropylacrylamide) (PNIPAM) is the most utilized. Its LCST (~32 °C) can be tuned near physiological temperatures, so it is well suited for biotechnological applications (*23, 24*). As one example, Pollock and Healy synthesized PNIPAM copolymers that immediately formed gels when injected into 37 °C buffers (*25*).

Interfacing polymers with biology

Chemically synthesized polymers are generally not designed to interact with specific biomolecules. Any interactions that do occur are not likely to approach the specificity of natural ligand-receptor pairings. Therefore, it is often desirable to impart specific biological functions to synthetic polymers during or after their synthesis. In most cases this means incorporating peptides or proteins. Peptides have generally been introduced by covalent coupling. An advantage of peptides is that they can be synthesized with reactive groups that do not cross-react with amino acid side chains. For example, DeForest et al. utilized two click reactions (thiol-ene and azide-alkyne) to introduce growth factor-mimetic peptides and protease-labile peptides into a PEG-based hydrogel in order to promote cell proliferation and cell-mediated remodeling (Figure 1-2) (*26*).

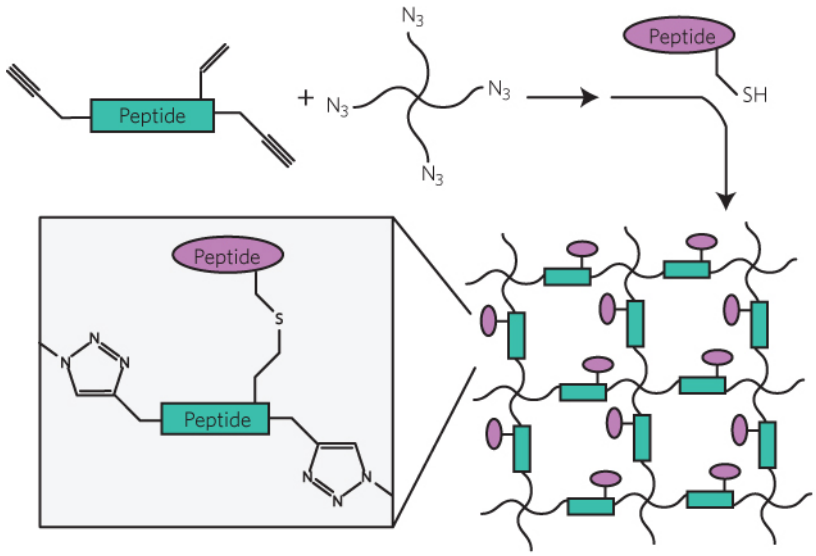

Figure 1-2. Example of peptide incorporation strategies. Difunctional alkyne-terminated peptides with pendant alkene groups can be directly crosslinked with tetrafunctional azide-terminated polymers to form a polymeric network by azide-alkyne cycloadditions. Thiol-bearing peptides can then be conjugated into the network by thiol-ene reactions. Adapted from DeForest et al. (*26*).

Unfortunately, there are limits on the length of peptides that can be conveniently chemically synthesized. Therefore, alternative bioconjugation chemistries are required to incorporate longer proteins such as antibodies. Although many techniques can be utilized for bioconjugation, it is most often performed by conjugation of amines to activated carboxylic acid esters or by conjugation of cysteine-derived thiols to maleimides (Figure 1-3) (*27-29*). One drawback of chemical conjugation is that the degree of conjugation is not necessarily uniform for each polymer chain, especially when the chains have multiple reactive sites (Figure 1-1). In addition, bioconjugation to proteins is often not site-specific. For example, multiple amines may be reactive on a protein surface. The protein may lose its activity if a crucial amine is reacted with (Figure 1-1) (*30*). An alternative strategy is to use non-covalent conjugation. Lackey et al. demonstrated such an approach by functionalizing polymers with biotin and then binding streptavidin proteins to the polymer through biotin-avidin interactions (*31*). Regardless of strategy, introducing bioactivity comes at the cost of additional chemical processing and purification steps.

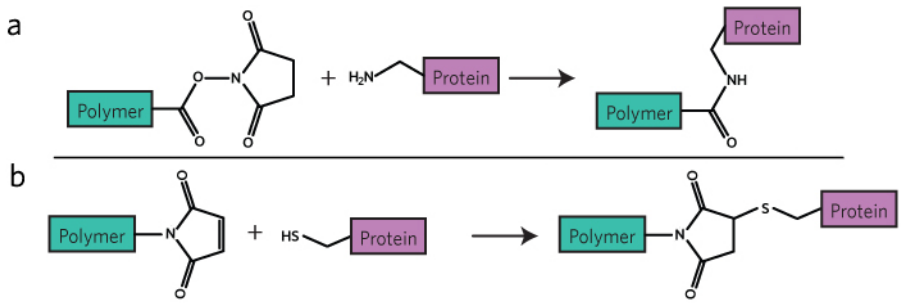

Figure 1-3. Common covalent protein bioconjugation strategies (a) An activated carboxylic acid ester reacts with a free primary amine from a protein (N-terminus or lysine). (b) A maleimide-functionalized polymer reacts with a thiol from a protein's cysteine side chain.

The alternative to conjugating bioactive peptides or proteins is to avoid using synthetic polymers altogether and to use naturally-derived polymers instead. These polymers have built in bioactivity and can be used to functionalize nanoparticles on their own. For example, hyaluronic acid is an extracellular matrix polysaccharide that is degradable by hyaluronidase enzymes, mediates cell activities by binding with CD44 receptors, and can independently functionalize nanoparticles (*32, 33*). Unfortunately, the library of bioactive polysaccharides is relatively small. On the other hand, there is a broad range of multi-functional proteins that might be used. For example, collagens can self-assemble into matrices, provide structural stability, present binding sites for cells and other proteins, and are degradable by proteases (*34-37*). Natural proteins are not without limitations, however. Proteins harvested from their native organisms can have batch to batch inconsistencies. Also, most proteins were not designed to specifically interact with solid surfaces. Any given protein might either not adsorb to a nanoparticle's surfaces, or adsorb non-site-specifically. Non-specifically adsorbed proteins can adopt non-uniform conformations, denature, or lose function (*38, 39*). Finally, natural proteins have predefined sets of functions and physical properties, so one protein may not fulfill all of the requirements of any given application.

Interfacing polymers with nanoparticles

A suitable connection between polymers and nanoparticle surfaces is of paramount importance to the mechanical properties of nanocomposites and the stability of colloidal NPHs. The first method for interfacing polymers with nanoparticles is by non-covalent adsorption during or after nanoparticle synthesis. For example, physisorption mediated by non-specific long and short-range van der Waals forces can occur (Figure 1-4a). For colloidal NPHs, this is typically performed with amphiphilic polymers having hydrophobic regions, which preferentially interact with the nanoparticle surfaces, and hydrophilic regions, which interact with aqueous environments (*40*). Non-covalent adsorption can also be mediated by electrostatic, hydrogen bonding, and chelation interactions (Figure 1-4b-d) (*41-43*). Although these bonds are non-covalent, the combined effect of multiple interactions occurring along a polymer chain can produce strong interfacial binding (*41*).

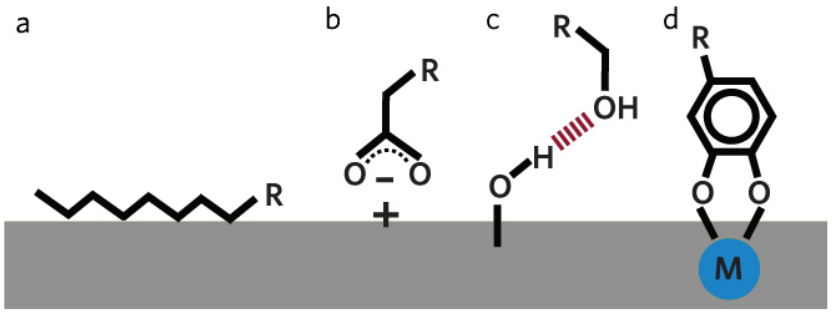

Figure 1-4. Examples of non-covalent binding interactions acting at surfaces. (a) Physisorption by non-specific van der Waals interactions (b) Electrostatic interactions. (c) Hydrogen-bonding. (d) Chelation of metal ions by catechols.

Nanoparticles can also be chemically bonded with polymers by "grafting to" and "grafting from" approaches (*44*). In the "grafting to" approach, presynthesized polymers are chemically attached to nanoparticle surfaces (Figure 1-5a). This is commonly performed by utilizing the bonding between gold surfaces and thiols or between metal oxides and silanes, though any covalent bond forming reaction also falls under this category (*43*). In contrast, "grafting from" involves immobilizing polymerization initiators onto the nanoparticles, then directly growing polymer chains off the surfaces (Figure 1-5b). This approach allows for the synthesis of higher density polymer brushes compared to grafting to techniques (*45*). However, grafting from requires an additional step (immobilizing the initiators), and sometimes requires the development of new chemical initiators (*45*).

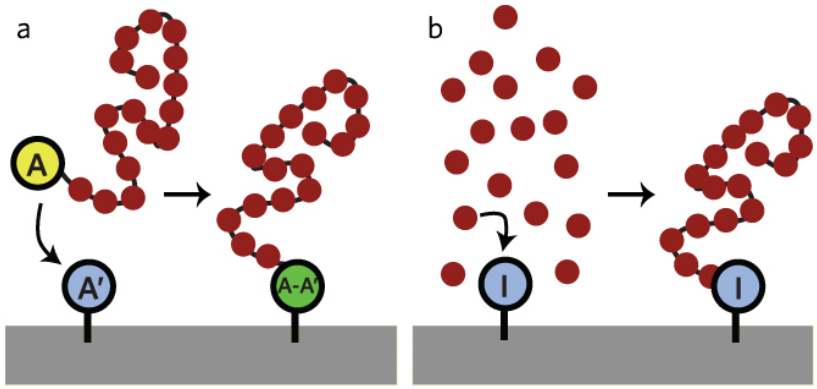

Figure 1-5. Schematic of nanoparticle functionalization strategies. (a) In the "grafting-to" approach, a presynthesized polymer is chemically bonded to reactive sites on the surface. (b) In the "grafting-from" approach, polymers are grown from the end of surface bound initiators.

1.2.2 Nanoparticles for Biotechnological Applications

A number of inorganic and carbon-based nanoparticles have been utilized for biotechnological applications (Table 1-1). The list includes clay, hydroxyapatite, silica, noble metal, semiconductor, carbon-based, and magnetic nanoparticles. These nanoparticles often exhibit valuable properties that are

not observed in larger scale materials of the same composition (e.g., superparamagnetism and luminescence) or that are difficult to obtain in polymeric systems (e.g., conductivity, and external field responsiveness). Nanoparticles are now especially attractive because new techniques have improved our ability to control their size, shape, and dispersity (*7, 46, 47*). Such factors are directly related to the nanoparticles' optical, mechanical, and electromagnetic properties (*12, 48*). The specific roles of nanoparticles will be reviewed in the context of NPHs with biotechnological applications.

Table 1-1. Overview of nanoparticles utilized for biotechnological applications.

Nanoparticle (NP)	**Properties**	**Applications**
Clays/Hydroxyaptatite/Silica	Stiff, biocompatible	Nanocomposites, drug delivery
Quantum Dots (CdTe, CdSe, ZnS, and CdS)	Luminescent	Imaging, sensing
Magnetic NPs (Maghemite, Magnetite)	Magnetic/superparamagnetic, biocompatible	Imaging, bioseparations, photothermal therapy, actuators, drug delivery
Noble metal NPs (Gold, Silver)	Conductive, surface-plasmon resonance, biocompatible	Imaging, drug delivery, photothermal therapy, sensing
Carbon-based NPs (Carbon Nanotubes, Graphene-derived nanoparticles)	Conductive, strong	Imaging, sensing, drug delivery, photothermal therapy, sensing, nanocomposites

1.2.3 Biotechnological Applications of Smart NPHs

Many NPH systems have already been synthesized and shown to have promising properties for a number of biology-related applications. The examples presented here will demonstrate how the design principles described in section 1.2.1 were addressed in previous work.

Nanocomposites

The judicious combination of nanoparticles and polymers can result in materials with greatly improved mechanical performance compared to either material alone. Nanoparticles incorporated into polymeric matrices are more effective at increasing strength and stiffness than larger scale particles, even when loaded at lower volume percents. (*49, 50*). This is due to their very high surface area to volume ratios which provide large interfacial areas for stress transfer with polymer chains (*50*). In addition, certain nanoparticles have a reduced sensitivity to flaws compared to their larger-scale counterparts (*51*). The dispersion of the nanoparticles within the polymer and the interfacial bonding between the polymer chains and nanoparticle surfaces are critical to providing mechanical enhancements (*9, 50, 52, 53*). Dispersion is critical because the advantages of using nanofillers are essentially negated if the nanoparticles are allowed to aggregate and segregate from the polymer phase. Meanwhile, interfacial bonding is critical because it allows the soft polymer to efficiently transfer stress to the stiff nanoparticles. To address these factors in a tissue engineering material, Zhang et al. grafted poly(L-lactide) chains from the surfaces of hydroxyapatite nanoparticles. The hydroxyapatite could then be uniformly dispersed within a poly(lactide-*co*-glycotide) matrix . Without the polymer coating, the hydroxyapatite would have aggregated during processing. Their nanocomposite included additional polymer chains that had been

coupled with integrin-binding arginine-glycine-aspartate (RGD) peptides to improve cell adhesion (*54*). In another example, Haraguchi et al. grafted long, stimuli-responsive copolymer chains from clay nanoplatelet surfaces to form hydrogels. The resulting hydrogels were mechanically robust, cytocompatible, and responded to changes in pH, temperature, and ionic strength by swelling or deswelling (*55*). Finally, in addition to mechanical enhancements, conductive nanofillers, such as carbon nanotubes, have been used to make electrically conductive nanocomposites (*56, 57*).

Biosensing

Certain nanoparticles are extremely sensitive to local changes in their environment and can be exploited for sensing applications. For example, carbon nanotubes and graphene-based nanoparticles change conductance when molecules bind to them. Myung et al. took advantage of this characteristic by synthesizing a reduced-graphene oxide (rGO)-based field effect transistor (FET), functionalizing the rGO surfaces non-covalently with small molecules, and then covalently linking antibodies to the small molecules. The antibody's target was detected at picomolar concentrations by measuring conductance changes through the rGO-FET (*58*). The optical properties of nanoparticles can also be utilized for sensing. For example, the color of gold nanoparticle solutions is dependent on interparticle spacing due to surface plasmon resonance effects. Chuang et al. used this property to develop a sensor for protease activity using a solution of gelatin coated gold nanoparticles. When proteases were added, the gelatin was cleaved, resulting in decreased spacing between the particles. This caused a color change that could be monitored by a spectrophotometer (*59*). Other NPHs made of metal nanoparticles or carbon-based nanoparticles have been utilized for electrochemical biosensing (*60*).

Imaging

A wide variety of imaging modalities have taken advantage of NPHs (*61*). For example, fluorescent semiconductor quantum dots (QDs) are used for in vitro and in vivo immunofluorescent labeling and imaging because they can be synthesized with tunable absorption/emission spectra and have long fluorescence lifetimes compared to traditional organic fluorophores and fluorescent proteins (*12, 62*). However, QDs are typically capped with hydrophobic surface ligands during their synthesis which hampers their dispersability in aqueous solutions. Wu et al. addressed this issue by solubilizing the QDs with amphiphilic, octadecylamine-modified polyacrylic acid. They then used the polymer's free carboxylic acids to chemically conjugate targeting antibodies (*63*). Thermoresponsive QD-based nanohybrids have also been engineered. Tagit et al. adsorbed a comb copolymer containing PNIPAM groups onto QDs. The luminescence emission of the modified QDs reversibly changed above and below PNIPAM's LCST (*64*).

Gold, carbon-based, and magnetic nanoparticles have been utilized with various imaging modalities. For example, similar targeting techniques to those described for QDs were used to functionalize gold nanoparticles with tumor-specific antibodies for imaging by X-ray computed tomography (*65*). Meanwhile, Zerda et al. used photoacoustic imaging to detect carbon nanotubes that were functionalized by amphiphilic PEG-grafted phospholipids. RGD peptides were conjugated to the PEG chains to target cancer cells (*11*). Instead of covalent bioconjugation, Amstad et al. took a non-covalent approach. Magnetic nanoparticles were mixed with PEG chains that were functionalized on one end with gallol and on the other with biotin. The gallol bound the polymer to the nanoparticle surface, allowing the biotin to freely interact with its binding partner, neutravidin. Finally, biotinylated

antibodies were attached to neutravidin's remaining biotin binding sites (*66*). The resulting magnetic nanoparticles were suitable for targeted imaging by magnetic resonance imaging (*61*).

Therapeutic delivery

Stimuli-responsive therapeutic release is highly sought after to improve the clinical efficacy of drugs. Various NPH systems have attempted to address this goal. For example, Popat et al. synthesized drug-loaded, mesoporous silica nanoparticles and grafted chitosan onto their surfaces. The chitosan formed a gel layer at physiological pH, greatly inhibiting drug release. At low pH, the chitosan gels disassembled, allowing drugs to exit (*67*). NPHs have also allowed for the on-demand release of drugs in response to external fields. One particularly effective example was demonstrated by Zhao et al. They made a porous, hydrogel nanocomposite using alginate and magnetic iron oxide nanoparticles. In the presence of a magnetic field, the entire gel became compressed, forcing the release of entrapped drugs, proteins, and cells (*68*).

Hyperthermia

Hyperthermia is a potential treatment for solid tumors which involves localized heating to temperatures that can kill cells. NPHs are particularly well suited for hyperthermia therapy because several nanoparticles can generate heat in response to external fields. Superparamagnetic nanoparticles generate heat when stimulated by alternating magnetic fields, while gold nanoparticles and carbon-based nanoparticles can be heated by near-infrared (IR) illumination (*61*). Shiotani et al. demonstrated a unique system that combined nanoparticle heat generation with polymer stimuli-responsiveness. They grafted PNIPAM containing copolymers with an LCST near 40 °C to gold nanoparticles. When irradiated with near-IR light, the heat generated by the gold induced PNIPAM's phase transition. This led to active accumulation of more nanoparticles at the irradiation site (*69*).

1.3 Genetic Engineering Approach to NPHs

The examples described thus far illustrate that the polymeric components of NPHs must fulfill multiple functions. Adding new functions (e.g., adding a monomer or block to a polymer, conjugating biomolecules, or introducing surface anchoring groups) comes at the cost of reduced yield and homogeneity due to the additional processing steps involved. Therefore, synthetic difficulty is the greatest limitation of using chemically synthesized polymers for NPHs. In contrast, uniform, multifunctional proteins are synthesized in nature everyday using a relatively small pool of chemical building blocks. Inspired by nature's abilities, scientists have sought to incorporate the physical, biological, and stimuli-responsive properties of natural proteins into synthetic, genetically engineered protein-based polymers (PBPs).

The use of PBPs is predicated upon the fact that, although they can be large and complex, many proteins are found to be built of shorter folded domains and peptide motifs that function modularly. These domains and motifs are able to maintain some or all of their properties and activities even when expressed outside of their native context. A diverse catalog of characterized motifs has been collected, and it is now possible to pick and choose members from the catalog and fuse them together as PBPs. To accomplish this, genetic engineering techniques are used to connect the DNA sequences which code for

the motifs. The resulting genes are then inserted into and expressed by a host organism such as *E. Coli* (Figure 1-6).

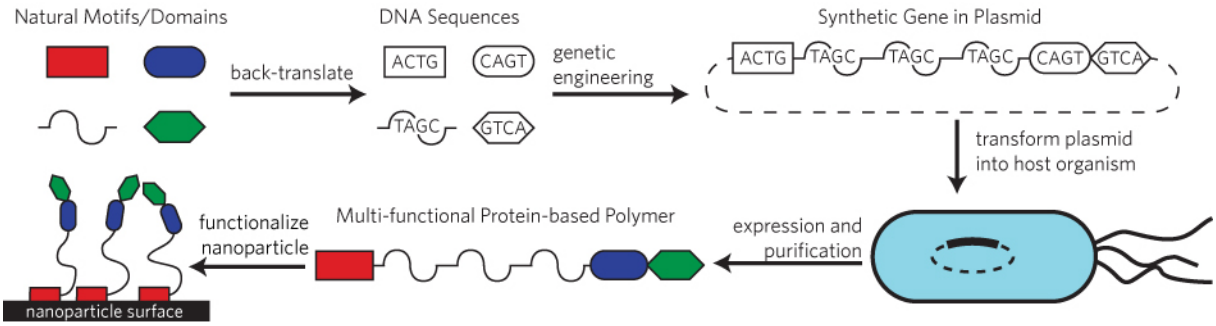

Figure 1-6. Schematic of genetically engineered PBP design and synthesis. Modular functional motifs are chosen for their physical or biological properties. Their corresponding DNA sequences are determined by back-translation. They are then combined into a synthetic gene in whatever order is desired by genetic engineering. Finally, they are expressed using a host organism.

There are many advantages to using PBPs compared to using chemically synthesized polymers or natural polymers and proteins. The first being that genetic engineering affords absolute control over a PBP's DNA sequence and resulting protein sequence. In addition, although the number of amino acids to choose from is small relative to the number of monomers available to polymer chemists, the ability to array all 20 amino acids in any combination generates a great diversity of physical and functional properties. Furthermore, by utilizing natural synthetic machinery, we are assured a product that is uniform in size, sequence, and stereochemistry and that does not require further chemical processing to add bioactivity. These characteristics are essentially unobtainable using traditional polymer synthesis. Stability may be a concern if complex tertiary structures need to be maintained when using natural proteins. This is much less of a concern for proteins built with short peptide motifs. Finally, PBPs are made with renewable resources, and they degrade into natural amino acids (*70-72*). The control and flexibility afforded by genetic engineering indicate that PBPs could be used as the polymeric component of NPHs.

1.3.1 Protein-based Polymer Design Factors

The design of PBPs for NPHs can be approached in the same way as for other polymers. We will consider the properties of the protein backbone, the introduction of bioactivity, and the methods for interfacing them with nanoparticle surfaces.

The protein backbone

The term "protein-based polymer" refers to synthetic proteins whose sequences are composed primarily of one or more tandemly repeated, structural peptide motifs. These repeated motifs make up most of a PBP's backbone and are primarily responsible for its physical properties. The motifs themselves are mostly based upon naturally occurring sequences found in secreted, structural proteins

(e.g. silks, elastins, and resilins) (Table 1-2). Amazingly, even the repetition of short peptide motifs within a PBP imparts many of the outstanding physical properties of the native proteins.

Table 1-2. Sampling of structural motifs used for PBPs

Function	**Sequence Motif**
Silk-like	GAGAGAS, GPGXX (*73*), SGRGGLGGQGAGAAAAAGGAGQGGYGGLGSQGT (*74*),
Elastin-like	VPGVG (*75*), VPAVG(*76*), LGGVG(*77*)
Resilin-like	SDTYGAPGGGNGGRP (*77*), GGRPSDSYGAPGGGN (*78*), AQTPSSQYGAP (*79*)
Random coil	AGAGAGPEG (*80*)

Silks, especially from spiders, exhibit extraordinary combinations of tensile strength, toughness, and ductility (*73*). Within silk sequences, alanine-rich motifs (e.g., GAGAGAS) contribute to stiffness by assembling into crystalline β-sheets, while glycine rich motifs (e.g., GPGXX) form flexible, non-crystalline regions that contribute to ductility. Many silk-like polypeptides (SLPs) have been synthesized using these motifs and then processed into mechanically robust films, hydrogels, microparticles, micelles, and fibers (*81, 82*). The physical properties of SLPs are tunable by controlling the motif repeat lengths and the ratio of crystalline to non-crystalline motifs (*83*). The ability of SLPs to form β-sheet crosslinks is potentially useful for nanocomposite synthesis, but could promote aggregation in colloidal NPH systems.

As its name suggests, elastin provides elasticity to tissues that require large deformations and recoil to their initial state during repeated cycles of stress (*84*). These tissues include arteries, lungs, skin, and cartilage (*85*). Elastin-like polypeptides (ELPs) are PBPs built from tandemly repeated motifs found in natural elastin. Like SLPs, they have been synthesized then processed into hydrogels, films, and fibers (*86*). Amazingly, ELPs exhibit thermoresponsive phase transitions akin to PNIPAM that can be utilized to introduce smart behavior. The properties of ELPs will be discussed at length later in the chapter.

Resilins are proteins found in the cuticle of insects and are best known for their contribution to insect flight and jumping. They are elastic and extensible like elastins. Most notably, resilins have resilience values (ability to recover after deformation) in excess of 90%. These values exceed that of commercial rubbers. In addition, they have long fatigue lifetimes (*78*). Only in the past decade have resilin like polypeptides (RLPs) based on resilin motifs been synthesized. These RLPs were demonstrated to exhibit extremely high resilience values just like the natural resilins (*79, 87*).

PBPs can also be designed as multi-block copolymers by combining motifs (*82*). For example, Teng et al. synthesized silk-elastin-like polypeptides composed of alternating SLP and ELP blocks. The silk domains formed crystalline β-sheet crosslinks while the elastin-like domains provided extensibility and resilience (*88*). The ability to precisely set block types, lengths and positions allows for exquisite control over the mechanical (stiffness, extensibility) and physical (porosity, swelling ratio) properties of the resulting materials.

Incorporating stimuli-responsiveness

Stimuli-responsive behavior can be easily genetically incorporated into PBPs by incorporating specific amino acids or peptide motifs. For example, Truong et al. showed that the adsorption and conformation of an RLP on gold was pH-dependent due to the presence of ionizable residues (*89*). Meanwhile, Winkler et al. demonstrated that the amount of β-sheet formation in SLPs could be controlled chemically, by switching the redox state of methionine residues, or enzymatically, by switching the phosphorylation state of tyrosine and serine residues (*90*). Stimuli-responsive self-assembly can also be introduced by inserting naturally associating protein sequences, such as leucine zippers. Leucine zippers are alpha-helical structural motifs that can associate with each other into supercoils of two or more helices (*91*). A PBP with a leucine zipper motif at each terminal flanking a central random coil sequence self-assembled into hydrogels (*80*). By rationally mutating the leucine zipper sequences, assembly and disassembly was engineered to respond to temperature and pH (*92*). Many other stimuli can potentially be incorporated into PBPs because the library of ligand-responsive and associating domains has only begun to be explored (*71*).

Incorporating bioactivity

Perhaps the greatest advantage of using genetically engineered proteins over chemically synthesized polymers is the ease with which bioactive motifs can be incorporated. Multiple bioactive motifs can be directly inserted into the backbone of PBPs during genetic engineering. In contrast to the previously described bioconjugation strategies, genetic engineering leaves no uncertainty in regards to the presence, number, or location of bioactive motifs. Every PBP backbone mentioned previously has successfully been functionalized with bioactive motifs in order to make materials suitable for drug delivery and tissue engineering. Sequences that have been added include those for cell adhesion, protease cleavage, carbohydrate binding, DNA binding, cellular penetration, and cross-linking (*93-96*). In one example, Charati et al. synthesized an RLP that included heparin binding sites, matrix metalloproteinase cleavable sites, and cell binding motifs on each chain. (*97*). Whole proteins can also be fused to PBPs instead of short peptide motifs if necessary (*98*). Finally, other drugs, polymers, or molecules can be site-specifically, covalently attached by introducing amino acid handles (e.g., cysteines) (*99*).

Interfacing PBPs with Surfaces

Genetic engineering can direct the oriented attachment of proteins to nanoparticle surfaces through many of the same pathways described for other polymers. Physisorption can occur, but, unlike natural proteins, specific sequences can be introduced that preferentially adsorb. For example, Wada et al. genetically fused a hydrophobic ELP with sequence $(VPAVG)_{12}$ to glutamine binding proteins. The ELP sequence mediated physisorption to hydrophobic surfaces and allowed the glutamine binding protein to be oriented towards the solution (*100*). Electrostatic complexation can also be engineered. Mattousi et al demonstrated this strategy by fusing a positively charge leucine zipper domain to a maltose binding protein. The charged leucine zipper preferentially bound to negatively charged QD surfaces (*101*). Natural surface binding motifs can be utilized as well. For example, silica exists naturally in the cell walls of diatoms. A peptide sequence from the diatom protein known as silaffin was implicated in mediating silica mineralization. When Nam et al. fused the silaffin-derived peptide to green

fluorescent protein, they found that the fusion protein was efficiently immobilized onto silica particles (*102*).

The ability to chemically bond to surfaces can also be engineered into proteins. For example, Mitchell et al. engineered a C-terminal cysteine followed by a spacer sequence onto bone morphogenetic protein-2. The thiol chemisorbed onto gold surfaces to provide oriented attachment of the protein. Meanwhile, Chan et al. demonstrated site-specific, covalent attachment of an engineered protein to glass surfaces using an enzymatically catalyzed reaction (*103*).

Certain natural peptide motifs already exist that bind to inorganic materials. For example, the silaffin-derived motif described earlier. However, many of the materials that comprise nanoparticles of interest do not exist in natural organisms. Thankfully, a powerful technique known as phage display has been adapted to generate peptide-based binding motifs for seemingly any surface of interest (*104*). To perform phage display, a combinatorial library of random, short peptide sequences is introduced onto bacteriophage coat proteins by genetic engineering such that each phage expresses one member of the library. Even for short, random sequences, a large library is theoretically created (a random 7 amino acid library can generate 20^7 unique sequences). The library is then mixed with a target material to allow for binding. Afterwards, unbound or weakly bound phage are washed away. The remaining phage are eluted from the target and amplified in bacteria to form a sub-library. The phage DNA is then sequenced and analyzed for consensus sequences. If none is found, the process can be repeated using the sub-library under more stringent binding conditions. The process is shown in Figure 1-7.

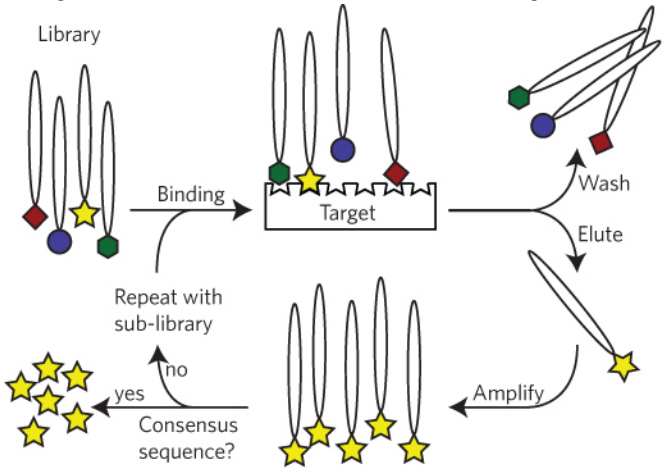

Figure 1-7. Schematic of the phage display process.

Phage display has already been utilized to identify peptides that bind many of the materials that comprise the nanoparticles listed earlier (i.e., gold, silver, silica, iron oxide, hydroxyapatite, cadmium sulfide, and carbon nanotubes) (*105-110*). Interestingly, like silaffin, the identified peptides not only bind to their target materials, they can also promote their mineralization (*105, 106, 108, 109*). These peptides have already been demonstrated to function if synthesized apart from the phage, or when attached to synthetic polymers (*111, 112*). Phage display thus provides a powerful tool for generating surface anchoring motifs that could be incorporated into PBPs.

1.3.2 Elastin-like Polypeptides (ELPs)

ELPs were chosen as the PBP backbone for the studies in the subsequent chapters. Therefore it is relevant to have a more detailed background on their properties and applications.

Natural elastin has several salient properties that make it worth imitating. Mechanically, elastin fibers behave like entropic elastomers. Under loading, energy is stored predominantly by reversible entropic changes. The alternative being storing energy internally in the chemical backbone, which promotes irreversible bond breaking (*113*). As a result, elastin fibers are exceptionally stable, having a half-life of approximately 70 years, during which they can experience millions of loading cycles (*114*). Elastin fibers are also extensible; they are capable of being extended to 100-220% of their original length (*115*). Elastin synthesis occurs by the self-assembly and crosslinking of precursor tropoelastin proteins. The tropoelastin building blocks are believed to align head to tail like a linear array of springs and to associate laterally through hydrophobic domains (*115, 116*). The lateral association is an entropically-driven process that can be controlled by temperature such that when tropoelastin solutions are heated above a certain temperature the proteins aggregate to form a coacervate (*113*). This stimuli-responsive behavior is qualitatively the same as the LCST response of PNIPAM and is known as an inverse temperature transition (ITT). Specifically, the ITT occurs when the entropically disfavored water that is hydrating hydrophobic elastin sidechains is released from the protein backbone to become bulk water. Finally, elastin has multiple biological effects as a ligand, including regulating chemotaxis and cell proliferation (*117, 118*)

Several types of repeating sequences fall under the umbrella of the ELP name, including proteins built of whole tropoelastin exon sequences (*119*). However, perhaps the most well characterized are ELPs based on repeats of the pentapeptide sequence valine-proline-glycine-valine-glycine (VPGVG) and its derivatives (*120*). The VPGVG sequence appears 15 times within the hydrophobic regions of the sequence of bovine tropoelastin. Ten of the fifteen occurrences are tandemly repeated in one 50 amino acid stretch. ELPs based on the VPGVG motif retain many of natural elastin's properties. Most notably, they retain the ITT response, shedding water of hydrophobic hydration and aggregating above a certain transition temperature (T_t). The resulting coacervates contain approximately 63% water by weight (*113*). Structurally, ELPs are considered to be random coils below their T_t, while above their T_t the secondary structure, if any, is still being debated (*84, 113*). Mechanically, ELPs are fatigue resistant and behave as near ideal entropic elastomers at the single molecule level and when crosslinked to form matrices (*72, 113, 121*). However, the molecular level origin of this elasticity is still disputed (*113, 121, 122*).

A major selling point of ELPs is their tunable T_t. By substituting amino acids within the VPGVG pentapeptide, the T_t can be raised or lowered. Most commonly the fourth position is replaced to create VPGXG-type ELPs, where X can be any amino acid other than proline and still retain a thermoresponsive behavior (*70, 123, 124*). The T_t shift depends on the number of substituted amino acids and the hydrophilicity of the inserted residue. More hydrophilic amino acids raise the T_t, while more hydrophobic residues lower it. For example, for ELPs of the same length, the T_t was 24 °C when 100% of the X residues were valine, the T_t was 50 °C when 20% were substituted with serine, and the T_t was 10 °C when 20% were substituted with isoleucine (*120*). The T_t can also be controlled by ELP length and concentration, the concentration and type of ions in solution, the pH, and the presence of organic solvents (*70, 125-127*). Therefore, although ELPs are considered thermoresponsive, their phase

transition can be induced at a constant temperature by applying environmental stimuli. This stimuli-responsiveness is at the heart of most of the applications for which ELP's have been applied.

1.3.3 Applications of Stimuli-Responsive ELPs

Protein purification

ELPs are a privileged class of PBPs because they can be expressed at high levels in *E. Coli* and conveniently and economically purified non-chromatographically with the aid of their unique phase transition behavior. The purification process is known as inverse transition cycling (ITC) (*98, 128*). After expression, ELPs exist in a complex mixture with other soluble and insoluble molecules. They can be selectively precipitated out of solution by adding salts and increasing the temperature to induce the ITT. The aggregated ELPs are separated by centrifugation and resolubilized in cold buffer. The cycle is completed by centrifugation below the T_t to remove insoluble matter. The cycle is repeated multiple times to increase purity (Figure 1-8a). ITC is also beneficial for the purification of other proteins (Figure 1-8b). Proteins fused to ELPs can be co-precipitated by ELP aggregation then separated by proteolytic cleavage or with self-cleaving intein tags with yields similar to those achieved using traditional chromatographic methods (*128-132*). Lower concentrations of ELP-fusion proteins can be purified by addition of free ELP to capture them from solution (*133*). ELP-promoted purification can also be realized by fusion of affinity labels (Figure 1-8c). For example, ELPs conjugated to staphylococcal protein A, bacterial metalloregulatory protein, and histidine clusters bound to their respective binding partners (antibodies, plasmid DNA, and heavy metals) and facilitated their separation by ITC (*134-136*).

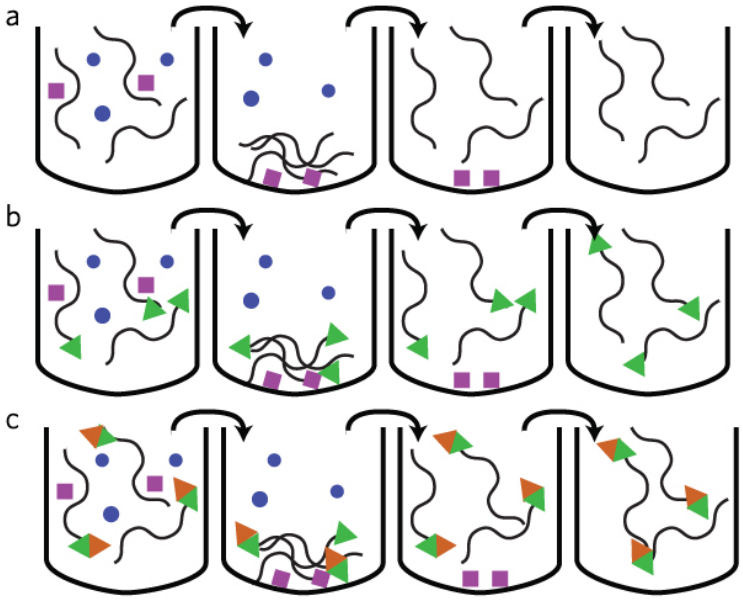

Figure 1-8. ELP and ELP-mediated purification. (a) Black curves represent ELP chains, squares represent insoluble impurities and circles represent soluble impurities. First the temperature is raised above the T_t to aggregate ELPs. Aggregates are then isolated by centrifugation. Next they are resolubilized in cold buffer and insoluble matter is isolated by centrifugation. Next the pure ELP supernatant is isolated and the process repeated if necessary. (b) Triangles represent a fused protein. The same process as (a) results in purified ELP-protein fusions. (c) Two triangles represent a ligand-receptor pair. The same process as (a) allows for ligands to be purified from complex mixtures by ELPs fused to ligand-binding sequences.

Therapeutic targeting and delivery

In the early 1990s, Urry et al. performed a litany of tests that all showed VPGVG-type ELPs to be remarkably biocompatible (*137*). ELPs have since been studied extensively for in vivo applications, including therapeutic delivery. Even passively, an ELP-antibody fusion was found to increase the antibody's circulating half-life by a factor of 24. However, the various ways that the stimuli-responsiveness of ELPs has been exploited are perhaps more interesting. Topcic et al. showed that an ELP could dynamically turn antibody binding on and off with changes in temperature (*138*). In another example, the coacervation of ELPs into viscous aggregates was used to form drug delivery depots that could increase the residence time of fused proteins and chemical therapeutic agents (*139-142*). Meanwhile, local ELP aggregation at tumor sites was achieved with a combination of targeted hyperthermia and T_t engineering. Mild hyperthermia (<43 °C) is an adjunct treatment for tumors. Meyer et al. demonstrated that an ELPs engineered with a T_t above 37°C and below 43 °C accumulated twice as much in the area of heated tumors compared to an ELP with a higher T_t (*143*). Bidwell et al. then demonstrated that ELPs genetically engineered with c-Myc inhibitor peptides could reduce breast tumor growth in conjunction with targeted hyperthermia (*96*).

ELPs can be engineered to self-assemble into nanoscale therapeutic delivery vehicles in a thermoresponsive manner by controlling their degree of amphiphilicity (Figure 1-9). Assembly occurs

due to segregation of hydrophobic ELP domains away from water. For example, conjugation of hydrophobic drug molecules to one end of an ELP induced nanoparticle formation. These nanoparticles were extremely effective at delivering drugs to tumor cells (*144*). Amphiphilicity has also been introduced genetically by creating di- and triblock ELPs. By controlling the block lengths and relative hydrophilicities, nanoscale spherical micelles were assembled above the T_t of the hydrophobic blocks (*145-149*) Further genetic engineering has led to pH and metal ion-dependent micelle assembly (*150*) as well as multivalent display of cell receptor ligands, cellular entry motifs, growth factors and whole proteins (*151-155*).

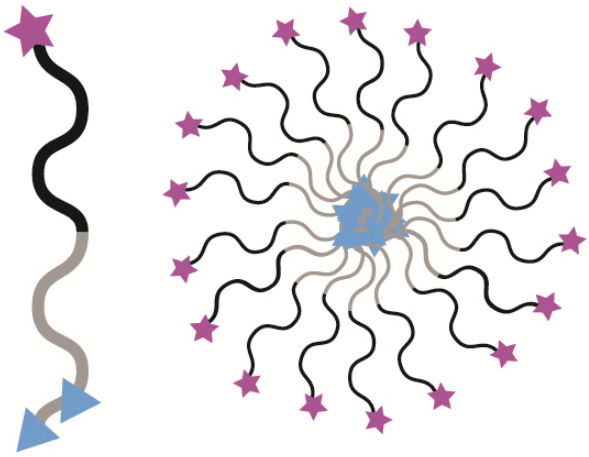

Figure 1-9. Schematic of ELP amphiphile self-assembly into nanoscale therapeutic delivery vehicles. Different amphiphilic architectures can generate nanoscale micelles. The hydrophilic region (black curve) can be an ELP block with a high T_t or a hydrophilic sequence. The hydrophobic region (grey curve) can be a low T_t ELP block but need not be if conjugates such as drugs (triangles) are sufficiently hydrophobic. Targeting ligands, or proteins, or cell penetrating peptides (stars) can decorate the surface after self-assembly.

Cell and Tissue Engineering

The biocompatibility and mechanical properties of ELPs make them good candidates for cell and tissue engineering. As mentioned previously, genetic engineering provides ample opportunity to introduce smart behavior in terms of ELP-cell and ELP-biomolecule interactions (*71*). However, less has been explored in terms of utilizing ELP stimuli-responsiveness. Betre et al. encapsulated chondrocytes within a viscous ELP coacervate and demonstrated their viability (*156*) Wright et al. utilized the ITT to self-assemble ELP hydrogels using triblock ELPs with "plastic-like" hydrophobic end blocks with the sequence poly((V/I)PAVG) and elastin-like hydrophilic midblocks with sequence poly(VPG(V/E)G) (Figure 1-10) (*157-159*). Meanwhile, Mie et al. utilized two ELPs to create a thermoresponsive cell culture surface. One ELP was first adsorbed to a substrate, and then a second ELP bearing a cell-binding motif was captured on the surface by inducing the ITT. Cells were subsequently cultured on the surfaces. When the temperature was lowered, the ELPs separated, releasing the cells from the surface. (*160*).

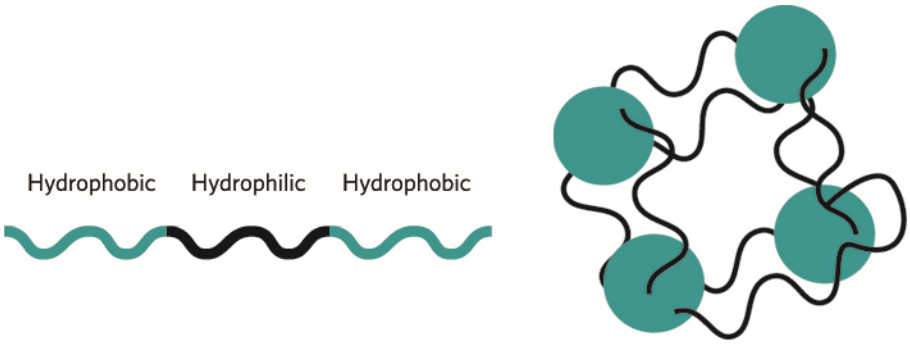

Figure 1-10. Schematic of hydrogel network formation by a triblock ELP. Above the T_t of the hydrophobic blocks, phase segregation occurs resulting in physical crosslinks between hydrophobic blocks bridged by the hydrophilic midblock.

1.4 Current State of the Art in PBP-Nanoparticle Hybrids

There are currently very few examples of PBP-nanoparticle hybrids in the literature. Several examples have followed the same general protocol. An SLP was fused with a peptide derived from phage display (silver-binding), a natural motif (silaffin), or a whole protein (hydroxyapatite binding) then cast into films and fibers. The respective inorganic precursors (silver ions, silicic acid, or calcium and phosphate ions) were then added. In each case, nanoparticles were mineralized within the SLP matrices. The silver nanoparticles provided anti-bacterial activity, while the hydroxyapatite nanoparticles increased SLP stiffness and toughness (*74, 161, 162*). A silk-elastin-like polypeptide (SELP) has also been mixed with clay nanoplatelets. No specific motif was used to interact with the clay platelets but the SELPs were found to change the dispersion of platelets based on their backbone charge (*163*). Finally, several groups have combined ELPs with gold nanoparticles in order to measure temperature and pH-dependent absorption spectra (*164-166*). The relative dearth of papers in this field suggests that many possibilities have yet to be explored, especially in terms of synergistically combining the stimuli-responsiveness of nanoparticles with the stimuli-responsiveness of PBPs.

1.5 Summary

1. Smart biomaterials are able to interact with biomolecules/cells and react to external cues.
2. Combinations of nanoparticles and polymers (NPHs) are promising smart biomaterials
3. To create functional NPHs, polymers must be designed with appropriate physical/stimuli-responsive properties, bioactivity, and to interface with nanoparticle surfaces.
4. Synthesizing all of the necessary functions into polymers can be prohibitively difficult.
5. Genetically engineered PBPs can be made multifunctional by modular incorporation of motifs
6. PBPs can be synthesized with a broad variety of physical/stimuli-responsive properties, bioactive motifs, and surface anchoring pathways.
7. The biocompatibility, high-yield synthesis, and thermoresponsiveness of ELPs make them especially attractive PBPs.
8. PBP-nanoparticle hybrids have yet to be extensively explored.

Chapter Two: A Method for Efficient, Seamless Cloning of Protein-based Polymer Genes

2.1 Abstract

This chapter describes the development of a new method to genetically engineer tandemly repeated DNA sequences for the construction of protein-based polymer (PBP) genes. A plasmid containing a specific layout of restriction endonuclease (RE) sites was designed specifically to facilitate simple, accurate and seamless multimerization of DNA sequences. As a proof-of-principle, this method was used to prepare a series of elastin-like polypeptide (ELP) genes.

2.2 Introduction

The rate at which new PBPs can be created and tested is inherently limited by the rate at which we can synthesize their genes. This is because, unlike chemically synthesized polymers, it is unavoidable to synthesize any new PBP without first engineering its corresponding gene. Unfortunately, PBP gene synthesis is not trivial; the highly repetitive nature of their DNA sequences precludes the use of more traditional genetic engineering methods. The same is true of the tandem repeats used for the synthesis of various therapeutic proteins (*167-170*). Therefore, it is critical to establish methods for simple, flexible, and rapid synthesis of long, repetitive gene sequences.

A number of genetic engineering methods have already been devised specifically to generate tandemly repeated DNA sequences (*75, 171-180*). Typically, these methods follow one of three pathways: concatemerization—the one-pot, head-to-tail ligation of monomeric units to each other, polymerization—the use of polymerase chain reactions (PCR), or iteration—a recursive, stepwise construction pathway (*181*). Concatemerization and polymerization are particularly well suited for rapid formation of a library of multimer lengths. The downside is that a large number of transformants must be screened and sequenced with no guarantee that the gene size of interest will be present (*180*). In addition, both methods generally become less applicable as the length of the target gene increases due to unwanted DNA circularization or PCR limitations (*171, 174, 179*). Concatemerization and PCR methods are also often not suitable for the simple creation of block copolypeptides, limiting their flexibility. Meanwhile, iterative methods allow for precise control of gene length but can be time consuming, especially for the construction of longer multimers. Previous cloning methods have managed to address multiple needs, including ensuring head-to-tail connections, and formation of seamless junctions (*173, 177, 178*). Unfortunately, these methods remain laborious, inefficient, error-prone, or limited in the length of the sequence that can be attained. Here we present a cloning method built upon the advances of previous PBP gene synthesis schemes that is amenable to both concatemerization and iteration, while also addressing various drawbacks of previous methods. Please note that, after completion of this work, an analogous method was published by McDaniel et al. (*182*).

2.3 The Genetic Engineering Scheme

The key aspects of our PBP gene synthesis method are the arrangement and choice of REs. Both type IIS REs—endonucleases which cleave DNA at a fixed distance from an asymmetric recognition site, and type IIP REs—endonucleases which recognize palindromic sequences and cleave at symmetrical

sites within or directly adjacent to the sequence, are utilized. As illustrated in Figure 2-1a, the gene cassette "monomer" to be multimerized is flanked by two unique type IIS RE sites. Meanwhile, two unique type IIP sites are located further downstream and upstream, respectively. In practice, only one of the two type IIP sites is required.

The overall arrangement of monomer and RE sites is diagrammed in Figure 2-1b. For the type IIS REs, we chose BpiI and Eco31I and designed their cleavage sites to generate compatible, non-palindromic four-base overhangs to ensure unidirectional DNA insertion. We chose BamHI and XhoI for the type IIP REs because they are compatible in the same buffer system used for the type IIS REs, preventing the need for sequential digestions. Other combinations of type IIS and IIP REs should presumably exist that would fit the same criteria. For the monomer, we chose a sequence which codes for an ELP with the protein sequence $[(\mathrm{VPGVG})_2\mathrm{VPGKG}(\mathrm{VPGVG})_2]_5$. The periodically spaced lysine groups are the defining characteristic of the ELP sequence, so we adopted the naming convention of K*n,* where *n* denotes the number of VPGXG pentapeptides in the sequence. The monomer sequence is thus identified as K25. The sequence, including RE sites and monomer, was synthesized in the pJ54 vector by DNA 2.0 Inc. Although we utilized DNA 2.0's proprietary vector, a number of common cloning vectors, including pUC19, contain no BpiI sites and one Eco31I site. This means that other suitable vectors could be prepared without significant difficulty.

A round of iterative construction is detailed schematically in Figure 2-1a and more specifically in Figure 2-1b. First, vector DNA is generated by digestion with BamHI and BpiI, while compatible insert DNA is generated by digestion with BamHI and Eco31I. Ligation of the products leads to placement of the insert upstream of the vector gene. Importantly, the original architecture of RE sites is completely regenerated by this process. Subsequent rounds of cloning can then proceed using the exact same protocol using the products of previous rounds. Gene length can increase exponentially each round in this way. The presence of the second type IIP REase site (XhoI) allows for cloning to occur using an analogous process, but the insert DNA gets added downstream of the vector gene. At any round, genes with compatible sticky ends can be inserted to create block copolypeptides.

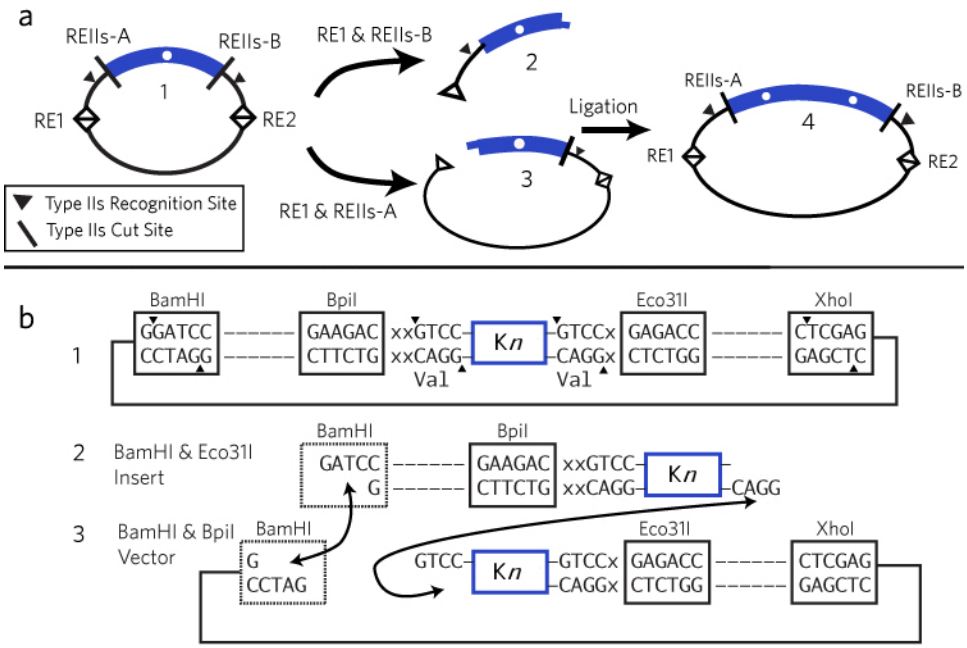

Figure 2-1. Description of our iterative cloning method. Generic (a) and detailed (b) schematics of the iterative cloning process. (a1 & b1) The vector containing the gene sequence to be multimerized. Directly upstream and downstream of the gene are two Type IIs restriction enzymes sites: REIIs-A (BpiI) and REIIs-B (Eco31I). Farther upstream and downstream are two type IIP RE sites: RE1 (BamHI) and RE2 (XhoI). (a2 & b2) An insert fragment is generated by cutting with RE1 and REIIs-B. (a3 & b3) A compatible vector is created by cutting with RE1 & REIIs-A. (a4) Subsequent ligation yields a seamless dimer of the original sequence with the same organization of RE sites (Note: An analogous method utilizing RE2 allows for insertion at the 3` end of the vector gene).

The RE architecture also allows for gene multimerization using a concatemerization pathway. A double digestion with both type IIS REs generates a monomer with sticky ends that can anneal to other monomers to form a library of multimers. The library can then be ligated to a vector treated with one or both Type IIS REs (Figure 2-2). Concatemerization also completely regenerates the initial RE architecture. This pathway proceeds analogously to previous methods which used single type IIS REases (*173, 179*). Although it suffers from the same shortcomings of previous concatemerization methods, it could be used to rapidly generate multimers that could then be used as building blocks for the iterative pathway. Previous improvements to concatemerization pathways which use "adapter" sequences to obviate the need for vector dephosphorylation or the "double initiator" method which prevents vector recircularization could also be utilized within our scheme (*179, 183*).

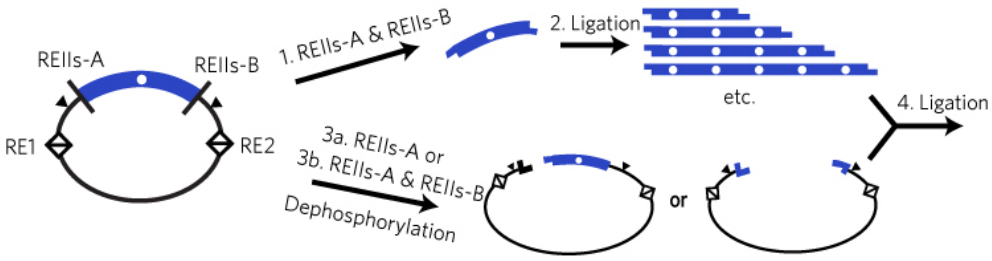

Figure 2-2. Schematic of concatemerization pathway. Step 1: The vector is cut with REIIs-A & REIIs-B to generate insert DNA. Step 2: The insert DNA is concatemerized by ligation to generate various length products. Step 3: Cutting with a single Type IIs REase or both IIs REases generates a compatible vector which must then be dephosphorylated. Step 4: The library of inserts from step 2 or an insert size purified from the library is ligated with the vector DNA.

2.4 Results

As shown in Figure 2-3, our method allowed for the controlled synthesis of genes corresponding to multiples of the original monomer, K25. We synthesized ELP genes up to 150 pentapeptides (K150) in length, but this by no means represents an upper limit on the achievable length. To demonstrate that the genes were functional, we transferred K150 to a suitable expression vector and expressed it to yield a monodisperse product (Figure 2-4).

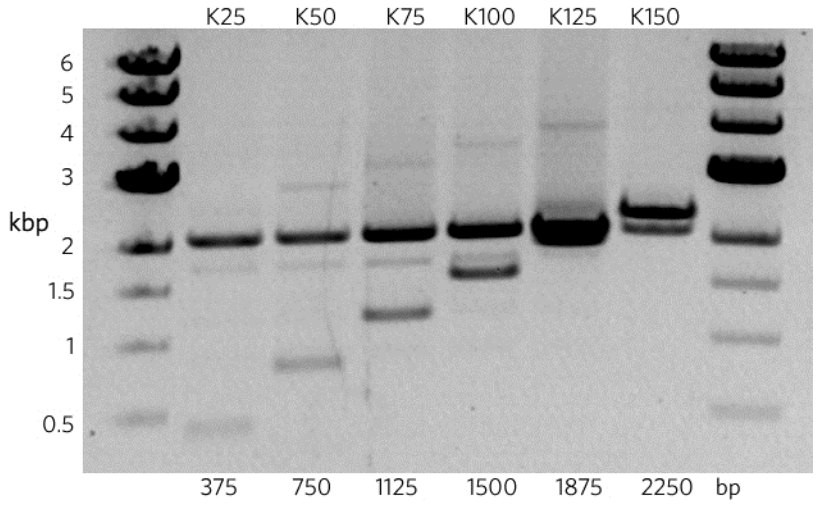

Figure 2-3. DNA size analysis. Agarose gel electrophoresis of the library of ELP plasmids. Plasmids were digested with BpiI and Eco31I to generate the 2151 base pair vectors and the ELP gene fragments. The initial ELP monomer size is 375 bp. The ELP gene fragment sizes in base pairs are shown at the bottom.

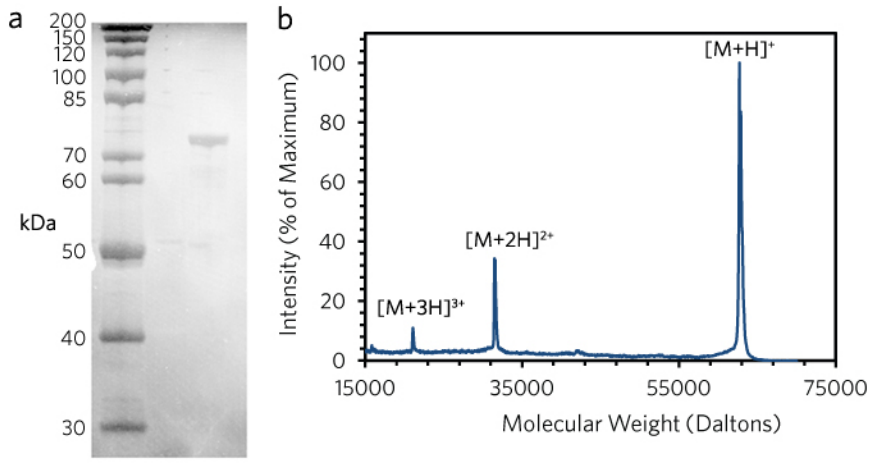

Figure 2-4. Protein characterization. (a) SDS-PAGE analysis on a copper stained gel shows that there is one pure product after purification of K150. (Note: ELPs commonly migrate to higher apparent molecular weights) (b) MALDI-TOF MS analysis also shows a single dominant peak as well peaks from the multiply ionized product. The observed molecular weight (62713 Da) is within 0.11% of the expected molecular weight (62778 Da assuming N-terminal methionine cleavage).

2.5 Advantages of Our Cloning Method

The cloning method we developed has multiple advantageous features and also addresses limitations of previous methods. First of all, the use of type IIS REs makes the ligation sites seamless, meaning no sequence scar is left from the RE recognition site. Lewis et al. also used a three enzyme system in their construction of a silk like PBP. However, their method relies on the complementary ends generated by type IIP REs, BspEI and XmaI, which results in the incorporation of unwanted nucleotides (*172*).

Our method is simple and fast. We aimed to maintain the number of DNA manipulation steps per round of cloning to a minimum. For each round there are only two restriction digests and one directional ligation step (no blunt ends). This makes the protocol essentially no different and no less efficient than required when using only type IIP restriction enzymes. Previously, Won et. al. also developed a multimerization strategy using two type IIS REs, but each round of cloning required three restriction digests, PCR, DNA dephosphorylation, DNA phosphorylation, and two ligation steps (*174*).

Our method is also efficient because there are a minimum of possible side reactions. The method known as recursive directional ligation (RDL) which also proceeds by an iterative process quotes success rates for finding positive clones of 30-80% (*175*). This is most likely due to the possibility for circularization of both the vector and insert. Although vector recircularization can be reduced by the addition of a dephosphorylation step, insert circularization cannot. Our method avoids this issue entirely by never generating a fragment capable of circularization. Although non-viable side-products can form when using our method (head-to-head ligation of vector or insert at BamHI sites) or RDL (insert circularization) which can deplete the reactant concentrations, efficiency did not appear to be an issue. Therefore, we found that very few colonies needed to be screened to find positive clones (we typically

picked two). Regardless, efficiency could be further improved by replacing the BamHI site with an RE site which leaves non-rotationally symmetric sticky ends such as AvaI to prevent any head-to-head side reactions (*177*).

Ideally any multimerization strategy should allow for complete control over DNA sequence and length. When it comes to repeat number, this control is afforded by the use of an iterative process instead of PCR or concatemerization-based processes because the size of the product is predetermined. This avoids the need for extensive screening of colonies. By not using any PCR steps, we prevent the introduction of errors or unwanted additions that can occur when performing PCR on highly repetitive sequences (*174*). Admittedly, PCR-based methods are the better choice if a library of gene lengths is desired (*182*).

Finally, our method is flexible. When utilizing RDL, the most important step is the choice of compatible REases. Because RDL utilizes REases that cut split palindromic sequences, portions of the recognition sites must match a portion of the coding region of the monomer (*175*). There is no guarantee that two such enzymes exist for any given sequence. Other methods also suffer from this lack of sequence flexibility (*157*). In contrast, the use of type IIS REase obviates the need to choose new REases for each new target sequence. Therefore, although we created an ELP gene, the same set of enzymes could have been used to multimerize almost any DNA sequence.

2.6 Conclusion

We have designed a method for gene multimerization based on a specific RE architecture which combines the advantages of a number of previous methods. It is seamless, flexible, efficient, rapid, accurate, and simple to perform. Furthermore, it can be utilized without modification for concatemerization when a library of repeat lengths is desired. Most importantly, the enzymes in this method are suitable for the multimerization of nearly any DNA sequence. New protein sequence motifs with potentially valuable properties are constantly being identified. (*87, 184*) The ease and reliability of our method in combination with complementary techniques will allow for rapid synthesis and tuning of the next generation of functional PBPs based on these new sequences.

2.7 Materials and Methods

Materials: K25 DNA was synthesized and obtained as an insert in the pJ54 vector from DNA 2.0 Inc. (full sequence and plasmid map in the appendix). Oligonucleotides were synthesized by Integrated DNA Technologies, Inc. Restriction endonucleases were purchased from Fermentas Inc. and New England Biolabs. T4 DNA Ligase was purchased from New England Biolabs. DNA was purified using kits from QIAGEN Inc. The pET-28b(+) expression vector, Novablue competent cells, and BLR(DE3) *E. coli* strains were obtained from EMD Novagen. All protein expression was carried out in Terrific Broth (*185*). DNA sequencing was performed by the University of California, Berkeley DNA sequencing center. Matrix-assisted laser desorption ionization time of flight mass spectrometry (MALDI-MS) was performed on an Applied Biosystems Voyager-DE.

Gene Synthesis: Synthesis began with the K25 "monomer" sequence (Figure 2-5). The sequence included appropriate restriction enzyme sites upstream and downstream from the ELP sequence (Figure 2-1).

The codon usage was designed to approximate the codon frequencies used by *E. coli* using an in-house script.

```
   BamHI             BpiI     Val
 1 GGATCCTTCA CATATGCGAA GACAAGTCCC CGGGGTCGGT GTTCCGGGAG TCGGGGTGCC
61 GGGAAAAGGG GTGCCGGGTG TTGGAGTGCC GGGCGTGGGT GTCCCGGGCG TCGGGGTTCC
121 GGGCGTCGGA GTCCCGGGTA AAGGTGTTCC GGGCGTTGGT GTTCCTGGGG TGGGCGTTCC
181 AGGGGTTGGT GTACCTGGTG TCGGTGTGCC TGGTAAAGGC GTCCCGGGTG TTGGCGTACC
241 TGGGGTCGGC GTGCCTGGCG TAGGCGTGCC AGGTGTAGGA GTGCCCGGTA AAGGAGTTCC
301 GGGTGTTGGT GTGCCTGGCG TGGGCGTGCC GGGCGTAGGT GTTCCAGGTG TGGGCGTGCC
361 TGGTAAGGGG GTACCAGGAG TTGGCGTCCC AGGCGTAGGA GTCCTGAGAC CGTCATATGT
421 ACTCGAG                                     Val   Eco31I
     XhoI
```

Figure 2-5. K25 sequence with flanking restriction sites and the first and last valine codons emphasized in bold.

Gene multimerization: Standard molecular biology protocols were used for DNA engineering. All RE reactions were performed in 1X Buffer Green from Fermentas. In a typical round of cloning ~1 μg of K*n* plasmid was digested with BamHI and BpiI to generate vector DNA while a K*m* plasmid was digested with BamHI and Eco31I (20 units for 4 hours) to generate insert DNA. The products were then isolated by agarose gel electrophoresis followed by gel extraction and purification. The isolated products were then ligated, in a 10 μL reaction with an approximately 1:4 (v/v) vector to insert ratio for 1 hour at room temperature using 400 units of T4 DNA ligase. The product was then transformed into Novablue competent cells using the manufacturer's protocol. The putative K*(m+n)* bearing colonies were confirmed by DNA sequencing using the primers ELPSeqF and ELPSeqR (Table 2-1). The process was repeated as necessary to reach the desired gene lengths.

Expression Vector Construction: The K150 gene was used for further expression studies. To remove the BpiI site and introduce an NcoI site, synthetic oligonucleotides N1 and N2 were annealed and inserted into BamHI and BpiI digested K150 to form K150N. To remove the Eco31I site and introduce a stop codon, the same procedure was used to insert annealed oligonucleotides C1 and C2 into Eco31I and XhoI digested K150 to form K150-NC (Oligonucleotide sequences shown in Table 2-1). To perform annealing steps, 45 μM solutions of complementary oligonucleotides were mixed with 10X T4 DNA ligase buffer, heated to 95 °C in a water bath and allowed to gradually cool to room temperature over the course of several hours. The oligonucelotides added DNA coding for a GVG sequence to the N-terminus and a VPG sequence to the C-terminus. K150-NC was then excised using NcoI and XhoI and transferred to pet28b which was also digested with NcoI and XhoI. The transformants were then confirmed by DNA sequencing using the primers p28F and p28R (Table 2-1). K150's protein sequence was MGVG$[(VPGVG)_2VPGKG(VPGVG)_2]_{30}$VPG.

Table 2-1. List of oligonucleotides used in this study

Identifier	Oligonucleotide Sequence (5′ to 3′)
N1	GATCCATGGGTGTTGGT
N2	GGACACCAACACCCATG
C1	GTCCCGGGTTAAGCAGCTC
C2	TCGAGAGCTGCTTAACCCG
ELPSeqF	GAGAGTAGGGAACTGCCAGG
ELPSeqR	CGCGAGCCCATTTATACCTG
p28F	GATGCGTCCGGCGTAGAG
p28R	GCTAGTTATTGCTCAGCGG

Protein Expression: K150-NC was expressed in *E. Coli* strain BLR(DE3). For expression, a single colony of K150NC was inoculated in a 50 mL starter culture of LB supplemented with 30 μg/mL of kanamycin. This culture was grown overnight at 37°C with shaking at 250 RPM. 10 mL of the starter culture was then added to 1 L of Terrific Broth also supplemented with 30 μg/mL of kanamycin. This culture was grown at 37°C with shaking at 250 RPM to an OD600 of ~0.8 before expression was induced by addition of IPTG to a final concentration of 1 mM. Expression was halted after 3 hours at which point the cells were centrifuged at 4000 RCF for 20 minutes at 4 °C. The cell pellet was resuspended in 40mL of 10mM sodium phosphate buffer, pH 10. Cell lysis was performed using sonication (Power Level 5, 10 seconds pulses followed by 20 second delays for 2 minutes of pulse time) using a Misonix Sonicator 3000. Insoluble matter was removed from the lysate by centrifugation at 30000 RCF for 30 minutes at 4 °C. The supernatant was then treated with PEI at a final concentration of 0.5% w/v to remove DNA. This solution was once again centrifuged at 20000 RCF for 20 minutes 4 °C and the supernatant kept for further purification.

Purification: The ELP was purified from solution by three rounds of inverse transition cycling (ITC) (*128*). For each round of ITC the ELP was heated to 35°C and NaCl was added at a concentration of 0.75 M-2 M. The insoluble ELP was then pelleted by centrifugation (15000 RCF, 15 minutes, 35 °C) followed by resolubilization on ice in 10 mM sodium phosphate buffer (Na_2HPO_4), pH 10. The resolubilized solution was then centrifuged at 20000 RCF for 15 minutes at 4 °C to remove insoluble impurities. The purified protein was dialyzed against deionized water for several days using a regenerated cellulose dialysis membrane with a molecular weight cutoff of 6000-8000 Da. The dialyzed product was then lyophilized.

Purity and Molecular Weight Characterization: The purity of purified ELP was determined by copper-stained SDS-PAGE and (MALDI-MS). MALDI-MS was performed using a 30% Acetonitrile, 0.1% TFA solution and a sinapinic acid matrix. 1 uL of 200 pmol/uL K150 was added to 12 μL of matrix solution then 1.5 μL of the mixture was spotted on the MALDI-MS sample plate.

Chapter Three: ELP-Hydroxyapatite Bionanocomposites

3.1 Abstract

This chapter describes the development of stimuli-responsive hybrids of elastin-like polypeptides (ELPs) with hydroxyapatite (HAP), the mineral component of bones and teeth. An anionic oligopeptide inspired by natural bone-associated proteins was genetically fused to ELPs. The resulting ELPs bound to and stabilized nano-hydroxyapatite particles in solution. The HAP-binding ELPs were also incorporated into bone cement mixtures, resulting in significant increases in strength compared to pure cements. In addition, the thermoresponsiveness of the ELPs was exploited in order to increase the initial stability and injectability of the cements.

3.2 Introduction

3.2.1 Nature's Biocomposites

Nature is replete with examples of organic-inorganic nanocomposites composed of stiff, nanoscale minerals and "soft" biomacromolecules (*186-188*). These biocomposites are made with a relatively limited set of building blocks (e.g., proteins, polysaccharides, and minerals), yet they exhibit remarkable combinations of stiffness and toughness, properties that usually come at the expense of the other (*186, 189*). For example, abalone shell nacre, a brick and mortar-like composite of calcium carbonate platelets and an organic matrix, is over 1000 times as tough as single crystals of calcium carbonate (*190*). These mechanical enhancements have led to the intense study of biological composites (e.g., bone, teeth, nacre, and crustacean exoskeletons) and to the development of high-performance, synthetic analogs (*41, 191-198*). Several factors have been found to contribute to the mechanical properties of natural biocomposites based on previous studies. These factors include hierarchical spatial organization of constituents, increased flaw tolerance of nanoscale minerals, and optimized mineral aspect ratios (*51, 199-202*).

Despite being present at small weight percents compared to the inorganic phase, organic phase macromolecules have also been cited to influence the mechanical properties of biocomposites. They are believed to direct mineral formation and morphology by stabilizing amorphous phases and by accelerating or inhibiting mineralization (*203-207*). In addition, they act as nanoscale glues (*208, 209*). In this role, the organic macromolecules bind to the mineral phase, transfer stress from mineral to mineral, and dissipate energy through the breaking of "sacrificial bonds". These bonds form through non-covalent intra-chain, inter-chain, and interfacial interactions (*208-211*). The energy that must be dissipated to break these non-covalent bonds during loading is believed to contribute to the fracture resistance of biocomposites. In both bones and nacre, proteins have been implicated as the glue-like macromolecules (*212*). Specifically, non-collagenous proteins (NCoPs), such as bone sialoprotein and osteopontin, have been suggested as the possible glue proteins in bones. These proteins belong to the small integrin-binding ligand N-linked glycoprotein (SIBLING) family of proteins, are mostly unstructured, and are known to bind to collagen and integrin receptors (*213*). Therefore, the glue-like NCoPs are essentially natural versions of the multifunctional protein-based polymers (PBPs) described

in chapter 1. Considering their importance in nature, it would be beneficial to explore the rational design of synthetic glue protein analogs in order to create higher-performance synthetic nanocomposites.

3.2.2 Calcium Phosphate Cements

Calcium phosphate cement (CPC) bone defect fillers are commonly used biomedical materials that could potentially benefit from the incorporation of an organic phase. CPCs are synthesized by mixing of calcium orthophosphate precursor powders and an aqueous phase. The precursor powders are unstable in water and immediately dissolve and then reprecipitate into a more stable calcium phosphate phase. The resulting materials are purely inorganic, brittle and composed predominantly of nanocrystalline hydroxyapatite (HAP) (*214*). CPCs are valued for their osteoconductivity, biocompatibility, and ability to be molded into complex defect sites (*214, 215*). However, due to their insufficient strength, CPCs are only approved for filling of non-load bearing defects (*216*). Significant improvements to CPCs could expand their medically suitable application sites and reduce the need for autografts, which are limited in supply, and allografts, which can be immunogenic (*217*). Previous attempts have been made to improve CPCs by the addition of off-the-shelf polymers and proteins such as chitosan, polyethylene glycol, gelatin, and albumin (*215, 218-220*). Some strengthening has been achieved with these polymeric additives; however, no clear structure-property relationships have been determined due to the wide variety of chemical backbones that have been used.

3.3 Overview of the Study

The goal of this study was to design PBPs to mimic natural biocomposite glue proteins and to investigate the effects of the glue-like proteins on CPCs. Backbone-backbone and backbone-inorganic interactions are believed to be crucial determinants of glue protein functionality (*209*). Therefore, by tuning those interactions, we sought to determine structure-function relationships to guide the design of improved polymeric additives for CPCs. We chose to use ELPs to accomplish this because of their thermoresponsive and genetically tunable properties.

3.4 Results and Discussion

3.4.1 ELP Protein Design

We designed a set of ELPs (Table 3-1) with varying backbone charges and with or without a HAP-binding motif (E8) (*221*). We believe that these ELPs are a suitable starting library for studying sequence property relationships because they provide different possible modes of interfacial and intra/intermolecular interactions (Figure 3-1). The ELP backbone genes were synthesized using the cloning method described in Chapter 2. The backbone sequences were then transferred to expression vectors containing the desired N-terminal and C-terminal sequences in-frame (details in Methods).

Table 3-1. List of synthesized ELPs

Name	N-terminus	Backbone	C-terminus
V125	MSGVG	$(VPGVG)_{125}$	VPG
V125-E8	MSGVG	$(VPGVG)_{125}$	VPGSEEEEEEEE
V125-E8E8	MSEEEEEEEEGPG	$(VPGVG)_{125}$	VPGSEEEEEEEE
K125	MSGVG	$[(VPGVG)_2VPGKG(VPGVG)_2]_{25}$	VPG
E125	MSGVG	$[(VPGVG)_2VPGEG(VPGVG)_2]_{25}$	VPG

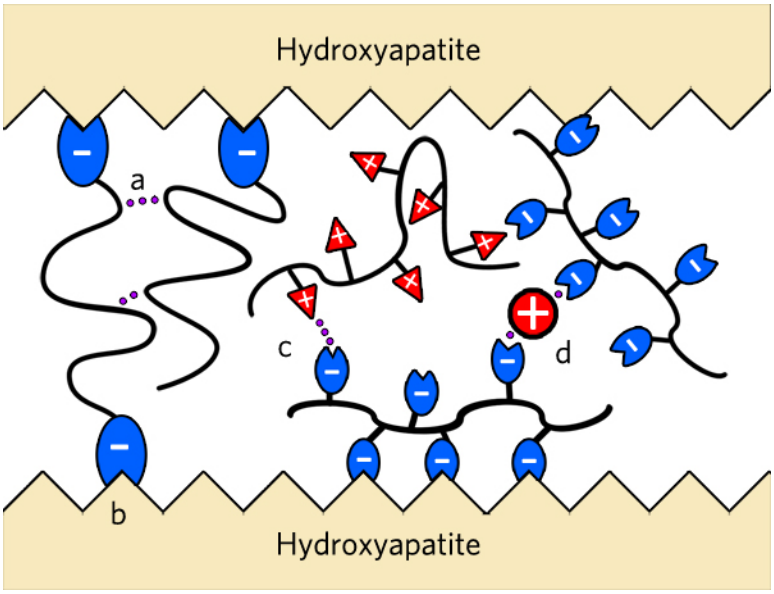

Figure 3-1. Schematic of possible ELP-ELP and ELP-HAP interactions: (a) backbone-backbone van der Waals or hydrogen bonding; (b) ELP-HAP binding; (c) backbone-backbone electrostatic interactions; and (d) ion-mediated crosslinks.

The purified proteins span a 2 kDa range from ~51-53 kDa and were verified to be within 0.5% of their expected molecular weights by MALDI-TOF MS (Figure 3-2).

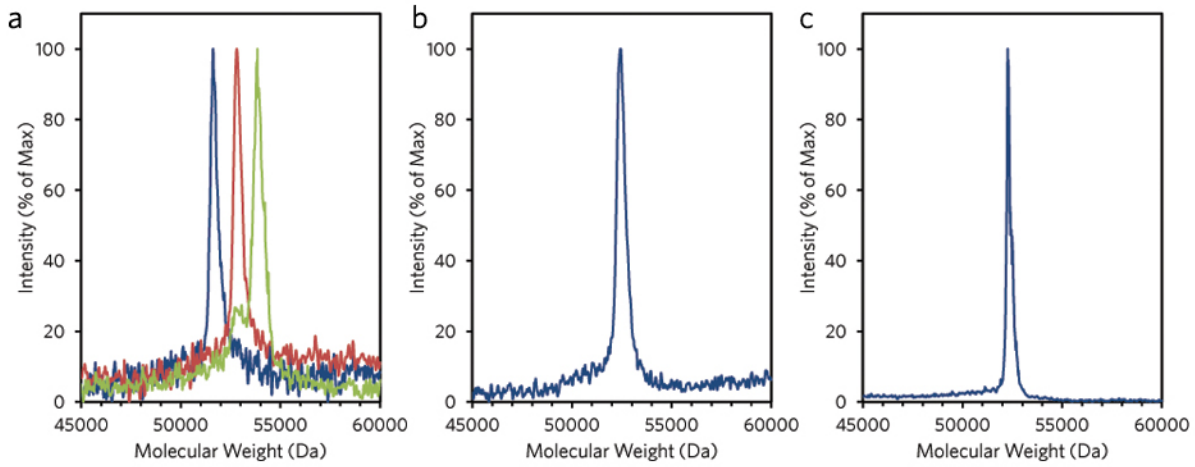

Figure 3-2. Molecular weight characterization. MALDI-TOF MS spectra of (a), from left peak to right peak, V125, V125-E8, & V125-E8E8; (b) E125; and (c) K125.

The resulting ELPs included uniformly neutrally (V125), negatively (E125), and positively (K125) charged backbones. The ELP length of 125 pentapeptides was chosen such that the neutral backboned ELP (V125) would have a T_t in a range of biological interest (between room temperature and physiological temperature). This ELP could then be used to investigate the effects of the inverse temperature transition (ITT) on composite properties. The negatively (E125) and positively (K125) charged backbones were designed with the same backbone length as V125 to allow us to exclude polymer molecular weight as a factor in our experiments. These polyelectrolyte ELPs were created in order to investigate the effects of polymer backbones with dispersed charges. Their backbones might interact electrostatically with each other, with solution ions, or with HAP. A silk-elastin PBP with similarly separated charged residues was previously shown to influence the disperson of clay nanoplatelets during the casting of PBP-clay nanocomposite films (*163*). To create the HAP binding ELPs, we linked an octaglutamic acid (E8) motif to either the C-terminal or both termini of V125 to generate V125-E8 & V125-E8E8, respectively. High concentrations of negatively charged sidechains are common to several NCoPs in bones and teeth including osteopontin, dentin matrix protein, and osteocalcin (*222-224*). In fact, the E8 motif is found within the sequence of bone sialoprotein. The negatively charged sidechains are believed to play a role in HAP binding, calcium ion binding, and regulating mineralization (*223*). Previous works have already shown that HAP binding can be conferred to short peptides and small molecule drugs by conjugating them with oligoglutamic or oligoaspartic acid sequences (*221, 225*). The variety of polymer architectures and uniformity in backbone length and charge distribution found in our small library demonstrate the power of using PBPs in endeavors such as this; it would be difficult to create a similar library using conventional polymer chemistry.

3.4.2 ELP-ELP and ELP-ion interactions

We characterized protein-protein and protein-ion interactions by measuring ELP transition temperatures (T_ts) (Figure 3-3, Table 3-2). Two solutions with equal ionic strengths were used. One

contained 10 mM Ca^{+2} ions while the other did not. As expected, the most hydrophobic ELPs, V125 and V125-E8, transitioned at the lowest temperatures, 27 °C and 33 °C, respectively (Figure 3-3). V125-E8 showed a small (2 °C) response to the presence of calcium ions. These proteins are above their T_ts under physiological conditions and, therefore, should engage in intermolecular and intramolecular van der Waals interactions.

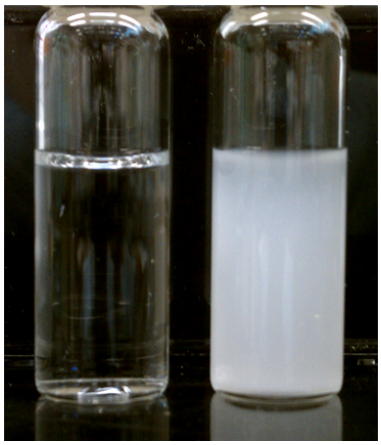

Figure 3-3. Photos of an ITT. 1 mg/mL solution of V125 at 23 °C (left, clear) and 37 °C (right, turbid).

No strong turbidity change was seen up to 95 °C in the calcium free V125-E8E8 solution. We believe that the charged end groups may have suppressed its transition or that its bola-amphiphilic nature may have resulted in the formation of soluble micelles with hydrophobic ELP backbones forming the cores and hydrophilic, E8-enriched coronas. In contrast, V125-E8E8 in the presence of calcium ions had a 40 °C T_t. This suggests that if the E8 motifs are sufficiently neutralized by calcium, as may occur during CPC setting reactions or due to mineral binding, V125-E8E8 might also be near its T_t at physiological temperatures. Both E125 and K125 had T_ts out of the physiological temperature range. Unlike K125 and V125, E125 showed a calcium ion dependent shift in T_t to a lower temperature. This indicates that E125's negatively charged side chains were interacting with calcium ions and could form the type of ion-mediated sacrificial bonds depicted in Figure 3-1d. These types of bonds have been shown to be active in the energy dissipating mechanisms of osteopontin and in mussel byssal fibers.(*210, 226*) Finally, we created 50:50 mixtures of K125 and E125 and demonstrated that backbone-backbone charge-charge interactions such as those depicted in Figure 3-1c occurred. This was indicated by the lower transition temperature of the mixture compared to either protein alone.

Table 3-2. List of ELP transition temperatures in °C in 20 mM Tris-Cl, pH 7.4

Name	**+150 mM NaCl**	**+120 mM NaCl, 10 mM $CaCl_2$**
V125	27	27
V125-E8	33	31
V125-E8E8	No Transition	40
K125	51	51
E125	71	62
K125/E125 50:50	43	44

3.4.3 ELP-HAP Interactions

We characterized sequence-dependent protein-mineral interactions using ELP-HAP binding assays (Figure 3- 4). In short, ELPs and HAP crystals were mixed in solution to allow binding. Afterwards, HAP and any bound ELP were separated by centrifugation and the remaining ELP concentration in solution was quantified. The binding assays confirmed that, despite the small size of the E8 motif relative to the full protein (1.25% or 2.5% of the length in amino acids), the E8 ELPs were imparted with an ability to bind HAP. At the same HAP to ELP mass ratio, E125, which has 25 glutamates, does not appear to bind to HAP as well as the E8 elastins did. This may be due to greater competition for binding sites; the distributed glutamates likely lead to a more extended conformation for E125 on HAP surfaces compared to the E8 ELPs. In addition, E8 likely has a higher affinity because binding of its glutamate sidechains decreases charge-charge repulsion within the highly charged E8 motif and places the other glutamates in close proximity to the mineral surface for cooperative binding. These results are consistent with previous studies that highlighted the importance of negative charge clustering over total negative charge when determining HAP affinity (*227*). K125 showed little to no binding activity despite reports suggesting the importance of cationic residues for HAP binding (*227, 228*). Therefore, K125 likely does not present its basic residues in a manner suitable for binding. Finally, the neutral ELP, V125, showed no binding activity to HAP. These results demonstrate that ELPs can be used to investigate sequence dependent protein binding to nanoparticle surfaces. Future modification by genetic engineering or chemical modification will allow us to test the role of binding motif length or to perform testing on other synthetic and naturally-derived HAP binding motifs (*229-231*). Engineereed HAP-binding ELPs might also be suitable in the future as therapeutic bone-mineral targeting agents if they are connected to drugs or therapeutic peptides.

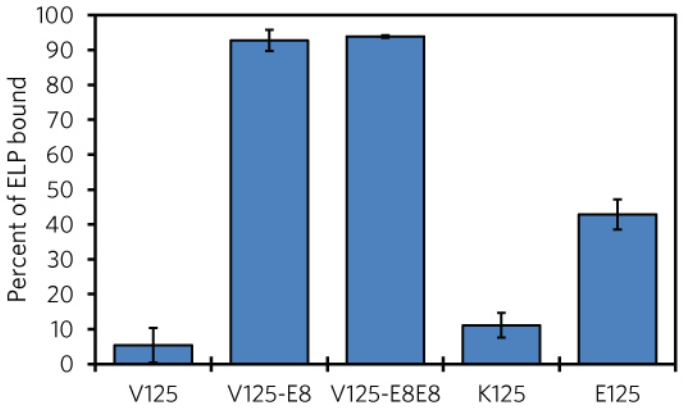

Figure 3-4. HAP binding analysis. The octaglutamic acid terminated ELPs bind to HAP crystals far more than the negatively charged E125 ELP. Non-negatively charged ELPs showed negligible binding to HAP.

We synthesized nanohydroxyapatite (nHAP) crystals using a hydrothermal method in order to investigate their colloidal behavior when mixed with ELPs in solution (Figure 3- 5).

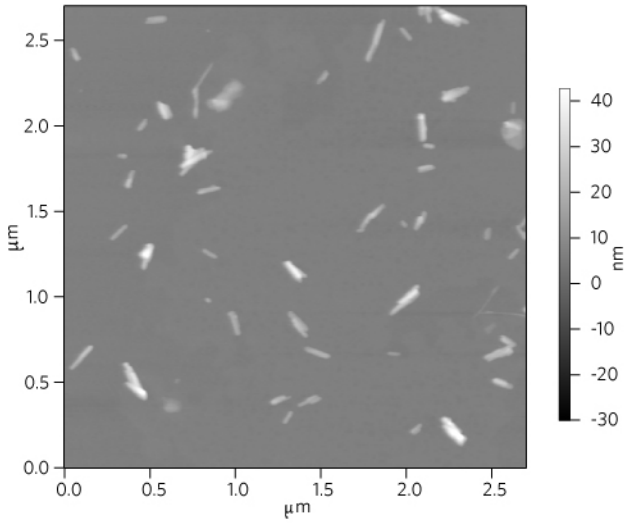

Figure 3-5. AFM image of aggregated nHAP crystals used for dispersion assays.

---

nHAP-ELP mixtures were observed in order to determine their time dependent sedimentation behavior. Complete sedimentation occurred within 30 minutes after nHAP crystals were dispersed by bath sonication in V125, K125, or E125 solutions. Meanwhile, consistent with the binding results, V125-E8 and V125-E8E8 containing solutions decreased the rate of sedimentation (Figure 3-6a). In V125-E8 solutions there was no visible sedimentation for several hours. This can be explained by the formation of a brush layer on the nHAP surfaces after V125-E8 bound which sterically hindered particle aggregation (Figure 3-6b). V125-E8E8 solutions also sedimented at a slower rate. We attribute this to initial binding

and steric stabilization followed by polymer bridging which led to particle aggregation and sedimentation (Figure 3-6c) (*232*). Like many nanoparticles, nHAP is prone to aggregation in the absence of stabilizers, limiting its effectiveness as a material for composite reinforcement (*9, 233*). These results demonstrate that ELPs can be used as thermoresponsive, colloidal dispersants for nHAP as was demonstrated previously for ELP-bound gold nanoparticles (*234*). ELP dispersed nHAP might someday be used in nHAP-reinforced composite materials (*233*). Meanwhile, telechelic ELPs such as V125-E8E8 may be used to bridge similar or dissimilar materials depending on the terminal amino acid sequences. This property may be useful for the development of composite hydrogel networks (*235*).

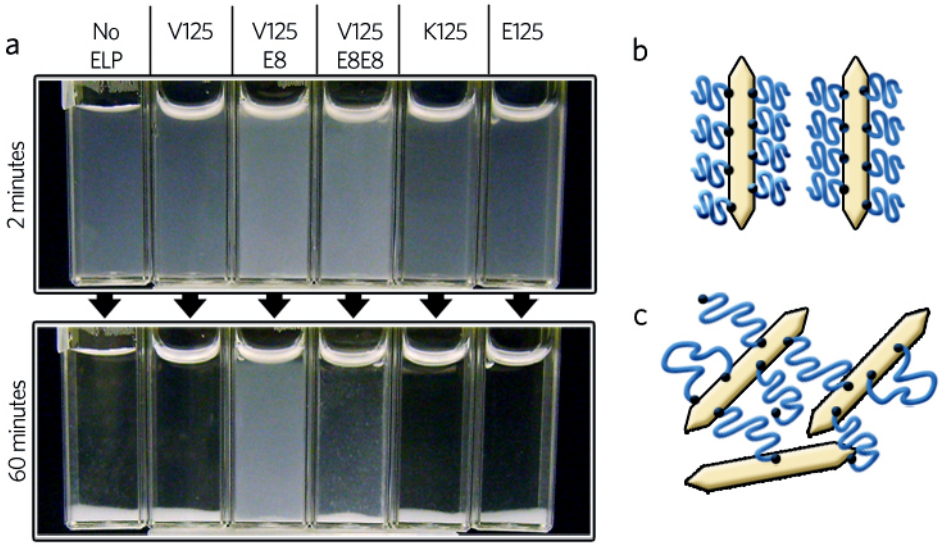

Figure 3-6. Dispersion assay. (a) ELPs mixed with nHAP particles quickly sediment except in the case of octaglutamic acid-displaying ELPs. V125-E8 has the more pronounced effect. (b) Schematic of V125-E8 binding providing steric protection against aggregation. (d) Schematic of V125-E8E8 causing particle bridging and thus having less of a protective effect.

3.4.4 ELP-CPC composite materials

In order to investigate the effects of our ELP constructs on the mechanical properties of ELP-HAP composites, we synthesized and characterized ELP-containing CPCs. The HAP-forming CPC formulation composed of dicalcium phosphate anhydrous (DCPA, $CaHPO_4$) and tetracalcium phosphate (TTCP, $Ca_4(PO_4)_2O$) was used (*236*). In the absence of ELPs, the maximum powder to liquid (P/L) mass ratio which allowed for suitable mixing and handling was 3:1. 10 wt% solutions of ELPs were used for fabricating CPC samples. Higher percentages became difficult to handle due to their viscosity. When 10 wt% solutions of V125-E8 and V125-E8E8 were mixed with the CPC powders there were significant changes to the cements' rheological and mechanical properties. CPC powders mixed with water at a 3:1 P/L ratio formed moldable putties, while E8 containing ELPs formed viscous fluids at the same ratio. The effect was more pronounced for V125-E8 compared to V125-E8E8. This behavior is consistent with the HAP dispersion assay and suggests that the E8 ELPs acted as plasticizers by binding

to the CPC precursor particles and promoting their dispersion. A similar effect has been demonstrated with sodium citrate and industrial superplasticizer modified CPCs. Dispersion in those cases was due to electrostatic repulsion (*237, 238*). The increased fluidity of E8 ELP containing cements allowed for mixing at increased P/L ratios because less water was required to solvate the cement particles. Increased P/L ratios have been shown to result in less porous, mechanically stronger cements. Therefore, samples were tested at P/L ratios of 4.25:1 for V125-E8 and 4:1 for V125-E8E8. Both ELPs resulted in CPCs with significantly increased compressive strengths. The strengths went from ~36MPa for control cements to ~57MPa for both V125E8 and V125E8E8-containing cements ($p < 0.001$) (Figure 3-7).

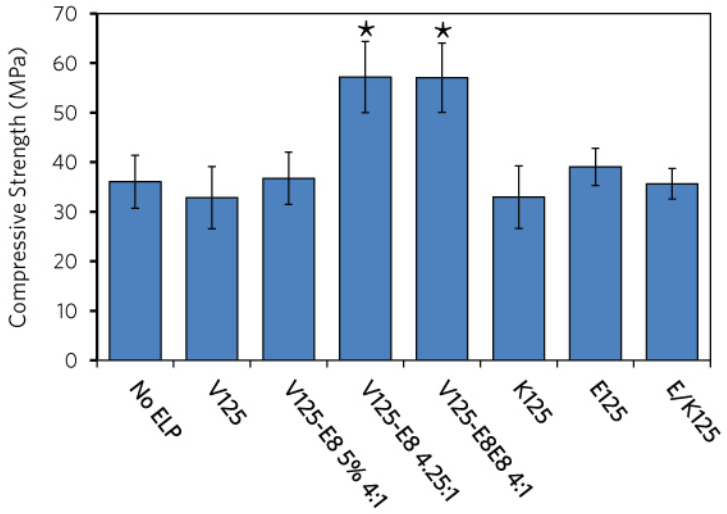

Figure 3-7. Compressive strength of ELP-CPC composites. V125-E8 and V125-E8E8-containing cements have enhanced strength. E/K125 was formed with a liquid phase containing a 10wt% 50:50 mixture of E125 and K125.

Although increasing P/L ratios can increase strength by reducing porosity, the E8 ELPs appeared to have an intrinsic strengthening effect (*237*). As evidence, when 5 wt% V125-E8 solutions were used at a P/L ratio of 4:1, the compressive strength (~37MPa) was not significantly increased compared to control (Figure 3-7). If the increased strength was due purely to decreased porosity, then similar strength improvements should have been found for the 5% and 10% formulations. In addition, the E8 elastins appeared to have qualitatively larger pores compared to the control cement, which has been seen previously in plasticized CPCs (Figure 3- 8a-c) (*238*). These pores may be the result of air entrainment arising from the ELPs' surfactant-like structures (*239*). Regardless, this porosity should decrease strength. This fact once again points to the presence of an intrinsic strengthening mechanism. At higher magnifications, it was apparent that the ELPs altered the crystal growth process (Figure 3- 8d-f). V125-E8-containing cements appeared to have larger crystallites with more rounded edges compared to the sharply faceted crystallites seen in control cements. V125-E8E8 containing cements appeared to also have more rounded crystallites in addition to a number of wide and flat crystallites. The exact effect of these morphological changes is unknown. The E8 elastins might also have become physically occluded

into the crystal lattices as the crystals precipitated. There is some evidence that this may occur in natural biomineralized systems and it has been shown to occur in other synthetic systems (*240-242*). In fact, occlusion of macromolecules within mineral crystals can increase the mechanical properties of the crystals (*241*).

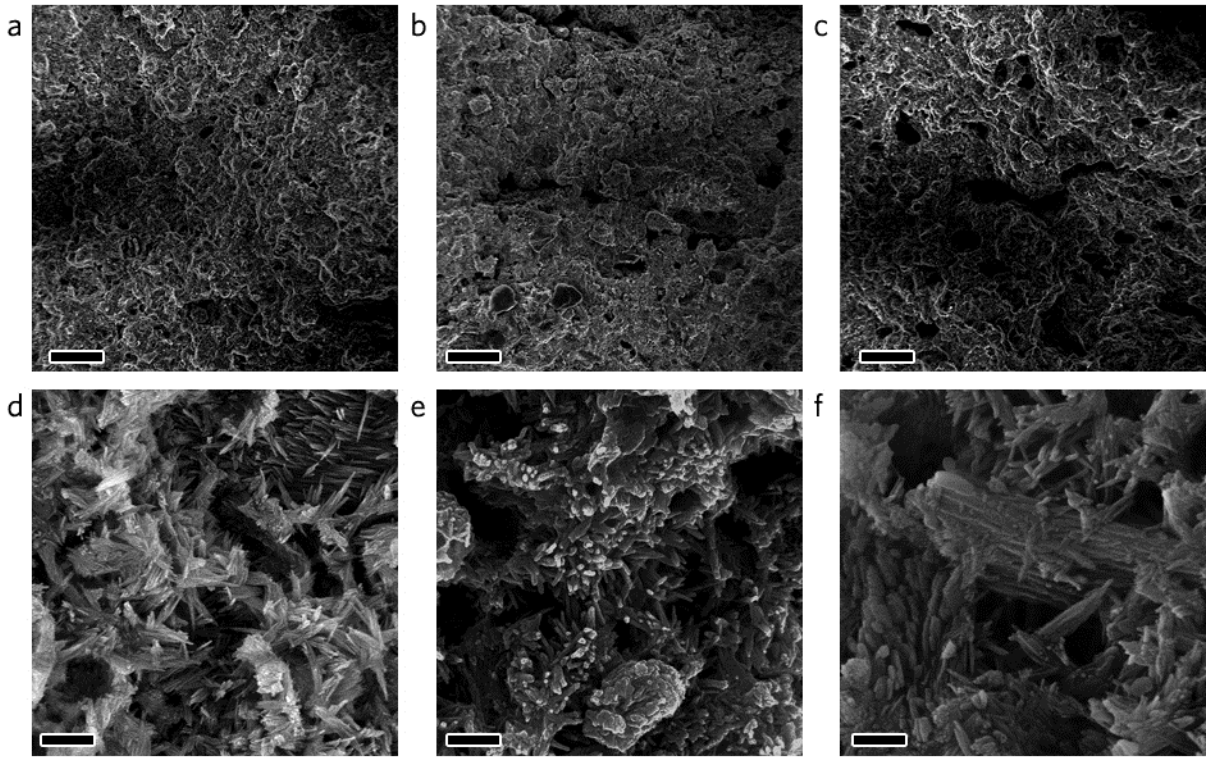

Figure 3-8. SEM analysis of ELP-CPC composites. (a, d) No ELP control; (b, e) V125-E8 containing cements; and (c, f) V125-E8E8 containing cements. Top row scale bars are 50 μm and bottom row scale bars are 500 nm. Top row images show the different porosities and bottom row images show different crystal morphologies.

The promising improvements in compressive strength led us to further characterize the flexural strength and work of facture of E8 ELP containing cements using three-point bending tests (Figure 3-4B). No significant difference was found when V125 was used as the additive compared to control samples. However, the flexural strength was found to improve from 9.4MPa for control samples to 14.6 MPa or 14.1 MPa for V125-E8 or V125-E8E8 containing samples, respectively (Figure 3-9a). The work-of-fracture increased from 13.1 J/m^2 to 21.2 J/m^2 or 20.9 J/m^2 for V125-E8 or V125-E8E8 containing samples, respectively (Figure 3-9b).

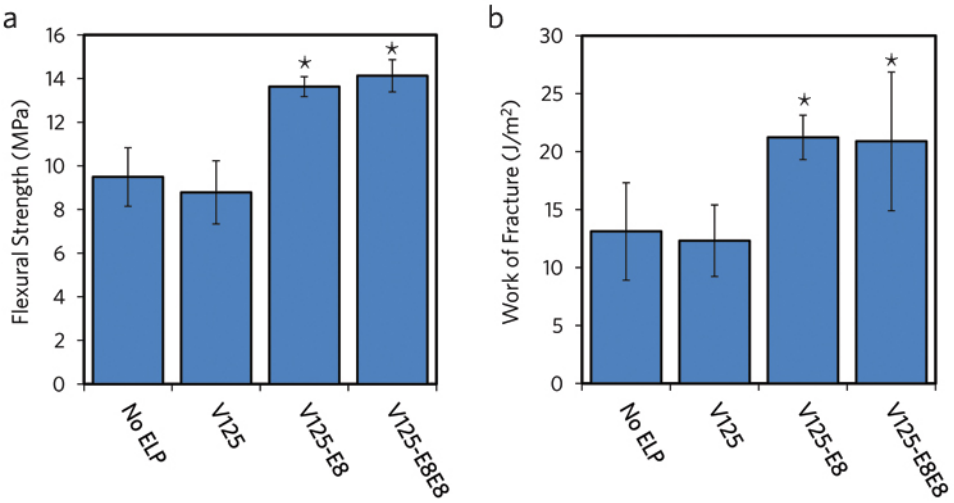

Figure 3-9. Three-point bending characterization. The flexural strength (a) and work of fracture (b) of V125-E8 and V125-E8E8 containing cements was improved compared to controls.

The uniformly charged ELPs were also tested as CPC additives. A 50:50 mixture of K125 and E125 was also tested in order to investigate the effect of electrostatic backbone-backbone interactions (Figure 3-1c). Using 10 wt% solutions, the use of V125, K125, E125, and 50:50 K125/E125 solutions did not change the suitable P/L ratio nor did they have statistically significant effects on the compressive strength of the resulting materials (Figure 3-7a). For V125 and K125 we can attribute this to the lack of significant interactions with the inorganic phase. Previously, polyanionic polymers such as alginate and polyacrylic acid were shown to alter CPC mechanical properties, presumably due to interactions between the polymers' carboxylic acid groups and calcium ions released during cement setting (*218, 243-245*). The lack of an effect from the addition of E125 may be due to its lower charge density or weaker HAP binding ability compared to the previously used anionic polymers. 50:50 mixtures of E125 and K125 showed no effects despite the protein-protein and protein-ion interactions available to these proteins suggested by the transition temperature experiments. The lack of strong interactions with HAP may have prevented those energy dissipating bonds from actively playing a role in altering the mechanical properties. For each of these ELP-CPC composites, we cannot rule out that the mineral to protein ratio was not optimal. There should be an ideal quantity of polymeric additive to yield the best properties (*211*). Previous studies showed that only certain inorganic to organic ratios yielded strength improvements, after which there were decreases in performance (*219*). These results show that ELP incorporation provides sequence-dependent mechanical property improvements to CPCs under multiple loading modes. Based on these results, future work can combine ELPs with other additives to further improve the mechanical properties (*246*).

3.4.5 Injectability and Washout Resistance of ELP-CPC Composites

We demonstrated that incorporation of V125-E8 allowed for formation of an injectable CPC-based bone composite with increased stability in fluids. Because of the aforementioned fluidity of CPCs containing E8 elastins, mixtures of CPC particles and V125-E8 could be injected through a 16 gauge

needle, even at a P/L ratio of 4:1 (Figure 3-10). The injectability of CPCs is important for minimally invasive techniques such as vertebroplasty and for implantation sites that are poorly accessible or narrow (*247*).

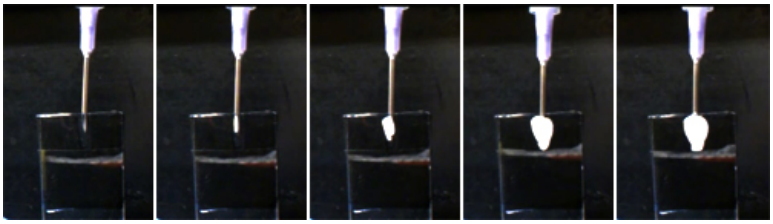

Figure 3-10. ELP-CPC injectability. Selected frames of a video demonstrating that the plasticizing effect of V125-E8 allows the CPC mixtures to be injected into molds.

Washout tests qualitatively determine the stability of cements by immersing them in solutions and visualizing the loss of material to the surrounding solution. In clinical practice, the washout of material can be medically hazardous and limits the utility of injectable formulas (*248*). When E8 containing cements reached physiological temperatures, they became cohesive putties due to the ELPs' inverse temperature transitions. The effect of this cohesiveness was readily apparent in washout tests. An E8-containing cement remained as a single mass when placed into a physiological buffer whereas control cements disintegrated (Figure 3-11). Therefore, the thermoresponsive cohesiveness observed in our cements is promising for surgical applications as it allows for highly injectable and washout resistant, cements.

Figure 3-11. Washout test on ELP-CPC composites. After mixing, cements were immediately immersed in 37 °C HEPES buffer. CPCs without ELP (left) were unstable and disintegrated while the E8-ELP containing mixtures remained as cohesive masses.

3.5 Conclusion

We designed biomimetic ELPs in order to fabricate novel bionanocomposite materials. We characterized their protein-protein interactions, protein-ion interactions, HAP binding abilities, and mechanical properties in the form of ELP-CPC composites. This study demonstrates the flexibility and power of using genetically engineered proteins as tools for studying sequence-property relationships of

nanocomposite materials. By imparting ELPs with varying modes of inter/intra molecular bonding and interfacial bonding we were able to demonstrate sequence specific property changes in ELP-HAP mixtures. Our results showed that interfacial binding to HAP through octaglutamic acid motifs was critical for imparting functionalities such as nanoparticle dispersion and mechanical property improvements. In the absence of binding, the physical properties of the protein had no effects. Using our genetic engineering method we can further explore the relationship between polymer structure and composite properties by changing and combining factors such as binding motif length, the motif itself, and molecular weight. New backbone-backbone interactions can be explored using other PBP backbone motifs or through the incorporation of known peptide-based associative or folded domains (*163, 249-251*). Meanwhile, genetic insertion of bioactive motifs (*252*) and incorporation into other bone-composite fabrication techniques (*253*) will expand the ELP's functionality. Furthermore, ELPs appear suitable for determining sequence-property relationships in more fundamental studies on biomineralization or in single-molecule force spectroscopy experiments (*121, 210, 253, 254*). We believe that our results are not limited to applications involving HAP; they can be expanded to explore composites with other nanoparticles. Through further iterative, rational design and combination with methods for synthesizing organized architectures, our approach may yield strong and tough materials for future load-bearing applications (*41, 198*).

3.6 Materials and Methods

Nomenclature: The ELP backbones were composed of repeating sequences of the form $[(VPGVG)_2VPGXG(VPGVG)_2]_n$ where X was either valine (V) glutamate (E), or lysine (K). The backbones were named after the one letter amino acid code corresponding to the X position followed by the number of elastin-like pentapeptides in the sequence. Functional protein terminal sequences were indicated by the addition of a descriptor to the protein's name (i.e., E8).

Genetic engineering: Cloning was performed in XL-1 Blue *E. coli* (Agilent Technologies) and constructed genes were confirmed by DNA sequencing (UC Berkeley DNA Sequencing Facility) using the same sequencing primers as listed in Table 2-1. Synthetic oligonucleotides (oligos) were used for construction of the monomers V5, E5, and K5. (Appendix Table A-1). Unlike the original K25 monomer sequence described in Chapter 2, the monomer DNA sequences were designed to completely avoid using any uncommon *E. Coli* codons. All oligos were first phosphorylated in 1X T4 DNA ligase buffer with T4 polynucleotide kinase (10 units) in 20 μL reactions (6 μM oligo concentrations, 37°C, 40 minutes). For V5, two pairs of complementary phosphorylated oligonucleotides were annealed separately (V5L-F/V5L-R and V5R-F/V5R-R). For E5 and K5, four pairs of complementary, phosphorylated oligonucleotides were annealed separately (Figure 3-12a-b). Annealing was performed by mixing the 20 μL phosphorylation reactions of complementary oligos. The mixtures were then heated to 95 °C and allowed to gradually return to room temperature over the course of several hours. The oligos were designed such that each annealed product corresponded to the first or second half of a monomer sequence. The two halves could be joined by complementary sticky ends. The annealed products were ligated into the K25 vector (Chapter 2) that had been prepared by reaction with BamHI and Eco31I (V5) or BpiI and Eco31I (E5, K5) and dephosphorylation with Antarctic Phosphatase. For E5 and K5, various length concatemers composed of combinations of the four possible monomer DNA sequences

were formed (Figure 3-12c-d). Four possible monomer sequences were synthesized in order to reduce the DNA sequence repetitiveness. Gene multimerization then proceeded as described in Chapter 2 up to a length of 125 pentapeptides.

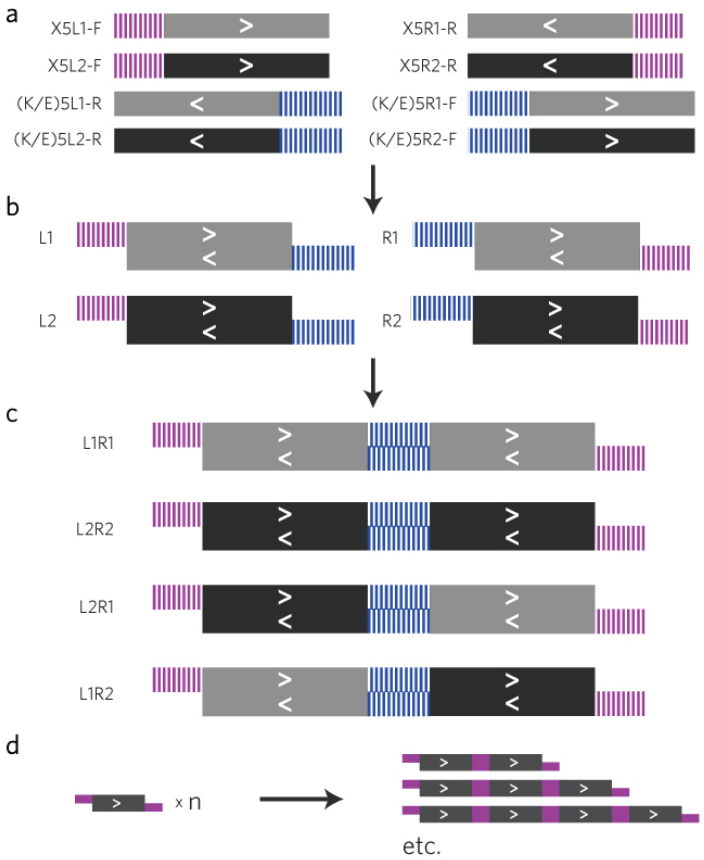

Figure 3-12. Schematic of E*n* and K*n* gene construction. (a) Schematic of eight oligonucleotides needed for gene construction. Arrows point from the 5′ end to the 3′ end. Corresponding shades are complementary. Dashed regions are sticky ends. (b) Complementary oligonucleotides are first annealed separately. (c) The annealed oligonucleotides are combined to create four possible monomer DNA sequences that all code for the same amino acid sequence. (d) Each product from (b) can combine together to generate multimers. Arrow indicates the coding sequence direction.

---

pET28b expression vectors were prepared by insertion of oligos coding for N-terminal and C-terminal cassettes. The terminal sequences flanked two Eco31I sites. The oligos were phosphorylated, annealed then ligated into pET28b plasmids that had been prepared by NcoI and BamHI digestion (Table 3-4, Figure 3-13).

Table 3-3. List of oligonucleotides used to prepare terminal sequence vectors

Oligo	Oligo Sequence (5′ to 3′)	Terminal Sequence
N-F	CATGAGCGGCGTTGGCGTCCTGAGACC	MSGVG
N-R	GTGACCAGTGGGTCTCAGGACGCCAACGCCGCT	
C-F	CACTGGTCACGGTCTCGGTCCCGGGTTAATAA	VPG--
C-R	GATCTTATTAACCCGGGACCGAGACC	
NE8-F	CATGAGCGAAGAGGAAGAAGAGGAAGAAGAAGGCCC GGGTGTCCTGAGACC	MSEEEEEEEEGPG
NE8-R	GTGACCAGTGGGTCTCAGGACACCCGGGCCTTCTTC TTCCTCTTCTTCCTCTTCGCT	
CE8-F	CACTGGTCACGGTCTCGGTCCCGGGTAGCGAAGAG GAAGAAGAGGAAGAAGAATAATAA	VPGSEEEEEEEE--
CE8-R	GATCTTATTATTCTTCTTCCTCTTCTTCCTCTTCGCTA CCCGGGACCGAGACC	

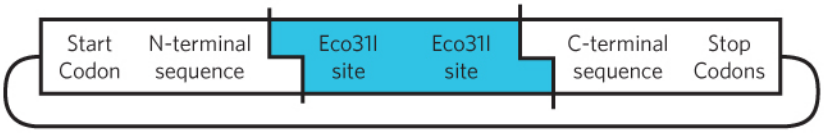

Figure 3-13. Schematic of a modified expression vector formed by insertion of a terminal sequence cassette into a pet28b vector. The desired N-terminal and C-terminal sequences flank two Eco31I sites that are later used as the insertion site for the ELP genes.

The V/E/K125 genes were liberated by BpiI and Eco31I digestion then ligated into the modified expression vectors that had been digested with Eco31I.

Protein Synthesis and Purification: The ELP plasmids were transformed into BLR(DE3) *E. Coli* for expression. ELP expression was performed in shake flasks of Terrific Broth supplemented with 30 μg/mL kanamycin with shaking at 225RPM, 37°C for 24 hours (*98*). The cells were isolated by centrifugation, resuspended in 10 mM Tris-Cl, 2 mM EDTA, pH 8.0 and lysed by probe sonication (10 seconds on, 25 seconds off, power level 7.5 for 3.5 minutes of on time) (Sonicator 3000, Misonix, Farmingdale, NY). The cell lysate was centrifuged at 30,000 x g for 30 minutes and the soluble fraction was mixed with poly(ethlyeneimine) (PEI M_w ~ 750,000) to form a 0.5% PEI solution. The PEI solution was centrifuged at 20,000 x g for 15 minutes and the supernatant was subjected to 3-4 rounds of inverse transition cycling for purification. NaCl or ammonium sulfate was used as the precipitating salt and resuspension was performed in phosphate buffered saline, pH 7.4, during each round (*255*). A modified method was used for purification of V125-E8E8. V125-E8E8 solutions were not treated with PEI. The solutions were instead adjusted to pH 4.2 with HCl to precipitate acid insoluble molecules. After

centrifugation at 20,000 x g for 15 minutes, the soluble fraction went through inverse transition cycling, but the protein pellet was resolubilized with 50 mM sodium citrate buffer, pH 4 rather than with phosphate buffered saline each round. The ITC-purified proteins were dialyzed into deionized water then lyophilized. MALDI-TOF MS was performed using a sinapinic acid matrix in a 30% acetonitrile, 0.1% TFA solution on an Applied Biosystems Voyager DE system.

Transition temperature measurements: ELP transition temperatures were measured using ELPs dissolved to a concentration of 10 mg/mL in 20 mM Tris-Cl, pH 7.4 with either 150 mM NaCl or 120 mM NaCl and 10 mM $CaCl_2$. 50 uL solutions of each ELP were placed in an MJ Mini thermocycler (Bio-Rad) and ramped up from 10 °C to 95 °C in 1° increments. At each temperature, the solutions were inspected for bulk solution turbidity. After the onset of turbidity, the temperature at which no further increases in turbidity were perceptible was designated as the transition temperature.

Hydroxyapatite binding assays: For HAP binding assays, each ELP was mixed with polycrystalline HAP particles (Alfa Aesar) to form 1.6 mg/mL ELP, 40 mg/mL HAP solutions in 20 mM Tris-Cl pH 7.4. The solutions were rotated end-over-end for 24 hours at room temperature. The soluble fraction was isolated after centrifugation at 10000 x g for 10 minutes. The concentration of ELP in the soluble fraction was determined using a bicinchoninic acid assay (Thermo-Scientific). Each protein was used to create its own standard curve.

Hydroxyapatite dispersion: For HAP dispersion assays, each ELP was mixed with nHAP crystals. The nHAP crystals were hydrothermally synthesized from a solution of linoleic acid, sodium linoleate, ethanol, $CaNO_3$ and Na_3PO_4. as previously described (7). They were washed thoroughly with several rounds of ethanol and 400 mM sodium phosphate, pH 9 solutions to remove the linoleic acid. 1.0 mg/mL solutions of nHAP in 20 mM Tris-Cl, pH 7.4 were bath sonicated for half an hour. An equal volume of 2.0 mg/mL ELP solutions in the same buffer were then added to the nHAP solutions. The mixtures were sonicated for an additional 10 minutes then transferred to a tabletop for monitoring of sedimentation.

Calcium Phosphate Cement Synthesis: The components of the calcium phosphate cements (CPC) are tetracalcium phosphate (TTCP) and dicalcium phosphate anhydrous (DCPA). TTCP with an average particle size of ~15 μm was purchased (Ensail Beijing Co. Ltd). DCPA was synthesized from a solution of $CaCO_3$ and H_3PO_4 as previously described except the reaction time was extended to 24 hours (*256*). The DCPA and TTCP powders were thoroughly mixed at a 1:1 molar ratio. To fabricate cements, the powders were mixed in PTFE mixing bowls with ice-cold water or ELP-solutions at P/L weight ratios ranging from 3:1 to 4.25:1. Washout tests were performed by hand molding the cements into spheres and immediately immersing them into a simulated physiological solution (1.15 mM $CaCl_2$, 1.2 mM Na_2HPO_4, 133 mM NaCl, 50 mM HEPES, pH 7.4)) at 37 °C (*215*). Injection testing was performed by immediately placing the CPC mixtures into a chilled syringe with an attached 16 gauge needle.

Mechanical Testing of ELP-CPC composites: The CPC mixtures were formed into cylinders 3 mm in diameter and 6 mm in height using stainless steel molds for compression testing or into bars 1.5 mm in height, 2 mm in width and 25 mm in length using PTFE molds for 3-point bending tests. The mixtures

were molded by hand with the aid of the blunt end of a 7/64 inch drill bit. The ends of the molds were covered with glass slides then placed into a 37 °C, 100% relative humidity chamber for 20 hours. The specimens were removed from their molds after 20 hours and immersed in the simulated physiological solution at 37 °C for four hours prior to mechanical testing. Testing was performed on an Instron model 5544 mechanical testing machine. Samples dimensions were measured by digital calipers. All tests were performed immediately after being removed from solution. For compression tests, a crosshead speed of 1 mm/min was used. For 3-point bending tests, a 20 mm span and 0.5 mm/min crosshead speed were used. Work-of-fracture for 3-point bending samples was calculated as the area under the load-displacement curve divided by the specimen's cross-sectional area (*215*). Six or more, and five or more samples of each ELP-CPC mixture were tested for compression and bending tests, respectively. Statistical analysis was performed using one-way ANOVA and Tukey's Honestly Significant Difference Test.

Microstructural Analysis: Immediately after mechanical testing, the CPC samples were immersed in ethanol to halt the setting reaction then dried in a 50 °C oven. The fracture surfaces of selected samples were sputter coated with gold and visualized using a scanning electron microscope (Hitachi S5000).

Chapter 4: Remote Activation of Stimuli-Responsive Graphene-ELP Hybrid Nanoparticles and Composite Hydrogels

4.1 Abstract

This chapter describes the development of stimuli-responsive hybrids of elastin-like polypeptides (ELPs) and graphene-derived nanoparticles. Hybrid particles formed by adsorption of ELPs to graphene oxide and reduced-graphene oxide were thermoresponsive, pH responsive, and near-infrared (IR) light responsive. Additional rationally engineered ELPs were designed to simultaneously adsorb to graphene-coated surfaces and to mediate cell binding and spreading. Finally, ELP-graphene hybrids were incorporated into ELP hydrogels. The nanocomposite hydrogels exhibited rapid, site-specific near-IR responsive bending actuation.

4.2 Introduction

4.2.1 External Field-Responsive Nanomaterials

Smart materials that can respond to external fields are particularly attractive for biomedical applications. This is because it is often infeasible or impractical to use other stimuli (e.g., pH, temperature, ionic strength, or solvent changes) without harming cells and biomolecules, especially in vivo. In addition, many external fields can be rapidly applied and removed with good spatial and temporal resolution and in non-invasive or minimally-invasive manners. Certain nanoparticles naturally respond to magnetic fields, electric fields, radiofrequency waves, or light. Exposure to these stimuli can generate force, heat, current, or luminescence. The external field-responsiveness of nanoparticles has already proven useful for creating shape-memory materials, actuators, electronics, and therapeutics (*10, 257-259*).

4.2.2 Graphene-Derived Materials

In the last decade, graphene and its derivatives have emerged as potentially useful stimuli-responsive nanomaterials. Pristine graphene is a two-dimensional sheet of sp^2-hybridized carbons that exhibits exceptional mechanical, thermal, electronic, and optical properties (*260-263*). Single-layer graphene sheets can be synthesized by chemical vapor deposition or by direct exfoliation from graphite (*264, 265*). However, these methods are generally insufficient for applications that require solution-processability, cost-effectiveness, and bulk-scale quantities. For those applications, the graphene-derived nanosheets (GNs), graphene oxide (GO) and reduced graphene oxide (rGO), are often utilized (*266-268*). GO is synthesized by the oxidation and subsequent exfoliation of graphite. The oxidation process introduces various defects and hydrophilic functional groups to the faces of each graphite sheet (e.g., hydroxyls and carboxylic acids). The oxidation process makes the graphite dispersable down to individual layers in low ionic strength aqueous solutions, but the sheets are non-conductive (*269*). rGO is synthesized by reduction of the functional groups on GO sheets. Reduction partially restores the conjugated carbon network to a more graphene-like state and renders rGO sheets conductive but poorly dispersable. Despite their limitations, GNs have been integrated into sensors, electronics, catalysts, and

composites (*269-273*). They have also been used for biotechnology in the development of therapeutics, imaging agents, biosensors, and bionanocomposites (*274-276*).

4.2.3 GO and rGO as Stimuli-Responsive Materials

The stimuli-responsive properties of GNs have been exploited in various studies. Park et al. demonstrated that GO is humidity responsive. They created a bilayer film that curled when the humidity was increased due to preferential swelling of the more hydrophilic GO layer (*277*). Meanwhile, the conductivity of rGO has been utilized to create thin film electromechanical actuators (*278, 279*). In these systems, the application of a current through an rGO layer generated heat, which expanded a neighboring polymer layer and resulted in bending. An exciting property of both GO and rGO is there light-responsiveness. Both GNs are able to generate heat when illuminated with near-IR light. This phenomenon has been exploited to generate photothermal therapeutic agents that can locally kill cells with heat (*274, 280*). For example, Robinson et al. conjugated polyethylene glycol chains to rGO particles. They then conjugated the RGD integrin-binding peptide to the PEG chains to promote tumor targeting (*280*). The GNs' photothermal responses have also been used to remotely initiate a shape-memory response in thermoplastic polyurethane, to actuate bilayer films, and to shrink hydrogels made of PNIPAM by inducing volume phase-transitions (*281-284*).

4.2.4 Methods to Functionalize GO and rGO Colloids

An issue that must constantly be addressed when using GNs is their poor colloidal stability. Unmodified GNs are extremely prone to aggregation due to strong intersheet attraction (*285-288*). Aggregation is particularly problematic in biological systems where the ionic strength cannot be lowered to favor colloidal stability. GNs have been chemically derivatized and functionalized with small molecules and polymers (covalently or non-covalently) to help prevent aggregation in aqueous or organic solvents (*289-294*). In most cases, the functionalization served no other purpose than to passively help disperse the GNs. The modifications also introduced little to no biological activity unless further modifications steps were taken (*280*). Natural biomolecules, such as nucleic acids, polysaccharides, amino acids, and natural proteins, have also been used to modify GN surfaces (*276, 295-304*). The intrinsic bioactivity of some of these molecules may introduce additional functionalities. However, tuning the physical properties of natural biomolecules is more difficult than with synthetic molecules. Amongst the strategies for GN functionalization, non-covalent modification with polymers presents certain advantages. It does not require additional chemical processing and purification steps and does not further disrupt the GNs' conjugated structures (*305*). The polymer chains can also provide tunable stimuli-responsive and biological capabilities.

4.3 Overview of this Study

GNs have great potential as biomaterials, but relatively few advances have been made in that direction. One hurdle to further development is the lack of convenient, tunable methods for functionalizing GNs with active biomolecules. Here we describe the synthesis of stimuli-responsive ELPs that can non-covalently bind to GO and rGO (Figure 4-1a). We also demonstrate how the

responsiveness of GNs and ELPs can be combined to generate behaviors such as light-induced aggregation and actuation for the first time in a protein-based system (Figure 4-1b,c).

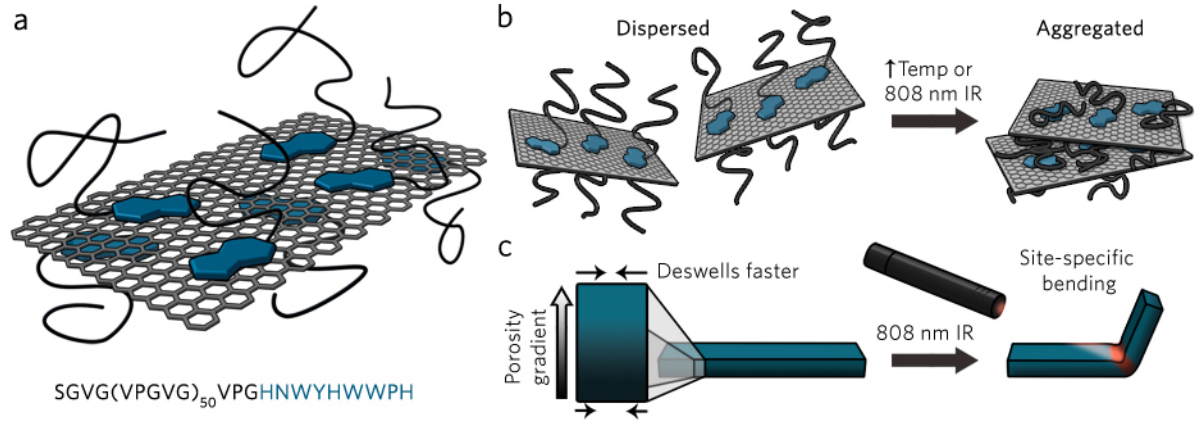

Figure 4-1. Schematic of ELP-GN hybrids. (a) ELPs engineered with graphene binding motifs bind to the surface of GNs. (b) The ELP-GN hybrids are well dispersed below their T_t but can be reversibly aggregated by increases in temperature or by near-IR illumination. (c) A GN-ELP composite hydrogel can be synthesized with a porosity gradient through its thickness. This hydrogel bends when illuminated by near-IR light.

4.4 Results and Discussion

4.4.1 Graphene-Binding ELP Synthesis

We first fused a GN-binding (GB) peptide sequence onto ELP sequences using genetic engineering (Figure 4-1a). The GB peptide (HNWYHWWPH) was derived from phage display against carbon nanotubes and had not previously been characterized against GNs (*110, 306*). We presumed that the GB peptide would be able to bind to GNs through π-π stacking interactions because it is enriched with aromatic amino acid residues. After initiating this study, phage display sequence results against graphite were published by other groups. Those sequences were not enriched with aromatic residues, but instead with methionines, histidines, and glutamines. However, the reason for this compositional difference and the relative affinities of the peptides to GNs is currently unknown (*307, 308*). The GB peptide was first fused to one or both termini of the neutral ELP backbone, $(VPGVG)_{50}$. The resulting expressed sequence for the GN-binding elastins (V50-GB and V50-GBGB) and the sequence of a control ELP (V50) can be found in Table 4-1. The ELP genes were expressed in *E. Coli* and typically yielded more than 100 milligrams of product per liter of culture. The ELPs' molecular weights were confirmed by mass spectrometry to be within 0.5% of their theoretical molecular weights (Figure 4-2). Each ELP's transition temperature (T_t) was also measured (Figure 4-3). The hydrophobic GB motif greatly decreased the T_t of the ELPs to which they were fused. This phenomenon is consistent with the effect seen when the X residues of VPGXG motifs were replaced with hydrophobic amino acids (*70*).

Table 4-1. ELP sequences used in this study.

Identifier	Sequence
V50	MSGVG$(VPGVG)_{50}$VPG
V50-GB	MSGVG$(VPGVG)_{50}$VPGHNWYHWWPH
V50-GBGB	MSHNWYHWWPHGPG$(VPGVG)_{50}$VPGHNWYHWWPH
V40-GB	MSGVG$(VPGVG)_{40}$VPGHNWYHWWPH
V40-RGDGB	MSGRGDSG$(VPGVG)_{40}$VPGHNWYHWWPH
E125	MSGVG$[(VPGVG)_2$VPGEG$(VPGVG)_2]_{25}$VPG
K50-GB	MSGVG$[(VPGVG)_2$VPGKG$(VPGVG)_2]_{10}$VPGHNWYHWWPH
V50-CK1	MSGVG$(VPGVG)_{50}$VPGKG

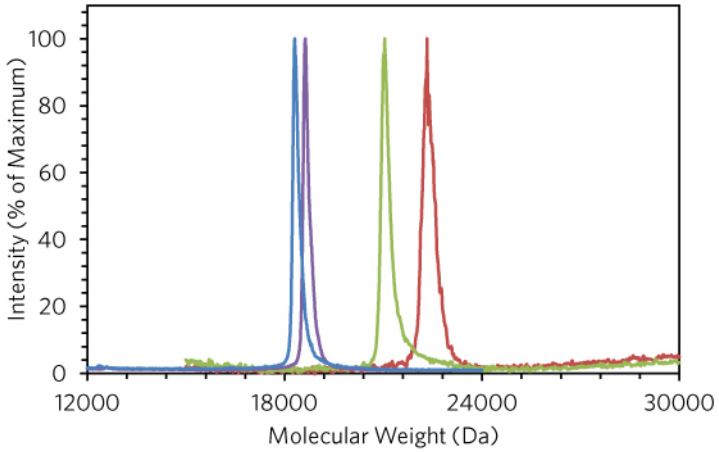

Figure 4-2. Molecular weight characterization of ELPs. From left peak to right peak with observed and theoretical molecular weights in parenthesis: V40-GB (18.3 kDa, 18.3kDa), V40-RGDGB (18.6 kDa, 18.6 kDa), V50 (21.0 kDa, 21.0 kDa), and V50-GB (22.3 kDa, 22.4 kDa).

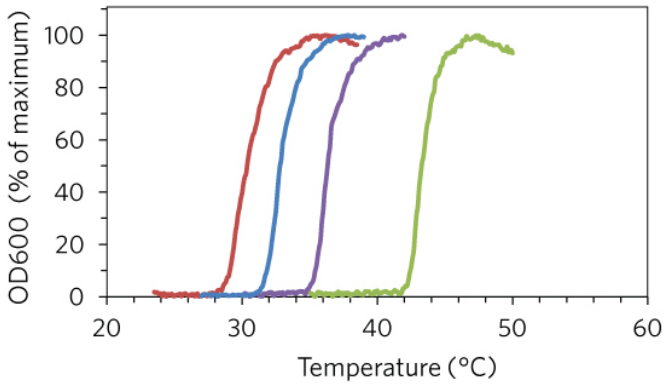

Figure 4-3. Transition temperature measurements of the ELPs used in this study. From left to right: V50-GB (29.4 °C), V40-GB (32.6 °C), V40-RGDGB (36.3 °C), and V50 (42.7 °C).

The strategy we adopted has certain advantages over other GN functionalization strategies. One advantage is that the GB peptides are synthesized along with the ELP backbone in one step. In contrast, synthetic GN-binding groups such as pyrene and solid-phase synthesized peptides would need to be conjugated to polymer chains in an additional step (*309-311*). An additional advantage compared with other biopolymers is that binding is preferentially directed to a specific part of the ELP backbone. Previous biopolymers (e.g., DNA, proteins) adsorbed to GNs, but there was no indication of which regions were bound or if the same region was always responsible for binding (*276, 304, 312, 313*). This can make it difficult to utilize other positions on the protein backbone for additional functions. An exception is hydrophobin, a natural protein that has a well-defined hydrophobic patch that can bind to graphene (*303*). However, the GB peptide is more than five times smaller than hydrophobin and likely does not require the maintenance of a folded structure like hydrophobin does.

4.4.2 Binding of ELPs to GNs

The behaviors of the engineered ELPs were first investigated by mixing them with GO and rGO solutions. Addition of V50-GB to GO solutions made the solutions slightly cloudy, but no sedimentation was observed. There were no additional observable effects for V50 and V50-GB containing solutions. Aggregation occurred when V50-GBGB was added to GN solutions. Therefore, it was excluded from further investigations. We suspect that the second GB motif may have led to bridging between GN sheets or to the formation of loops on the same sheet.

We then analyzed the binding of V50 and V50-GB to the GNs by atomic force microscopy (AFM) (Figure 4-4). AFM images confirmed that the GN sheets were exfoliated down to single layers (Figure 4-4a,c). No change was observed when we attempted to bind V50 to GO sheets (Figure 4-4b). When V50-GB was used, there was a clear height increase of ~1 nm across all of the sheets measured (Figure 4-4c). The height change was more pronounced (~3 nm increase) when rGO sheets were treated with V50-GB (Figure 4-4f). A height increase of ~1 nm was also observed when rGO was treated with V50. Based on the AFM analysis, we can conclude that the GB peptide promoted binding of ELPs to both GO and rGO. The larger height increase observed for V50-GB-rGO mixtures was consistent with the fact that rGO has more aromatic, hydrophobic areas available for binding compared with GO. The AFM images also indicate that non-specific physisorption of ELPs to rGO occurs in the absence of GB motifs. This likely occurs due to the high percentage of non-polar aliphatic groups on V50 and is consistent with a previous study which showed that a poly(VPAVG) sequence could non-specifically adsorb to hydrophobic polymer surfaces (*100*). Future studies might reduce non-specific binding by introducing more polar amino acids into the ELP backbone.

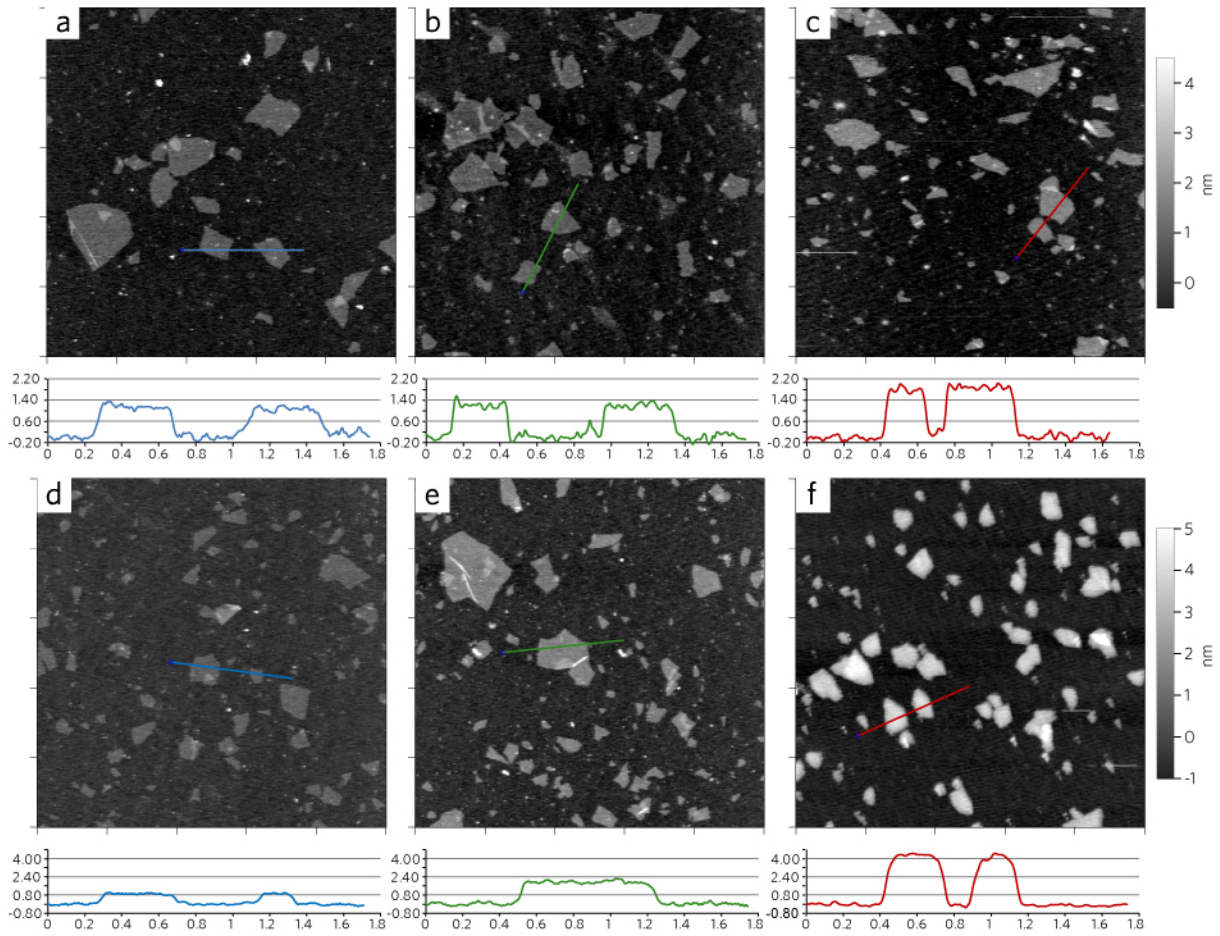

Figure 4-4. AFM images and height profiles of ELP binding to GNs. (a) GO sheets. (b) GO sheets dipped in V50. (c) GO sheets dipped in V50-GB. (d) rGO sheets. (e) rGO sheets dipped in V50. (f) rGO sheets dipped in V50-GB. All images are 5 μm x 5 μm.

The binding of V50-GB to the GNs was quantitated. Despite the stark difference observed in the AFM images, the amount of V50-GB that GO sheets bound (~5 times their mass) was not drastically different from the amount that rGO sheets bound (~6 times their mass) based on our results. (Figure 4-5). It may be possible that the ELP backbone of V50-GB non-specifically adsorbed to rGO surfaces and inhibited binding of additional ELP chains.

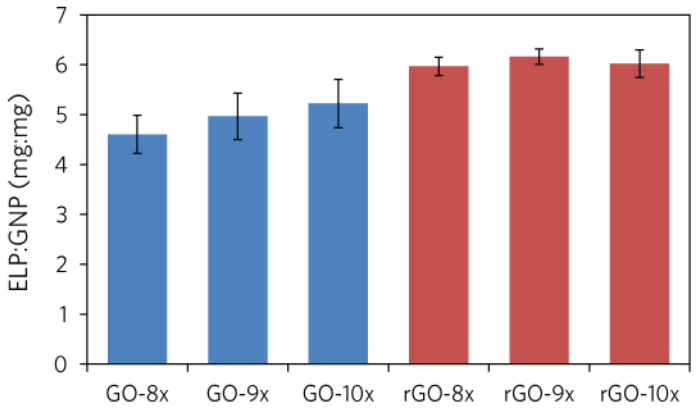

Figure 4-5. Binding of V50-GB to GO and rGO. V50-GB was added at eight, nine, or ten times the mass of GO or rGO in solution. The amount of unbound ELP was measured to determine the amount of ELP that was bound. The mass ratio of bound ELP to GN was not statistically different for the three conditions tested. This suggests that the GNs were saturated at all ELP concentrations.

The effects of ELP binding were clearly observed when we analyzed the colloidal stability of ELP-GN solutions. As can be seen in Table 4-2, the stability of GN dispersions against salt was significantly increased when V50-GB was added at a 6:1 ELP to GN weight ratio. Colloidal solutions of non-functionalized rGO aggregate at acidic pH values because rGO's ionizable groups are no longer able to provide electrostatic repulsive forces (*285*). On the other hand, V50-GB functionalized rGO was protected against pH-induced aggregation. The results of the colloidal stability tests using V50-GB indicate that it provided steric repulsive forces to prevent aggregation. The GB peptide's roles were to promote the formation of a brush-like layer of ELP chains and to anchor the ELPs strongly enough to prevent displacement by other GN sheets. Therefore, V50-GB behaved as a macromolecular surfactant. Meanwhile, V50 had only mild effects on colloidal stability. Interestingly, V50 had a slight protective effect on GO dispersions despite there being no evidence of binding between the two. Because the AFM analysis indicated that non-specific ELP adsorption could occur on rGO sheets, we also began to test the negatively charged ELP, E125. It had a slightly improved protective effect compared to V50. This is likely because E125's charged residues bolstered the electrostatic repulsion between sheets. Based on these results, we believe that ELPs, especially those with GB peptides, can be used to stabilize GN colloids in vivo as an alternative to the PEG chains that have been used ubiquitously in other studies (*280, 293, 314*). One caveat is that we performed our tests at 4 °C to avoid observing inverse temperature transitions (ITTs). In order to truly function in vivo, new ELPs with higher transition temperatures will need to be engineered. The improved colloidal stability of E125-rGO mixtures suggest that introducing glutamates to V50-GB would be a good strategy that could potentially raise the T_t and also provide increased repulsive forces.

Table 4-2. Maximum ionic strength or lowest pH before aggregation.

	GO	GO+V50	GO+V50-GB	
Maximum [NaCl] before aggregation	< 25 mM	At least 25 mM, less than 50 mM	At least 1.0 M	
	rGO	**rGO+V50**	**rGO+V50-GB**	**rGO+E125**
Maximum [NaCl] before aggregation	< 12.5 mM	At least 50mM, less than 100 mM	At least 1.0 M	At least 100 mM , less than 150 mM
Lowest pH before aggregation	7	6	Not observed	5

The ability of the V50-GB to function in organic solvents was also tested. Dimethyl sulfoxide (DMSO), N-N-dimethylformamide (DMF), and N-methyl-2-pyrrolidone (NMP) are good solvents for ELPs. However, there are conflicting reports as to whether or not graphite oxide can be exfoliated in NMP and DMF (*287, 288*). We were unable to directly disperse freeze-dried graphite oxide or rGO in any of these solvents. However, we were able to disperse V50-GB-GN hybrids into each of these solvents at relatively high GN concentrations (1 mg/mL) (Figure 4-6). Dispersing GNs in organic solvents is important because it allows GNs to be incorporated into polymers that cannot be processed in water (*290*).

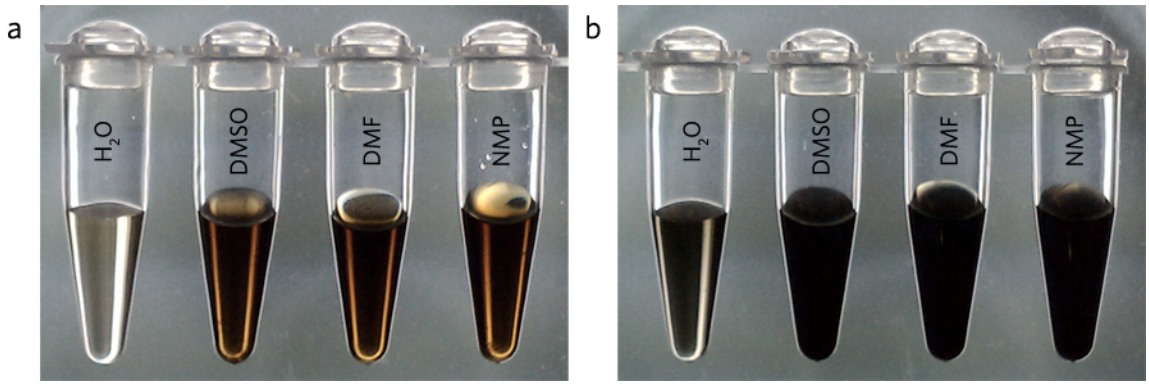

Figure 4-6. Transfer of ELP-GN hybrids into organic solvents. (a) V50-GB-GO hybrids at a GO concentration of 0.1 mg/mL in water and at a GO concentration of 1.0 mg/mL in DMSO, DMF, and NMP. (b) V50-GB-rGO hybrids in the same conditions.

4.4.3 Stimuli-Responsive Behavior of ELP-GN hybrids

Polymer-coated nanoparticles have been shown to exhibit the same stimuli-responsiveness as their polymer coatings. As examples, ELP-coated gold nanoparticles could be aggregated by inducing the ELP's ITT and PNIPAM-coated graphene could be aggregated by inducing PNIPAM's LCST transition (*234, 315*). Therefore, we continued our analysis of ELP-GN hybrids by testing their stimuli-responsiveness. V50-GO mixtures showed no response to heating other than the independent aggregation of the ELP (Fig 4-7a) V50-rGO mixtures, on the other hand, did show reversible thermoresponsive aggregation (Fig 4-7c). Meanwhile, both GO and rGO solutions mixed with V50-GB

underwent thermoresponsive aggregation and dispersion when heated and cooled (Figure 4-7b,c). These results are consistent with the results from the AFM analysis. Future work may be able to adapt this behavior for sensor systems. For example, if a target was able to alter an ELP's transition temperature by binding or through an enzymatic reaction it could be detected visibly due to particle aggregation.

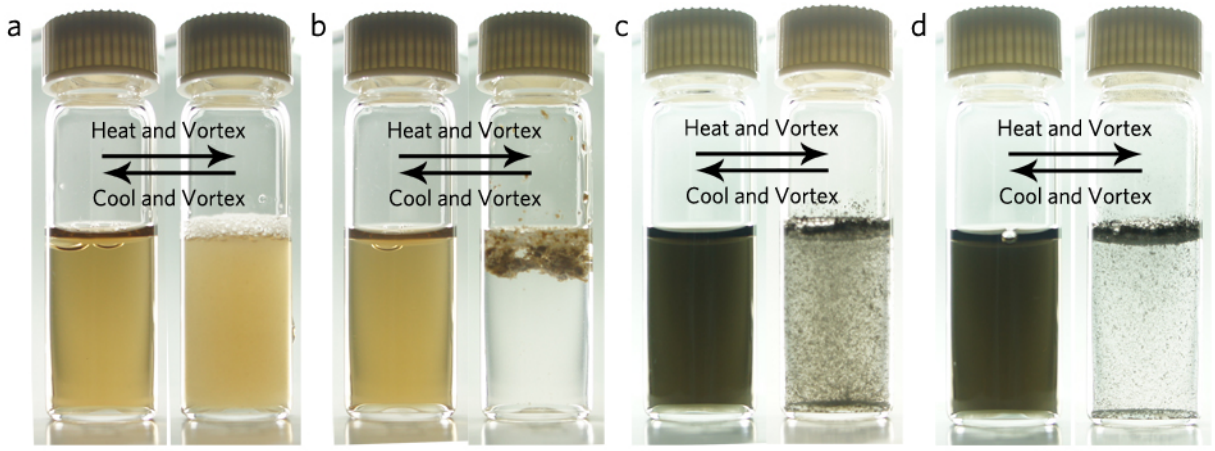

Figure 4-7. Thermoresponsive dispersion of ELP-GN hybrids. (a) GO + V50. (b) GO + V50-GB. (c) rGO + V50. (d) rGO + V50-GB.

We went on to demonstrate that thermoresponsive aggregation could be initiated remotely using near-IR light (Figure 4-1b). The progress of IR-induced aggregation can be seen for GO and rGO in Figure 4-8 and 4-9, respectively. In both cases, aggregation occurred at and above the laser spot site. Local heating at the laser spot site induced convective flow that caused particles to rise, while bringing new particles to the laser site, until the entire region above the laser spot was affected. In contrast, a carbon nanotube-thermoresponsive polymer hybrid irradiated by an IR laser showed aggregation only at the spot site (*316*). It is unknown why convection did not affect that system as it did ours. As mentioned previously, remote photothermal heating of GNs is a potential noninvasive treatment for tumors. In addition, local heating to induce an LCST transition or ITT was previously shown to improve the accumulation of PNIPAM-coated nanoparticles or freely soluble ELPs, respectively (*69, 317*). These results indicate that ELP-GN hybrids can be further engineered for photothermal therapy; the GNs would generate heat to kill cells and also induce the ITT to promote active accumulation of more GNs.

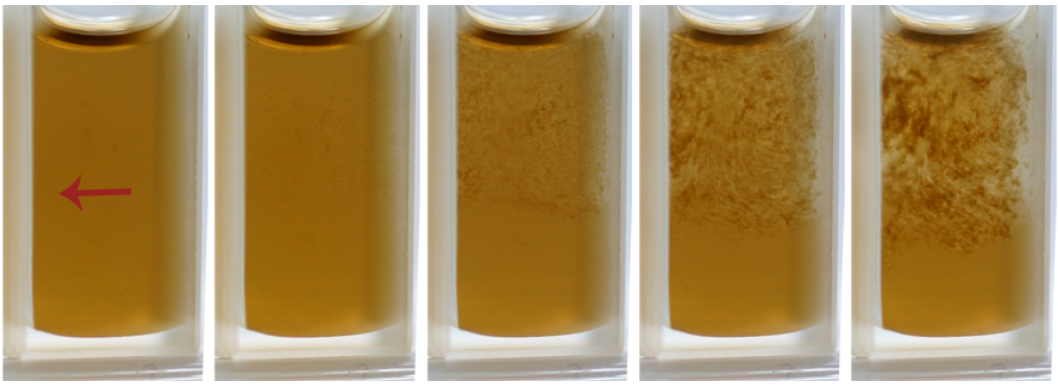

Figure 4-8. Near-IR induced aggregation of GO-V50-GB hybrids. Images are one minute apart starting one minute after the near-IR laser was turned on.

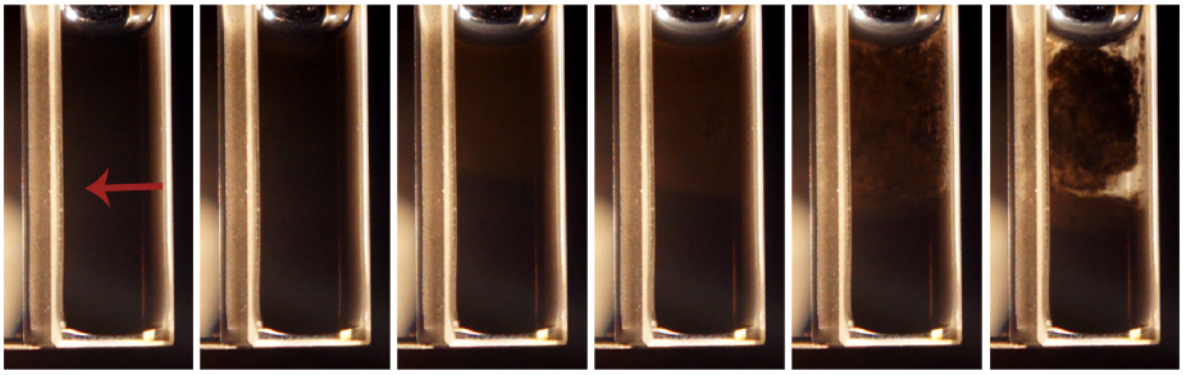

Figure 4-9. Near-IR induced aggregation of rGO-V50GB hybrids. Images are one minute apart starting at time zero.

We also demonstrated pH-responsive colloidal behavior. The hydrophilicity of E125 could be controlled by pH because the protein's glutamate residues are deprotonated at high pH and protonated at low pH. When we cycled the pH of E125-rGO mixtures from pH~9 to pH~4 and back, the GNs aggregated and then redispersed (Figure 4-10). This process was repeatable through several cycles. In the absence of E125, the acidification step led to irreversible rGO aggregation. This clearly demonstrates that pH-responsiveness can be genetically encoded into the ELP backbone.

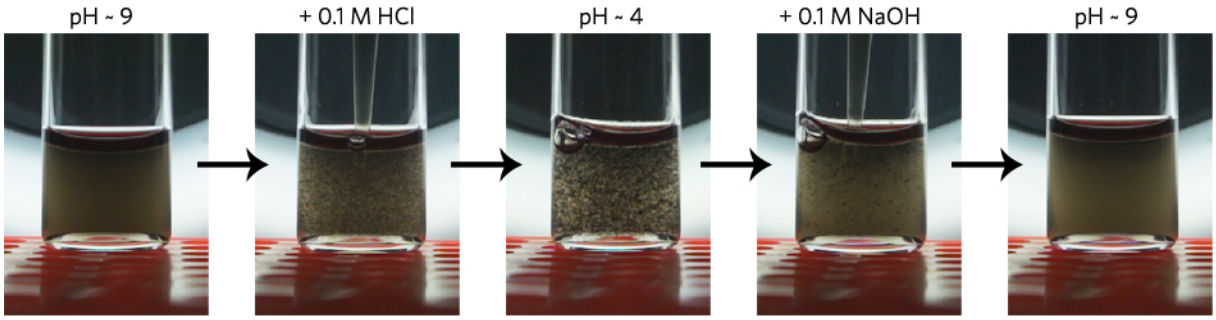

Figure 4-10. pH response of E125-modified rGO. Aggregation was induced by acidification then reversed by raising the pH back to basic.

4.4.4 Introduction of bioactivity

One of the greatest advantages of using a genetically engineered polymer is the ability to genetically introduce bioactive motifs rather than having to do it through chemical means (see Chapter 1). Genetic engineering also affords the opportunity to fine tune a polymer's physical properties. We demonstrated this versatility by genetically encoding an RGD motif onto the N-terminus of V40-GB to form V40-RGDGB (Table 4-1). The RGD peptide was incorporated on the opposite terminus from the GB peptide to ensure that it would be presented in an accessible manner, away from the rGO surface. The mass and transition temperatures of these ELPs were also determined and compared to the V50 ELPs (Figure 4-2, Figure 4-3). As expected, the shorter ELP chain had a higher T_t and the addition of the hydrophilic RGD peptide raised the T_t (*125*).

We tested the biofunctionality of the new ELPs by adsorbing them onto rGO surfaces then measuring the ability of these surfaces to promote the adhesion and spreading of a mouse pre-osteoblast cell line (MC3T3-E1 subclone 4) (Figure 4-11a). Both cell number and average cell area on V40-RGDGB treated surfaces were found to be significantly higher ($p < 0.05$) compared to V40-GB treated surfaces and statistically the same as untreated tissue culture polystyrene (TCPS) (Figure 4-11b-e). These results show that the ELPs can act as bifunctional linkers between rGO and cells. Modular addition to or replacement of the RGD group with other functional peptides can be carried out easily by further genetic engineering. This strategy can be used in lieu of the chemical conjugation, lengthy synthesis of bifunctional peptides, and surface chemistry modifications used in previous reports (*280, 307, 318*).

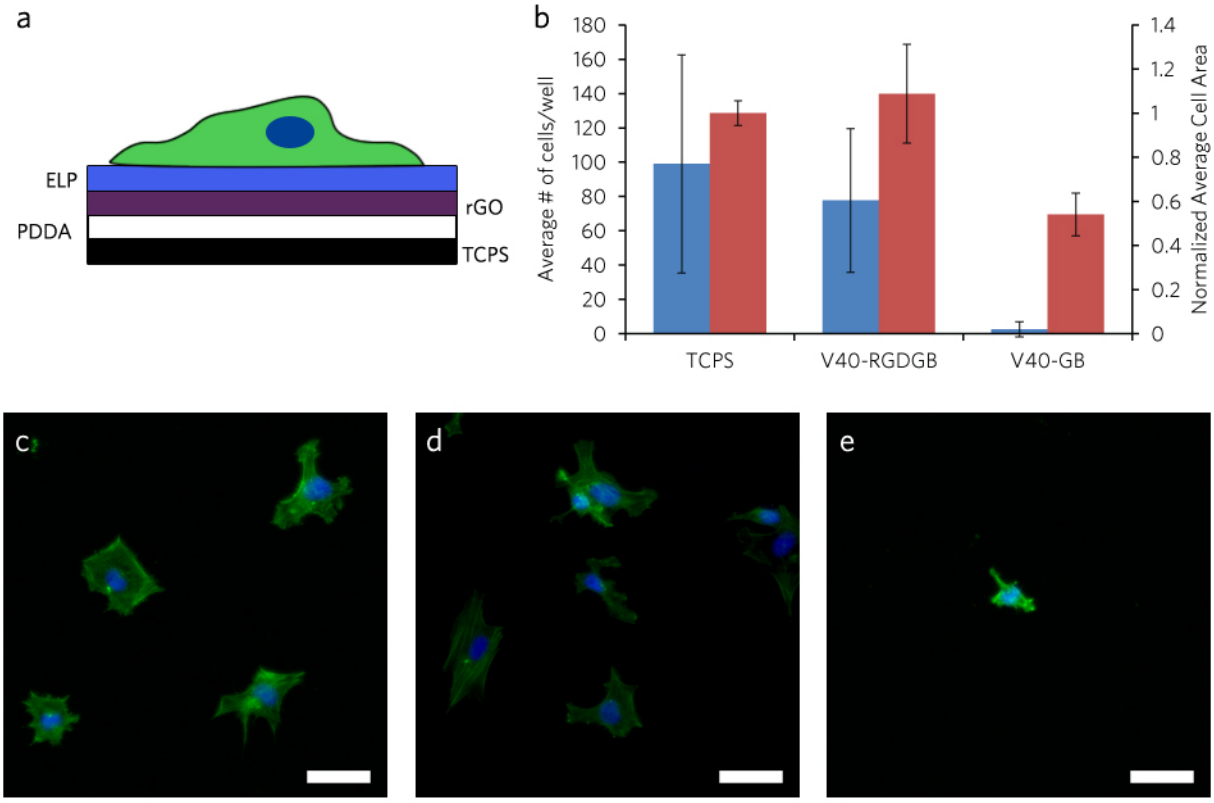

Figure 4-11. Cell adhesion and spreading on ELP-coated rGO. (a) Schematic of the layered structure that cells were grown on. Poly(diallyl dimethyl ammonium chloride) (PDDA) was used to coat TCPS substrates. rGO was then electrostatically adsorbed. Finally, V40-GB or V40-RGDGB was adsorbed to the rGO. (b) Average cell number per well (left bars) and average cell area (right bars). Fluorescent images of cells grown on (c) TCPS, (d) V40-RGDGB, and (e) V40-GB. Green: Actin labeled with fluorescein-phalloidin. Blue: Nuclei labeled with DAPI.

4.4.5 Synthesis of ELP-rGO Composite Hydrogels

We endeavored to encapsulate GNs into ELP hydrogels. GNs were initially mixed with K125, a polycationic ELP that can be crosslinked into hydrogels through its multiple free amines (*94, 319, 320*). Aggregation occurred immediately when they were mixed regardless of pH and mixing order (adding GN to K125 versus the opposite). We also attempted to use K50-GB, a polycationic ELP with a GB-peptide motif, but were met with the same results. In contrast, the polycationic polysaccharide, chitosan, was shown to successfully disperse GO (*295*). Chitosan has a higher charge density than the ELPs we tested. Therefore, we believe that the polycationic ELPs neutralized but did not reverse the surface charge of the GNs, which caused aggregation due to reduced electrostatic repulsion.

We designed an alternative crosslinking strategy that does not rely on polycationic ELPs. A four-arm polyethylene glycol crosslinker with N-hydroxysuccinimidyl (NHS) end groups (4-arm PEG-NHS) was combined with V50-CK1, an elastin designed to have one reactive primary amine at each terminal. Reaction of the NHS groups with the primary amines led to the formation of a hydrogel network where

every crosslinking site is separated by one V50-CK1 chain (Figure 4-12a,b). We adopted this strategy because hydrogels with the same network architecture were previously demonstrated to have superior mechanical properties compared to hydrogels created by conventional free-radical polymerization due to the uniform chain length between crosslinks (*321*). We then added V50-GB-functionalized rGO sheets as a third component of the crosslinking system (Figure 4-12a,c). Each V50-GB chain has a free N-terminal amine that can crosslink into the network. Thus, the rGO sheets behaved as multi-arm, physical crosslinkers. The gelation strategy successfully formed stable gels; there was no apparent particle loss when the gels were incubated in water or phosphate buffered saline (PBS).

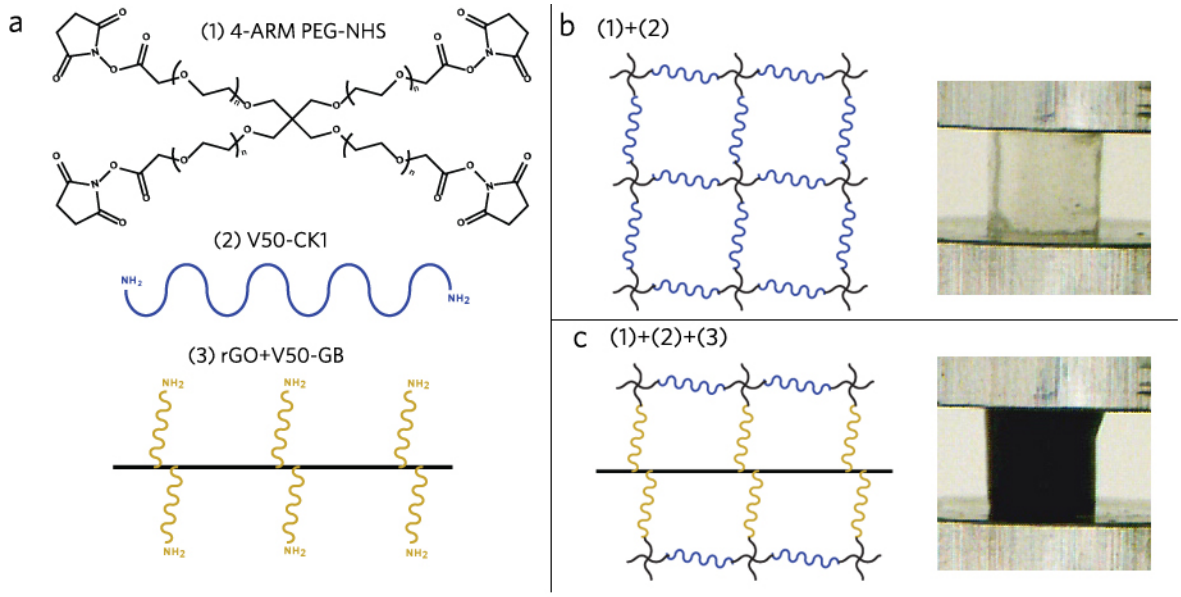

Figure 4-12. Crosslinking scheme. (a) Schematics of a 4-arm PEG-NHS crosslinker (1), the V50-CK1 bifunctional ELP (2), and a V50-GB functionalized rGO sheet (3). (b) Network formed by combining (1) and (2), and photograph of the resulting hydrogel (c) Network formed by incorporation of (3) and photograph of the resulting hydrogel.

4.4.6 Hydrogel Actuation

We utilized phase separation in order to generate ELP-rGO-based hydrogel actuators. Hydrogels made of ELPs are known to undergo temperature dependent swelling and deswelling processes in the same way as gels made of PNIPAM (*319*). Swelling and deswelling are dependent upon the diffusion of solvent into and out of the hydrogel network. Therefore, the rate at which thermoresponsive gels can change volume is dependent upon their dimensions. According to Tanaka and Fillmore, the shrinking rate is inversely proportional to the square of the gel's smallest spatial dimension (*322*). One method to increase the shrinking rate is to facilitate diffusion by making the gels more porous, and one method to increase porosity is to induce phase separation of the polymer from the solvent during hydrogel formation (*323*). The resulting hydrogels have polymer rich and polymer-depleted regions. Phase separation has been induced in PNIPAM systems by using mixed solvent systems (*324*). PNIPAM's LCST can decrease in mixed solvents due to cononsolvency effects, even

when PNIPAM is soluble in pure solutions of either solvent alone (*325*). Phase separation has also been observed when certain ELPs were crosslinked in water due to local occurrence of the ITT (*319*). This likely occurred because the T_t of crosslinked ELPs are significantly broader then the T_t of the same ELPs in solution (*326*). Therefore, ELPs are commonly crosslinked in organic solvents in which there is no ITT behavior (i.e., DMSO and DMF) in order to avoid phase separation (*319, 326*). No study has addressed the effects of phase separation on ELP swelling rates. Regardless, we suspected that it could be used to speed up swelling and deswelling of ELP hydrogels.

ELPs of constant composition shrink and expand relatively evenly with temperature (Figure 4-13a). This means that they can only behave as linear actuators. In order to generate bending actuators, we introduced a porosity gradient into ELP gels using a diffusion technique (Figure 4-13b). The nanocomposite hydrogel components were mixed in a 75% DMSO/25% DMF solution and molded into films ~0.5 mm in thickness. The top face of the films was left open to an environment of ~75% relative humidity. In this configuration, water was able to diffuse into the gel and preferentially induce phase separation near the exposed surface. In addition, water could hydrolyze the NHS groups on the crosslinker to reduce the crosslink density near the surface. The effect of this diffusion strategy on the morphology of the gel surfaces is seen in Figure 4-14. The vapor exposed surface (Figure 4-14a,b) had dramatically larger pores than the unexposed surface (Figure 4-14c,d).

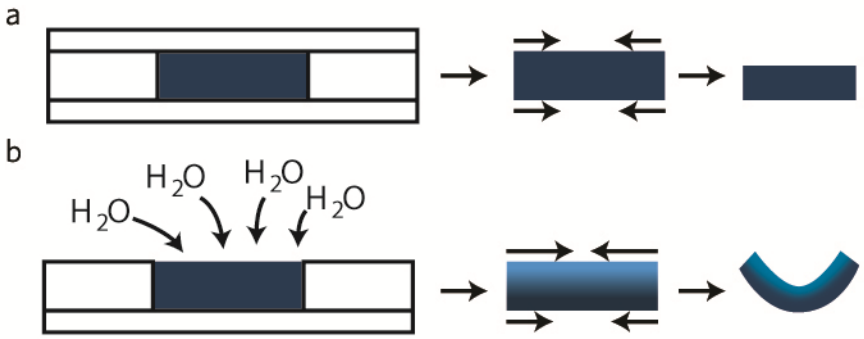

Figure 4-13. Actuation of homogenous gels and gradient gels. (a) Homogenous gels are crosslinked in closed cells. They shrink evenly upon heating. (b) Gradient gels are crosslinked with one face open to water vapor. Upon heating they shrink unevenly and bend.

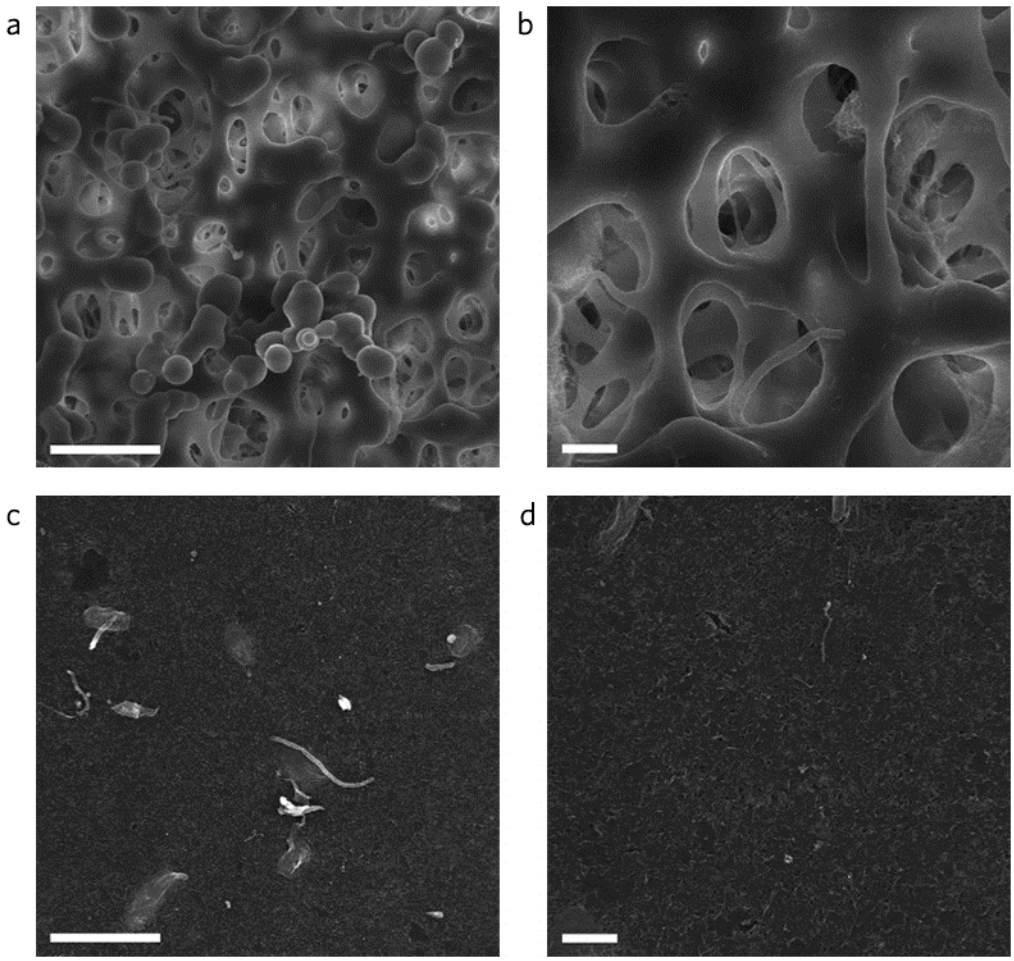

Figure 4-14. SEM analysis of gradient gels made with 0.8 mg/mL rGO. (a, b) Water vapor exposed surface. (c, d) Opposite surface. (a, c) Scale bars are 10 μm. (b, d) Scale bars are 2 μm.

When rectangular gradient films were placed in hot water, they immediately curled such that the exposed surface was on the inside (Figure 4-13b). This occurred because the vapor-exposed surface shrank much faster than the other side. The preferential shrinkage created a stress that caused the entire gel to curve. This is analogous to bilayer actuators except that only one material is needed (*327, 328*). A similar concept has been applied to photoresists that were given a crosslinking gradient through their thickness by control of UV light exposure (*329*). The gradient crosslinked photoresists curved in response to changes in solvent. Variable crosslinking has also been applied to create hydrogels that programmably folded into various shapes (*330*). These examples and our gradient gels demonstrate the ability of structural inhomogeneity to create complex behaviors.

Incorporating rGO into the gradient gels allowed us to bend the hydrogels remotely with near-IR light (Figure 4-1c). This technique provided much greater temporal and spatial control over the actuation of the hydrogels compared to changing the temperature of the entire solution. Local actuation is demonstrated in Figure 4-15 on the fingers of a hand-shaped hydrogel.

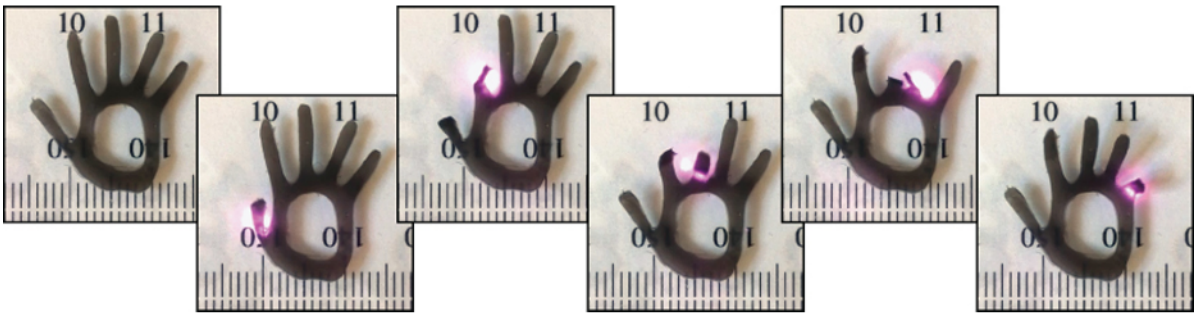

Figure 4-15. Site-specific bending and recovery on complex structures. A hand-shaped ELP-rGO composite hydrogel was molded. The fingers could be bent independently of one another by irradiation with a near-IR laser.

Hydrogel bending always occurred in the same direction, regardless of whether we illuminated the top or bottom surface (Figure 4-16). This further confirms that bending was the result of a structural gradient and not due to uneven IR absorbance on the opposite faces of the gels. The actuation was tunable by varying the concentration of rGO (Figure 4-17) and changing the laser intensity (Figure 4-18). Bending rates and angles both increased with increasing rGO concentration and laser intensity.

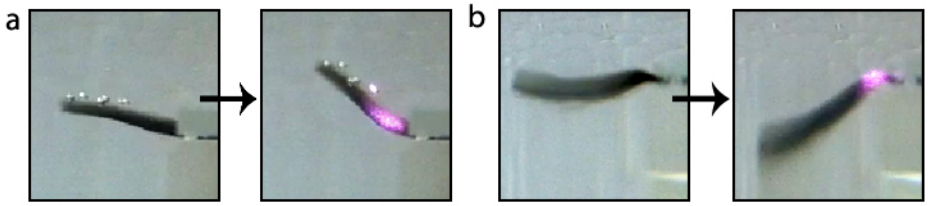

Figure 4-16. Directional bending. (a) Gel with vapor exposed layer facing up, bending upwards. (b) The same gel with the vapor exposed layer facing down, bending downwards. Illumination was from the top in both (a) and (b).

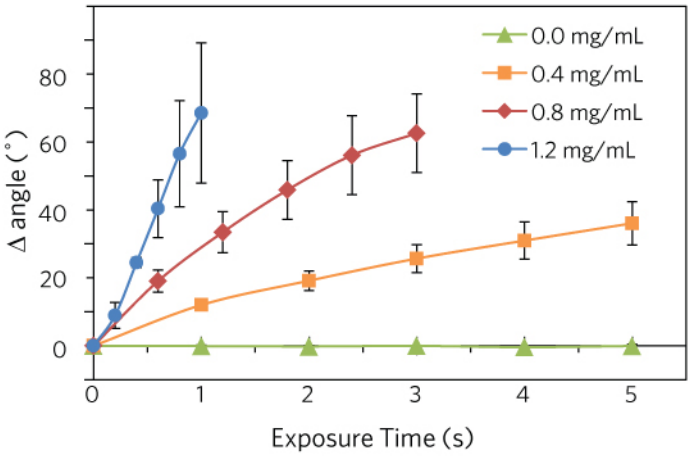

Figure 4-17. Dependence of bending rate and angle on rGO concentration.

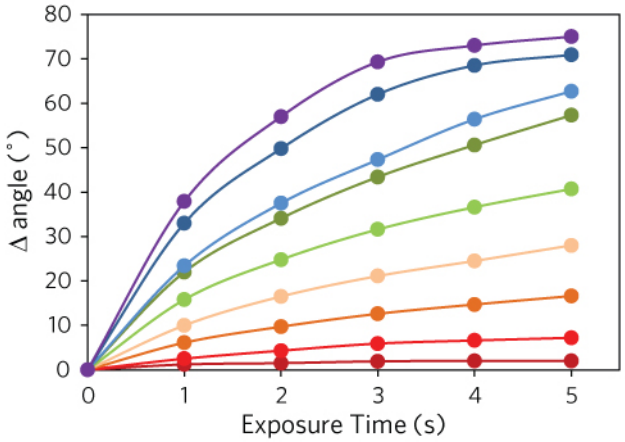

Figure 4-18. Effect of laser power on bending rate and angle. Laser power used in order from bottom curve to top curves: 15, 60, 105, 145, 195, 240, 285, 330, and 370 mW.

We also investigated whether or not the heat generated by the laser was hurting the performance of our actuators. We analyzed the bending trajectories of a gel over the course of 100 illumination cycles (Figure 4-19). The bending behavior was essentially unchanged over the course of the cycles which suggests that the gels are not being damaged. Lastly, we observed that we could control a gel's bending axis by controlling the path of the IR laser (Figure 4-20). This demonstrates the structural flexibility of our gradient gel actuators. Many shapes can be temporarily adopted by controlling the intensity, position, and paths of the near-IR lasers. In contrast, most stimuli-responsive folding materials were predesigned to bend at specific locations in order to adopt a single prescribed shape (*327, 331, 332*).

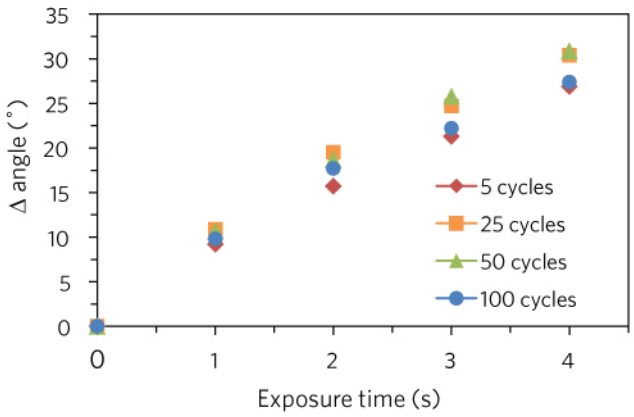

Figure 4-19. Endurance testing. There was no significant difference in the bending rate of the gels over the course of 100 cycles

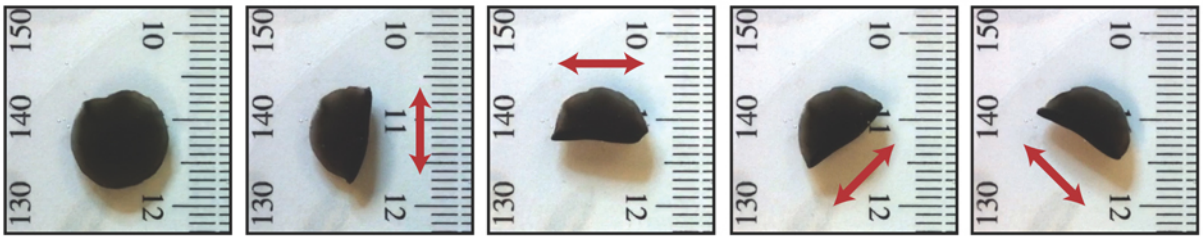

Figure 4-20. Laser path dependent folding. The arrows indicate the directions that the laser was rastered through the center of the gel.

To the best of our knowledge, our hydrogel is the first to undergo bending due to photothermal heating. The bending occurs on a short time-scale due to the unique porosity gradient. Although bending actuation using GNs has been demonstrated quite often using thin films, for biological applications a hydrated and porous network is more suitable for mimicking soft tissues. We believe that our gel actuators can be used for several applications. The simplest would be as microfluidic valves and switches (*283, 284, 333*). Our gels could also be used for fundamental cell studies because they can dynamically apply forces and biomolecule signals to cells in a spatially defined manner (*334-336*). Previously, in order to apply forces using a phase transition, hydrogels needed to be moved from one incubator to another of different temperature (*337*).

4.5 Conclusion

Here we demonstrated that simple incorporation of a short peptide sequence derived from phage display could impart a protein-based polymer with binding affinity towards graphene-derived nanosheets. Genetic engineering allowed for tuning of the physical and biological activities of the ELPs, while avoiding lengthy or inefficient chemical processing steps. The resulting ELP-GN hybrids are thermoresponsive in solution and as hydrogels. Furthermore, the light-responsiveness of GNs allows for

spatially and temporally controlled induction of ELP phase transitions. These hybrid materials have potential applications in diverse fields, including therapeutic delivery, tissue engineering, and microfluidics.

4.6 Materials and Methods

Molecular Cloning of ELPs: ELPs were engineered using the same techniques described in Chapters 2 and 3. The oligonucleotides used to insert the desired N- and C-terminal sequences into the pET-28b expression vectors are shown in Table 4-3.

Table 4-3. List of oligonucleotides used to synthesize the terminal sequence vectors in this study.

Oligo	Oligo Sequence (5′ to 3′)	Terminal sequence
CGB-F	CACTGGTCACGGTCTCGGTCCCGGGTCACAACT GGTACCACTGGTGGCCGCACTAATAA	VPGHNWYHWWPH--
CGB-R	GATCTTATTAGTGCGGCCACCAGTGGTACCAGT TGTGACCCGGGACCGAGACC	
NRGD-F	CATGAGCGGCCGTGGCGACTCCGGTGTCCTGAG ACC	MSGRGDSG
NRGD-R	GTGACCAGTGGGTCTCAGGACACCGGAGTCGCC ACGGCCGCT	
CK1-F	CACTGGTCACGGTCTCGGTCCCGGGTAAAGGCT AATAA	VPGKG--
CK1-R	GATCTTATTAGCCTTTACCCGGGACCGAGACC	

Protein Expression and Purification: The ELP genes were transferred to BLR(DE3) *E. Coli* for expression. 60 mL overnight starter cultures in LB Broth supplemented with 30 ug/mL of kanamycin were used. 12 mL of starter culture was then inoculated into every 900 mL of Terrific Broth and supplemented with 30 ug/mL Kanamycin. A 24 hour hyperexpression protocol was then followed as previously described. The ELPs were purified as described in Chapter 2 using three rounds of inverse transition cycling.

Protein Characterization: ELP molecular weights were verified by MALDI-TOF MS (Applied Biosystems Voyager DE). The matrix solution used was 10 mg/mL sinapinic acid in 30% acetonitrile, 0.1% TFA. 1 μL of marix was spotted on the sample plate and allowed to dry. The dried crystal was then crushed with an eraser covered in aluminum foil. 200 pmol/uL ELP solutions were prepared in water. 1 μL was then added to 12 μL of 10 mg/mL sinapinic acid in 30% acetonitrile, 0.1% TFA. 1.5 uL of the protein and matrix solution was then spotted onto the crushed crystals and allowed to dry before analysis.

Transition temperatures were measured using 1 mg/mL solutions of ELP in 10 mM Tris-Cl, 25 mM NaCl, pH 7.4. The ELP solution was placed in a glass cuvette with 5mm path length. The bottom half of the cuvette was placed in a stirred water bath. A light source was passed through the cuvette and the absorbance at 600 nm was measured using a spectrometer (Ocean Optics USB4000) as the

temperature of the water bath was increased. The temperature at which the rate of absorbance increased fastest was marked as the T_t.

GO synthesis: GO was synthesized from SP1 graphite (Bay Carbon) using a modified Hummer's method (*285*). Synthesis began with a preoxidation step. 25 mL of concentrated sulfuric acid was heated to 90 °C in a water bath. 5 g of potassium persulfate and phosphorous pentoxide were added and the temperature was lowered to 80 °C. 6 g of graphite powder was added and the solution was held at 80 °C with stirring for 4.5 hours. The reaction mixture was then poured slowly into 1 L of water and kept overnight. Finally, the reaction was filtered through a 0.2 μm pore size polyethersulfone filter and allowed to dry. 3 g of the dried product was then subjected to oxidation. 230 mL of concentrated sulfuric acid and a stirbar was added to a 4 L beaker and placed on an ice bath. When the solution reached ~0 °C it was placed on a stirring plate and 30 g of potassium permanganate was slowly added without allowing the temperature to exceed 10 °C. Once all of the potassium permanganate had dissolved, the solution was gradually heated to 35 °C and held for two hours. The reaction was returned to an ice bath then 460 mL of deionized water was slowly added without letting the temperature exceed 50 °C. The reaction was stirred for an additional two hours. Afterwards, an additional 1.4 L of water was added. 25 mL of 30% hydrogen peroxide was then added, causing the solution to turn yellow. The oxidized graphite was allowed to settle for one day and then the supernatant was decanted. The remaining solution with product was concentrated by centrifuging at 3000 x g for five minutes. The product was then applied to 0.2 μm pore size polyethersulfone filters and washed with 2.5 L of 10 wt% hydrochloric acid and 2.5 L of water. The product was dried on the filter then resuspended in water to ~2.0 wt% The graphite oxide slurry was subjected to extensive dialysis for one week then freeze dried to form a spongy brown mass. The graphite oxide was exfoliated to single GO sheets by suspending the freeze-dried material to the desired concentration in water and then subjecting it to bath sonication.

rGO synthesis: Reduction of GO to rGO was performed in batches using ascorbic acid as the reducing agent (*338*). 5.6 mg of GO was suspended in water to a concentration of 0.2 mg/mL then bath sonicated for ~2 hours. Half the volume was diluted in half with water to reach a concentration of 0.1 mg/mL. 80 μL of 35% ammonium hydroxide was then added to adjust the pH to between 9 and 10. The solution was then sonicated for an additional hour. Unexfoliated material was pelleted by spinning the solution for 20 min at 1950 x g. 50 mL of the supernatant was removed and added to a 100 mL round bottom flask. Ascorbic acid was then added to a concentration of 1 mM. The flask was closed with a rubber stopper then sealed tightly with parafilm and teflon tape. The flask was held in a silicone oil bath at 95 °C for 1 hour with stirring then cooled to room temperature with continued stirring. After reduction, we assumed that the mass of rGO was not significantly different than the GO precursor (0.1 mg/mL).

AFM Binding Analysis: Silicon wafer sections were treated with piranha solution (3:1 Sulfuric Acid: 30% hydrogen peroxide) for 10 minutes, rinsed with water and ethanol, and finally blown dry in a stream of nitrogen. The sections were then immersed in 1% solution of 3-Aminopropyltriethoxysilane (APTES) in ethanol for 30 minutes, rinsed with ethanol, blown dry in a stream of nitrogen, then baked in a 70 °C oven for 30 minutes. APTES treated wafer fragments were immersed in solutions of GO (4 ug/mL) for 2 minutes or rGO (5 ug/mL pH ~ 9) for 5 minutes, rinsed with water, and blown dry in a stream of nitrogen. Binding was performed by dipping the GO/rGO treated fragments in solutions of V50 or V50-

GB (0.5 mg/mL) for 20 minutes, rinsing with water, and then blowing them dry in a stream of nitrogen. Imaging was performed using an MFP3D AFM (Asylum Research, Santa Barbara, CA) in tapping mode and analyzed using Igor Pro 6.0 software.

ELP binding to GNs: rGO solutions were dialyzed against water that had been adjusted to a pH of ~9 to remove byproducts from the reduction process. The initial volume of rGO was divided by the final volume after dialysis to determine the final concentration of the stock solution (86.6 μg/mL). 100 μg/mL GO stock solutions were used for binding assays. 100 μL of V50-GB was added to 300 μL of the GN stock solutions at an 8:1, 9:1, or 10:1 mass ratio. The solutions were rotated end over end for 16 hours at 4 °C then placed in 0.5 mL, 100kDa cutoff centrifugal filters (Millipore). The filters were centrifuged at 5000 x g for 30 minutes at 4 °C. The concentration of V50-GB in the flow through was determined by comparison to a standard curve made with V50-GB using a bicinchoninic acid assay (Thermo-Scientific).

Colloidal Stability: Colloidal stability of GO was measured by adding 25 μL of 4.8 mg/mL V50, 4.8 mg/mL V50-GB, or water to 100 μL of 0.2 mg/mL GO on ice. 75 μL of cold NaCl of varying concentrations was then added to adjust the ionic strength to the desired values. The colloidal stability of rGO was measured by adding 25 μL of 2.4 mg/mL V50, 2.4 mg/mL V50-GB, 2.4 mg/mL E125, or water to 100 μL of 0.1 mg/mL rGO on ice. 75 μL of cold NaCl or HCl of varying concentration was then added to adjust the ionic strength or pH to the desired values, respectively. The solutions were kept at 4 °C and visibly monitored for signs of aggregation for one day.

Organic Solvent Assay: 0.1 mg/mL solutions of GO or rGO were mixed with V50-GB to a 6:1 ELP to GN mass ratio. The solutions were then heated to induce aggregation and pelleted by centrifugation. The supernatant was removed and replaced with ethanol. The solution was vortexed, pelleted again, and the supernatant was removed. The ethanol wash was repeated and then the pellet was allowed to dry in a vacuum chamber. The pellet was then resuspended to a GO or rGO concentration of 1.0 mg/mL in DMF, DMSO, or NMP and bath sonicated.

Thermoresponsive Characterization: 0.1 mg/mL solutions of GO or rGO were mixed with V50-GB to a 6:1 ELP to GN mass ratio. NaCl was added to reach a concentration of 25 mM. The solutions were heated to ~45 °C and vortexed to test for aggregation. The solutions were then cooled on an ice bath and vortexed again to test for resdispersion. The same solutions were placed in 10mm path length cuvettes and irradiated by an 808 nm near-IR laser (Lazerer Electronics). The laser power was set at ~0.4 W using a laser power meter (Molectron PowerMax 5100) and a DC power supply.

pH-responsive Characterization: 0.1 mg/mL solutions of rGO were diluted by 25% with E125 solutions. The final E125:rGO mass ratio was 6:1 and the initial pH was ~9. 0.1 M HCl was then added to reach a pH of ~4 to induce aggregation. The pH was then brought back to ~9 by 0.1 M NaOH. This process was repeated two more times to test for reversibility.

Cell Culture and Adhesion Assays: Mouse pre-osteoblast cells (MC3T3-E1 subclone 4) were obtained from ATCC and cultured in α-MEM supplemented with 10% fetal bovine serum (FBS) and

antimicrobial agents (penicillin, streptomycin). The media was changed every two days. Cell growth was carried out in a 37 °C, 5% CO_2, >95% relative humidity incubator.

24-well TCPS plates were used for cell adhesion. Wells were treated with 500 μL of 0.55 mg/mL PDDA (100-200 kDa molecular weight, 45 minutes, room temperature), then 0.5 mg/mL rGO, (45 minutes, room temperature), and then 0.5 mg/mL of ELP (V40-GB or V40-RGDGB, overnight, 4 ˚C). The wells were rinsed gently three times with water after each incubation step. The wells were then blocked with 7.5 mg/mL of heat-denatured bovine serum albumin (BSA) fraction V in Dulbecco's phosphate buffered saline (dPBS) (Corning cellgro) to prevent non-specific adsorption. Heat denaturation was performed by incubating the BSA at 80 °C for 10 minutes. When the cells reached ≥ 95% confluency, they were washed once with PBS. Cells were detached by incubating them for three minutes at 37 °C with 0.05% trypsin in 2mM EDTA. Trypsin was neutralized with four volume equivalents of α-MEM supplemented with 2% FBS. The cell suspension was pelleted at 2000 rpm for five minutes and the pellet was resuspended in 2 mM EDTA in dPBS. The cells were pelleted again and resuspended in dPBS. The cells were pelleted a third time and resuspended in α-MEM at a density of 1.2 million cells/mL. This suspension was incubated at 37 °C for 30 minutes. During the 30 minute incubation, excess BSA was washed out of the wells of the 24-well plate three times with dPBS. The cells were diluted to 120,000 cells/mL with α-MEM and 500 μL was seeded into each well. Cells were also plated into bare TCPS wells. The plate was incubated at 37 °C for 45 minutes, after which, the cells were washed thrice with dPBS with calcium and magnesium (Corning cellgro) and fixed with 4% formaldehyde in dPBS for 10 minutes at room temperature. The cells were washed three times with dPBS, permeabilized with 0.2% Triton X-100 in dPBS, then washed three more times with dPBS. Fluorescent staining was performed by 30 minute incubation at room temperature in a solution containing a 1:320 dilution of 5 mg/mL DAPI and a 1:1000 dilution of 8.712 μg/mL fluorescein-phalloidin. The plates were washed three final times with dPBS prior to imaging.

Six locations near the center of each well were imaged for DAPI and FITC at 100X magnification. Care was taken such that the images did not overlap with each other. The number of cells per well and average cell area of the cells in each well were calculated with CellProfiler (*339*). Outlier cell counts (greater than two population standard deviations from the mean) were excluded. Statistical analysis was performed using one-way ANOVA and the Student-Newman-Keuls post-hoc analysis. P-values less than 0.05 were considered statistically significant.

Gel Synthesis: V50-GB functionalized rGO was prepared by mixing the two components at a 6:1 mass ratio. The solution was then heated to 37 °C to induce aggregation and then pelleted by centrifugation at 1950 x g in a swinging arm centrifuge. The pellet was further centrifuged at 5000 x g in a fixed angle rotor (Beckman JA-20). The supernatant was removed and replaced with half the initial volume of deionized water. NaCl was added to a concentration of 5 mM. The rGO was pelleted by heating and centrifugation again and resuspended again in the same volume of deionized water. This mixture was frozen and lyophilized. The lyophilized product was weighed and, under the assumption that it remained a 6:1 V50-GB to rGO ratio, resuspended in a 75% DMSO/25% DMF solution to an rGO concentration of 5 mg/mL. V50-CK1, triethylamine, and 4-arm PEG-NHS (Succinimidyl Carboxy Methyl ester) crosslinker (CreativePEGWorks) were prepared in the same solvent. The four components were mixed such that the final percent weight by volume of V50-CK1 would be 13% (assuming each mg of V50-CK1 added 1 μL to the volume). The TEA concentration to add was determined by the formula, [primary

amines from V50-GB] + [primary amines from V50-CK1] + 20·(mg of rGO). The 4-Arm PEG-NHS was added so that the NHS concentration would equal the concentration of primary amines under the assumption that each crosslinker had 3.3 arms. The value of 3.3 was determined empirically based on testing with various crosslinker concentrations. The crosslinker was always added last and mixed on ice to prevent rapid crosslinking before thorough mixing could occur.

To create gradient gels, molds were cut out of parafilm that had been layered on glass to a thickness of ~0.45 mm. The pre-gel mixtures were then pipetted into the molds. The gel was allowed to stand at room temperature for 10 minutes before being put in a box containing a saturated solution of NaCl. The box was sealed and placed in a 37 °C incubator for 20 hours. The gels were removed from their molds then swelled in water to remove organic solvents and uncrosslinked materials.

SEM Analysis: The gradient gels were solvent-exchanged into ethanol by progressively increasing the ethanol concentration from 10% to 100% over the course of two days. The gels were then critical point dried in an attempt to maintain the pore structure. The dried gels were sputter coated with gold and mounted on gold stubs with carbon tape for SEM analysis (Hitachi S5000).

Laser Actuation: Gel bending was characterized by pinning one end of rectangular gels (~0.4mm x 2mm) between glass slides. The gel was then irradiated by the 808 nm near-IR laser near the pinning point. Bending rates were determined by measuring the angle between the laser spot and the end of the gel using individual video frames. Bending fatigue was tested by cycling the laser on for 5 seconds and off for 25 seconds, 100 times.

Chapter 5: Conclusions and Future Perspectives

As the complexity of our bioengineered systems increases to include more functions, it becomes increasingly difficult to reliably meet the physical and biological requirements we set out to achieve using traditional synthetic techniques and off-the-shelf materials. Yet, nature shows us that myriad functions can be rolled into one polymer and that the same polymer can be produced without variation using a cell's synthetic machinery. Thankfully, genetic engineering allows us to mimic nature and create protein-based polymers (PBPs) with the same fidelity as nature. It also lets us pull functions from nature's toolbox and insert them into wholly synthetic, but biologically active, materials. At the same time, we have created nanomaterials with exciting and useful properties that are never encountered in nature. Therefore, combining nanomaterials with genetically engineered PBPs is a pathway to advanced biomaterials with completely new capabilities. This dissertation described the steps I took to begin combining those materials.

We began by choosing a PBP backbone. Elastin-like polypeptides were chosen because of their excellent mechanical properties, biocompatibility, and tunable thermoresponsive phase transitions. ELPs also have a proven history of excelling in biomedical applications.

Before continuing, we set out to improve the way ELP genes are synthesized. The rate of gene synthesis limits our ability to rapidly generate and test new protein-based polymers. Previous approaches for making PBPs had poor fidelity, laborious protocols, inefficient yields, or uncontrollable product sizes. We developed an organization of restriction enzyme sites that permitted seamless cloning of PBPs, used a minimum of steps, was highly efficient, and resulted in well-defined products. Each cloning step regenerated the same organization of enzyme sites so each cloning step was the same. The use of TypeIIS restriction enzymes ensured that cloning was directional and seamless. Most importantly, they allowed for the same enzymes to work on any sequence. This method proved to be very effective in our synthesis of ELPs and can be used to accelerate the development of new PBPs.

Armed with an efficient gene synthesis protocol, we endeavored to create nanocomposites with hydroxyapatite, the mineral component of bones. Nature has a limited set of building blocks, but it still creates remarkably stiff and tough composite materials. Bone is one those materials. There are a number of proteins that are believed to contribute to the toughness of bone. We attempted to mimic the interfacial bonds formed by these proteins by engineering ELPs with a bioinspired HAP-binding sequence and varying backbone charges. In the end, we found that the presence of the HAP-binding sequence had the greatest effects in our systems. With a HAP-binding ELP, we were able to bind to and disperse HAP nanoparticles. When combined with calcium phosphate bone cements, HAP-binding ELPs significantly improved their mechanical strength, injectability, and stability. Further improvements to bone cements using PBPs may allow for their use in load-bearing defects.

Attaching polymers to nanoparticles is critical when making nanoparticle-polymer hybrids. However, unlike HAP, some materials don't have natural peptidic binding sequences. We demonstrated that we could use a phage-display derived peptide to attach ELPs to the surfaces of nanoparticles. Specifically, we used graphene oxide and reduced graphene oxide nanosheets (GNs). The GN binding ELPs had a dramatic stabilizing effect on the colloidal stability of GNs in solution. In addition, the ELP-graphene hybrids aggregated in response to near-IR illumination due to the combined stimuli-responsiveness of the two components (heat generation by the GNs and the phase transition of the ELPs). A simple genetic addition to the GN binding ELPs was shown to greatly increase the adhesion

and spreading of cells on ELP treated GN surfaces. Finally, we showed that a novel phase separation technique could introduce porosity gradients into ELP-GN composite hydrogels. These gradients were exploited to create hydrogels that bent in a rapid, site-specific, and reversible manner in response to remote illumination with near-IR light. We believe that the anchoring of PBPs to nanoparticles using phage display derived peptides can be generalized to any nanoparticles. The specific combination of ELPs and GNs may find applications in therapeutics and cell/tissue engineering.

Taken together, these results show that the tools exist to easily and efficiently immobilize PBPs on nanoparticle surfaces. It also clearly demonstrates that the capabilities of PBPs and nanoparticles can be combined to generate useful responses that neither material could achieve on its own (e.g., mechanical strength, remote aggregation and actuation).

As described in Chapter 1, the possibilities of PBP-nanoparticle hybrids are relatively unexplored. Our studies and previous work have covered only a small cross-section of possible combinations. For example, our most complex PBP only included a nanoparticle binding motif, a cell-binding motif, and an ELP backbone. However, more backbone types and bioactive motifs can easily be introduced. In addition, techniques are allowing for the improved incorporation of unnatural amino acids that will increase the range of physical and stimuli-responsive properties available. Finally, although we have focused on the advantages of PBPs over chemically synthesized polymers, future systems can combine the advantageous properties of both into polymer-nanoparticle hybrid materials.

References

1. D. G. Anderson, J. A. Burdick, R. Langer, Smart Biomaterials. *Science* **305**, 1923 (2004).
2. R. A. Pérez, J.-E. Won, J. C. Knowles, H.-W. Kim, Naturally and synthetic smart composite biomaterials for tissue regeneration. *Advanced Drug Delivery Reviews*, (2012).
3. S. Sirivisoot, B. S. Harrison, in *Principles of Regenerative Medicine,* A. Atala, R. Lanza, J. A. Thomson, R. Nerem, Eds. (Academic Press, London, UK, 2010).
4. R. Langer, D. A. Tirrell, Designing materials for biology and medicine. *Nature* **428**, 487 (2004).
5. A. R. Tao, S. Habas, P. D. Yang, Shape control of colloidal metal nanocrystals. *Small* **4**, 310 (2008).
6. T. Reid, Nanoparticle synthesis: Family gold. *Nature Nanotechnology*, (2009).
7. X. Wang, J. Zhuang, Q. Peng, Y. Li, A general strategy for nanocrystal synthesis. *Nature* **437**, 121 (2005).
8. K. Hidehiro, I. Motoyuki, Surface modification and characterization for dispersion stability of inorganic nanometer-scaled particles in liquid media. *Science and Technology of Advanced Materials* **11**, 044304 (2010).
9. A. C. Balazs, T. Emrick, T. P. Russell, Nanoparticle Polymer Composites: Where Two Small Worlds Meet. *Science* **314**, 1107 (2006).
10. T. H. Kim *et al.*, Selective and Sensitive TNT Sensors Using Biomimetic Polydiacetylene-Coated CNT-FETs. *ACS Nano* **5**, 2824 (2011).
11. A. De La Zerda *et al.*, Carbon nanotubes as photoacoustic molecular imaging agents in living mice. *Nat Nano* **3**, 557 (2008).
12. H. Mattoussi, G. Palui, H. B. Na, Luminescent quantum dots as platforms for probing in vitro and in vivo biological processes. *Advanced Drug Delivery Reviews* **64**, 138 (2012).
13. R. Gref *et al.*, Biodegradable long-circulating polymeric nanospheres. *Science* **263**, 1600 (1994).
14. S. Dai, P. Ravi, K. C. Tam, pH-Responsive polymers: synthesis, properties and applications. *Soft Matter* **4**, 435 (2008).
15. D. Crespy, R. M. Rossi, Temperature-responsive polymers with LCST in the physiological range and their applications in textiles. *Polymer International* **56**, 1461 (2007).
16. A. Lendlein, R. Langer, Biodegradable, Elastic Shape-Memory Polymers for Potential Biomedical Applications. *Science* **296**, 1673 (2002).
17. F. D. Jochum, L. zur Borg, P. J. Roth, P. Theato, Thermo- and Light-Responsive Polymers Containing Photoswitchable Azobenzene End Groups. *Macromolecules* **42**, 7854 (2009).
18. J. P. Magnusson *et al.*, Ion-Sensitive "Isothermal" Responsive Polymers Prepared in Water. *Journal of the American Chemical Society* **130**, 10852 (2008).
19. O. J. Cayre, N. Chagneux, S. Biggs, Stimulus responsive core-shell nanoparticles: synthesis and applications of polymer based aqueous systems. *Soft Matter* **7**, 2211 (2011).
20. E. G. Bellomo, M. D. Wyrsta, L. Pakstis, D. J. Pochan, T. J. Deming, Stimuli-responsive polypeptide vesicles by conformation-specific assembly. *Nat Mater* **3**, 244 (2004).
21. L. E. Gerweck, S. Vijayappa, S. Kozin, Tumor pH controls the in vivo efficacy of weak acid and base chemotherapeutics. *Molecular Cancer Therapeutics* **5**, 1275 (2006).

22. J. Jung, I.-H. Lee, E. Lee, J. Park, S. Jon, pH-Sensitive Polymer Nanospheres for Use as a Potential Drug Delivery Vehicle. *Biomacromolecules* **8**, 3401 (2007).
23. M. Bikram, J. L. West, Thermo-responsive systems for controlled drug delivery. *Expert Opinion on Drug Delivery* **5**, 1077 (2008).
24. M. A. Cole, N. H. Voelcker, H. Thissen, H. J. Griesser, Stimuli-responsive interfaces and systems for the control of protein-surface and cell-surface interactions. *Biomaterials* **30**, 1827 (2009).
25. J. F. Pollock, K. E. Healy, Mechanical and swelling characterization of poly(N-isopropyl acrylamide -co- methoxy poly(ethylene glycol) methacrylate) sol-gels. *Acta Biomater* **6**, 1307 (2010).
26. C. A. DeForest, E. A. Sims, K. S. Anseth, Peptide-Functionalized Click Hydrogels with Independently Tunable Mechanics and Chemical Functionality for 3D Cell Culture. *Chemistry of Materials* **22**, 4783 (2010).
27. K. L. Heredia, L. Tao, G. N. Grover, H. D. Maynard, Heterotelechelic polymers for capture and release of protein-polymer conjugates. *Polymer Chemistry* **1**, 168 (2010).
28. S. Sriwichai *et al.*, Electrochemically controlled surface plasmon resonance immunosensor for the detection of human immunoglobulin G on poly(3-aminobenzoic acid) ultrathin films. *Sensors and Actuators B: Chemical* **147**, 322 (2010).
29. G. T. Hermanson, *Bioconjugate Techniques*. (Elsevier Inc., ed. 2nd, 2008).
30. F. M. Veronese, Peptide and protein PEGylation: a review of problems and solutions. *Biomaterials* **22**, 405 (2001).
31. C. A. Lackey *et al.*, Hemolytic Activity of pH-Responsive Polymer-Streptavidin Bioconjugates†. *Bioconjugate Chemistry* **10**, 401 (1999).
32. T. A. Christopoulos *et al.*, Hyaluronidase and CD44 hyaluronan receptor expression in squamous cell laryngeal carcinoma. *Biochimica et biophysica acta* **1760**, 1039 (2006).
33. A. Kumar *et al.*, Development of hyaluronic acid–Fe2O3 hybrid magnetic nanoparticles for targeted delivery of peptides. *Nanomedicine: Nanotechnology, Biology and Medicine* **3**, 132 (2007).
34. R. T. Aimes, J. P. Quigley, Matrix metalloproteinase-2 is an interstitial collagenase. Inhibitor-free enzyme catalyzes the cleavage of collagen fibrils and soluble native type I collagen generating the specific 3/4- and 1/4-length fragments. *The Journal of biological chemistry* **270**, 5872 (1995).
35. M. Mizuno, R. Fujisawa, Y. Kuboki, Type I collagen-induced osteoblastic differentiation of bone-marrow cells mediated by collagen-alpha2beta1 integrin interaction. *Journal of cellular physiology* **184**, 207 (2000).
36. L. Yang *et al.*, Mechanical Properties of Native and Cross-linked Type I Collagen Fibrils. *Biophysical Journal* **94**, 2204 (2008).
37. G. He, A. George, Dentin matrix protein 1 immobilized on type I collagen fibrils facilitates apatite deposition in vitro. *The Journal of biological chemistry* **279**, 11649 (2004).
38. C. A. Haynes, W. Norde, Structures and Stabilities of Adsorbed Proteins. *Journal of Colloid and Interface Science* **169**, 313 (1995).
39. L. Fei, S. Perrett, Effect of Nanoparticles on Protein Folding and Fibrillogenesis. *International Journal of Molecular Sciences* **10**, 646 (2009).

40. X. Gao, Y. Cui, R. M. Levenson, L. W. K. Chung, S. Nie, In vivo cancer targeting and imaging with semiconductor quantum dots. *Nat Biotech* **22**, 969 (2004).
41. P. Podsiadlo *et al.*, Ultrastrong and Stiff Layered Polymer Nanocomposites. *Science* **318**, 80 (2007).
42. S. A. McClure *et al.*, Electrostatic Layer-by-Layer Assembly of CdSe Nanorod/Polymer Nanocomposite Thin Films. *ACS Applied Materials & Interfaces* **2**, 219 (2009).
43. K. G. Neoh, E. T. Kang, Functionalization of inorganic nanoparticles with polymers for stealth biomedical applications. *Polymer Chemistry* **2**, 747 (2011).
44. B. Zhao, W. J. Brittain, Polymer brushes: surface-immobilized macromolecules. *Progress in Polymer Science* **25**, 677 (2000).
45. C. Li, B. C. Benicewicz, Synthesis of Well-Defined Polymer Brushes Grafted onto Silica Nanoparticles via Surface Reversible Addition-Fragmentation Chain Transfer Polymerization. *Macromolecules* **38**, 5929 (2005).
46. Y. Jin *et al.*, Silica Nanoparticles with Continuously Tunable Sizes: Synthesis and Size Effects on Cellular Contrast Imaging. *Chemistry of Materials* **20**, 4411 (2008).
47. J. Park *et al.*, One-Nanometer-Scale Size-Controlled Synthesis of Monodisperse Magnetic Iron Oxide Nanoparticles. *Angewandte Chemie International Edition* **44**, 2872 (2005).
48. M. Hu *et al.*, Gold nanostructures: engineering their plasmonic properties for biomedical applications. *Chemical Society Reviews* **35**, 1084 (2006).
49. J.-J. Luo, I. M. Daniel, Characterization and modeling of mechanical behavior of polymer/clay nanocomposites. *Composites Science and Technology* **63**, 1607 (2003).
50. F. Hussain, M. Hojjati, M. Okamoto, R. E. Gorga, Review article: Polymer-matrix Nanocomposites, Processing, Manufacturing, and Application: An Overview. *Journal of Composite Materials* **40**, 1511 (2006).
51. H. Gao, B. Ji, I. L. Jäger, E. Arzt, P. Fratzl, Materials become insensitive to flaws at nanoscale: Lessons from nature. *Proceedings of the National Academy of Sciences* **100**, 5597 (2003).
52. P. Rittigstein, R. D. Priestley, L. J. Broadbelt, J. M. Torkelson, Model polymer nanocomposites provide an understanding of confinement effects in real nanocomposites. *Nat Mater* **6**, 278 (2007).
53. L. S. Schadler, in *Nanocomposite Science and Technology,* P. M. Ajayan, L. S. Schadler, P. V. Braun, Eds. (2003).
54. P. Zhang *et al.*, RGD-Conjugated Copolymer Incorporated into Composite of Poly(lactide-co-glycotide) and Poly(l-lactide)-Grafted Nanohydroxyapatite for Bone Tissue Engineering. *Biomacromolecules* **12**, 2667 (2011).
55. K. Haraguchi, K. Murata, T. Takehisa, Stimuli-Responsive Nanocomposite Gels and Soft Nanocomposites Consisting of Inorganic Clays and Copolymers with Different Chemical Affinities. *Macromolecules* **45**, 385 (2011).
56. S. R. Shin *et al.*, Carbon Nanotube Reinforced Hybrid Microgels as Scaffold Materials for Cell Encapsulation. *ACS Nano* **6**, 362 (2011).
57. C. J. Ferris, M. in het Panhuis, Conducting bio-materials based on gellan gum hydrogels. *Soft Matter* **5**, 3430 (2009).

58. S. Myung *et al.*, Graphene-Encapsulated Nanoparticle-Based Biosensor for the Selective Detection of Cancer Biomarkers. *Adv. Mater.* **23**, 2221 (2011).
59. Y.-C. Chuang *et al.*, An optical biosensing platform for proteinase activity using gold nanoparticles. *Biomaterials* **31**, 6087 (2010).
60. S. Guo, S. Dong, Biomolecule-nanoparticle hybrids for electrochemical biosensors. *TrAC Trends in Analytical Chemistry* **28**, 96 (2009).
61. J. Xie, S. Lee, X. Chen, Nanoparticle-based theranostic agents. *Adv Drug Deliv Rev* **62**, 1064 (2010).
62. X. Michalet *et al.*, Quantum Dots for Live Cells, in Vivo Imaging, and Diagnostics. *Science* **307**, 538 (2005).
63. X. Wu *et al.*, Immunofluorescent labeling of cancer marker Her2 and other cellular targets with semiconductor quantum dots. *Nat Biotech* **21**, 41 (2003).
64. O. Tagit *et al.*, Nanostructured thermoresponsive quantum dot/PNIPAM assemblies. *European Polymer Journal* **46**, 1397 (2010).
65. R. Popovtzer *et al.*, Targeted Gold Nanoparticles Enable Molecular CT Imaging of Cancer. *Nano Lett.* **8**, 4593 (2008).
66. E. Amstad *et al.*, Surface Functionalization of Single Superparamagnetic Iron Oxide Nanoparticles for Targeted Magnetic Resonance Imaging. *Small* **5**, 1334 (2009).
67. A. Popat, J. Liu, G. Q. Lu, S. Z. Qiao, A pH-responsive drug delivery system based on chitosan coated mesoporous silica nanoparticles. *Journal of Materials Chemistry* **22**, 11173 (2012).
68. X. Zhao *et al.*, Active scaffolds for on-demand drug and cell delivery. *Proceedings of the National Academy of Sciences* **108**, 67 (2011).
69. A. Shiotani *et al.*, Active Accumulation of Gold Nanorods in Tumor in Response to Near-Infrared Laser Irradiation. *Bioconjugate Chemistry* **21**, 2049 (2010).
70. D. W. Urry, Physical Chemistry of Biological Free Energy Transduction As Demonstrated by Elastic Protein-Based Polymers. *The Journal of Physical Chemistry B* **101**, 11007 (1997).
71. R. L. DiMarco, S. C. Heilshorn, Multifunctional Materials through Modular Protein Engineering. *Adv. Mater.*, (2012).
72. J. Carlos Rodríguez-Cabello, J. Reguera, A. Girotti, M. Alonso, A. M. Testera, Developing functionality in elastin-like polymers by increasing their molecular complexity: the power of the genetic engineering approach. *Progress in Polymer Science* **30**, 1119 (2005).
73. C. Vepari, D. L. Kaplan, Silk as a biomaterial. *Progress in Polymer Science* **32**, 991 (2007).
74. C. Wong Po Foo *et al.*, Novel nanocomposites from spider silk–silica fusion (chimeric) proteins. *Proceedings of the National Academy of Sciences* **103**, 9428 (2006).
75. D. T. McPherson *et al.*, Production and Purification of a Recombinant Elastomeric Polypeptide, G-(VPGVG)19-VPGV, from *Escherichia-Coli*. *Biotechnology Progress* **8**, 347 (1992).
76. A. C. Rincon *et al.*, Biocompatibility of elastin-like polymer poly(VPAVG) microparticles: in vitro and in vivo studies. *Journal of biomedical materials research. Part A* **78**, 343 (2006).
77. A. Bracalello *et al.*, Design and Production of a Chimeric Resilin-, Elastin-, and Collagen-Like Engineered Polypeptide. *Biomacromolecules* **12**, 2957 (2011).
78. C. M. Elvin *et al.*, Synthesis and properties of crosslinked recombinant pro-resilin. *Nature* **437**, 999 (2005).

79. L. Li, S. Teller, R. J. Clifton, X. Jia, K. L. Kiick, Tunable Mechanical Stability and Deformation Response of a Resilin-Based Elastomer. *Biomacromolecules* **12**, 2302 (2011).
80. W. A. Petka, J. L. Harden, K. P. McGrath, D. Wirtz, D. A. Tirrell, Reversible Hydrogels from Self-Assembling Artificial Proteins. *Science* **281**, 389 (1998).
81. A. Rising, M. Widhe, J. Johansson, M. Hedhammar, Spider silk proteins: recent advances in recombinant production, structure-function relationships and biomedical applications. *Cell. Mol. Life Sci.* **68**, 169 (2011).
82. O. S. Rabotyagova, P. Cebe, D. L. Kaplan, Protein-Based Block Copolymers. *Biomacromolecules* **12**, 269 (2011).
83. A. E. Brooks, R. V. Lewis, Probing the elastic nature of spider silk in pursuit of the next designer fiber. *Biomedical sciences instrumentation* **40**, 232 (2004).
84. B. Bochicchio, A. Pepe, A. M. Tamburro, Investigating by CD the molecular mechanism of elasticity of elastomeric proteins. *Chirality* **20**, 985 (2008).
85. L. B. Sandberg, N. T. Soskel, J. G. Leslie, Elastin Structure, Biosynthesis, and Relation to Disease States. *New England Journal of Medicine* **304**, 566 (1981).
86. J. C. Rodriguez-Cabello, J. Reguera, A. Girotti, F. J. Arias, M. Alonso, in *Ordered Polymeric Nanostructures at Surfaces*. (2006), vol. 200, pp. 119-167.
87. R. E. Lyons *et al.*, Design and facile production of recombinant resilin-like polypeptides: gene construction and a rapid protein purification method. *Protein Engineering Design & Selection* **20**, 25 (2007).
88. W. Teng, J. Cappello, X. Wu, Recombinant Silk-Elastinlike Protein Polymer Displays Elasticity Comparable to Elastin. *Biomacromolecules* **10**, 3028 (2009).
89. M. Y. Truong *et al.*, A pH-responsive interface derived from resilin-mimetic protein Rec1-resilin. *Biomaterials* **31**, 4434 (2010).
90. S. Winkler *et al.*, Designing recombinant spider silk proteins to control assembly. *International Journal of Biological Macromolecules* **24**, 265 (1999).
91. S. Banta, I. R. Wheeldon, M. Blenner, Protein Engineering in the Development of Functional Hydrogels. *Annual Review of Biomedical Engineering* **12**, 167 (2010).
92. C. Xu, V. Breedveld, J. Kopeček, Reversible Hydrogels from Self-Assembling Genetically Engineered Protein Block Copolymers. *Biomacromolecules* **6**, 1739 (2005).
93. L. Mi, S. Fischer, B. Chung, S. Sundelacruz, J. L. Harden, Self-Assembling Protein Hydrogels with Modular Integrin Binding Domains. *Biomacromolecules* **7**, 38 (2005).
94. E. R. Welsh, D. A. Tirrell, Engineering the Extracellular Matrix: A Novel Approach to Polymeric Biomaterials. I. Control of the Physical Properties of Artificial Protein Matrices Designed to Support Adhesion of Vascular Endothelial Cells. *Biomacromolecules* **1**, 23 (2000).
95. S. Halstenberg, A. Panitch, S. Rizzi, H. Hall, J. A. Hubbell, Biologically Engineered Protein-graft-Poly(ethylene glycol) Hydrogels: A Cell Adhesive and Plasmin-Degradable Biosynthetic Material for Tissue Repair. *Biomacromolecules* **3**, 710 (2002).
96. G. L. Bidwell, E. Perkins, D. Rancher, A thermally targeted c-Myc inhibitory polypeptide inhibits breast tumor growth. *Cancer Lett.* **319**, 136 (2012).
97. M. B. Charati, J. L. Ifkovits, J. A. Burdick, J. G. Linhardt, K. L. Kiick, Hydrophilic elastomeric biomaterials based on resilin-like polypeptides. *Soft Matter* **5**, 3412 (2009).

98. D. C. Chow, M. R. Dreher, K. Trabbic-Carlson, A. Chilkoti, Ultra-High Expression of a Thermally Responsive Recombinant Fusion Protein in E. coli. *Biotechnology Progress* **22**, 638 (2006).
99. M. R. Dreher *et al.*, Evaluation of an elastin-like polypeptide–doxorubicin conjugate for cancer therapy. *Journal of Controlled Release* **91**, 31 (2003).
100. A. Wada *et al.*, Design and Construction of Glutamine Binding Proteins with a Self-Adhering Capability to Unmodified Hydrophobic Surfaces as Reagentless Fluorescence Sensing Devices. *Journal of the American Chemical Society* **125**, 16228 (2003).
101. H. Mattoussi *et al.*, Self-Assembly of CdSe-ZnS Quantum Dot Bioconjugates Using an Engineered Recombinant Protein. *Journal of the American Chemical Society* **122**, 12142 (2000).
102. D. H. Nam, K. Won, Y. H. Kim, B. I. Sang, A novel route for immobilization of proteins to silica particles incorporating silaffin domains. *Biotechnology Progress* **25**, 1643 (2009).
103. L. Chan *et al.*, Covalent Attachment of Proteins to Solid Supports and Surfaces via Sortase-Mediated Ligation. *PLoS ONE* **2**, e1164 (2007).
104. G. Smith, Filamentous fusion phage: novel expression vectors that display cloned antigens on the virion surface. *Science* **228**, 1315 (1985).
105. Y. Huang *et al.*, Programmable Assembly of Nanoarchitectures Using Genetically Engineered Viruses. *Nano Lett.* **5**, 1429 (2005).
106. R. R. Naik, S. J. Stringer, G. Agarwal, S. E. Jones, M. O. Stone, Biomimetic synthesis and patterning of silver nanoparticles. *Nat Mater* **1**, 169 (2002).
107. B. H. Lower *et al.*, In Vitro Evolution of a Peptide with a Hematite Binding Motif That May Constitute a Natural Metal-Oxide Binding Archetype. *Environmental Science & Technology* **42**, 3821 (2008).
108. W.-J. Chung, K.-Y. Kwon, J. Song, S.-W. Lee, Evolutionary Screening of Collagen-like Peptides That Nucleate Hydroxyapatite Crystals. *Langmuir* **27**, 7620 (2011).
109. C. E. Flynn *et al.*, Synthesis and organization of nanoscale II-VI semiconductor materials using evolved peptide specificity and viral capsid assembly. *Journal of Materials Chemistry* **13**, 2414 (2003).
110. S. Wang *et al.*, Peptides with selective affinity for carbon nanotubes. *Nat Mater* **2**, 196 (2003).
111. C. Tamerler *et al.*, Molecular biomimetics: GEPI-based biological routes to technology. *Peptide Science* **94**, 78 (2010).
112. T. Schwemmer, J. Baumgartner, D. Faivre, H. G. Börner, Peptide-Mediated Nanoengineering of Inorganic Particle Surfaces: A General Route toward Surface Functionalization via Peptide Adhesion Domains. *Journal of the American Chemical Society* **134**, 2385 (2011).
113. D. W. Urry *et al.*, Elastin: a representative ideal protein elastomer. *Philosophical Transactions of the Royal Society of London. Series B: Biological Sciences* **357**, 169 (2002).
114. E. Petersen, F. Wågberg, K. A. Ängquist, Serum Concentrations of Elastin-derived Peptides in Patients with Specific Manifestations of Atherosclerotic Disease. *European Journal of Vascular and Endovascular Surgery* **24**, 440 (2002).
115. S. M. Mithieux, A. S. Weiss, in *Advances in Protein Chemistry*, A. D. P. David, M. S. John, Eds. (Academic Press, 2005), vol. 70, pp. 437-461.

116. C. Baldock *et al.*, Shape of tropoelastin, the highly extensible protein that controls human tissue elasticity. *Proceedings of the National Academy of Sciences*, (2011).
117. Z. Indik *et al.*, Production of recombinant human tropoelastin: Characterization and demonstration of immunologic and chemotactic activity. *Archives of Biochemistry and Biophysics* **280**, 80 (1990).
118. V. Groult *et al.*, Mechanisms of interaction between human skin fibroblasts and elastin: Differences between elastin fibres and derived peptides. *Cell Biochemistry and Function* **9**, 171 (1991).
119. F. W. Keeley, C. M. Bellingham, K. A. Woodhouse, Elastin as a self–organizing biomaterial: use of recombinantly expressed human elastin polypeptides as a model for investigations of structure and self–assembly of elastin. *Philosophical Transactions of the Royal Society of London. Series B: Biological Sciences* **357**, 185 (2002).
120. D. W. Urry, Molecular Machines: How Motion and Other Functions of Living Organisms Can Result from Reversible Chemical Changes. *Angewandte Chemie International Edition in English* **32**, 819 (1993).
121. A. Valiaev *et al.*, Hydration and Conformational Mechanics of Single, End-Tethered Elastin-like Polypeptides. *Journal of the American Chemical Society* **130**, 10939 (2008).
122. B. Li, D. O. V. Alonso, B. J. Bennion, V. Daggett, Hydrophobic Hydration Is an Important Source of Elasticity in Elastin-Based Biopolymers. *Journal of the American Chemical Society* **123**, 11991 (2001).
123. D. W. Urry *et al.*, Temperature of polypeptide inverse temperature transition depends on mean residue hydrophobicity. *Journal of the American Chemical Society* **113**, 4346 (1991).
124. J. Reguera, D. W. Urry, T. M. Parker, D. T. McPherson, J. C. Rodríguez-Cabello, Effect of NaCl on the Exothermic and Endothermic Components of the Inverse Temperature Transition of a Model Elastin-like Polymer. *Biomacromolecules* **8**, 354 (2007).
125. A. Girotti *et al.*, Influence of the Molecular Weight on the Inverse Temperature Transition of a Model Genetically Engineered Elastin-like pH-Responsive Polymer. *Macromolecules* **37**, 3396 (2004).
126. D. W. Urry, T. L. Trapane, K. U. Prasad, Phase-structure transitions of the elastin polypentapeptide–water system within the framework of composition–temperature studies. *Biopolymers* **24**, 2345 (1985).
127. Y. Cho *et al.*, Effects of Hofmeister Anions on the Phase Transition Temperature of Elastin-like Polypeptides. *The Journal of Physical Chemistry B* **112**, 13765 (2008).
128. D. E. Meyer, A. Chilkoti, Purification of recombinant proteins by fusion with thermally-responsive polypeptides. *Nature Biotechnology* **17**, 1112 (1999).
129. M. R. Banki, L. A. Feng, D. W. Wood, Simple bioseparations using self-cleaving elastin-like polypeptide tags. *Nature Methods* **2**, 659 (2005).
130. W.-Y. Wu, C. Mee, F. Califano, R. Banki, D. W. Wood, Recombinant protein purification by self-cleaving aggregation tag. *Nat. Protocols* **1**, 2257 (2006).
131. K. Trabbic-Carlson, L. Liu, B. Kim, A. Chilkoti, Expression and purification of recombinant proteins from Escherichia coli: Comparison of an elastin-like polypeptide fusion with an oligohistidine fusion. *Protein Science* **13**, 3274 (2004).

132. D. Lan *et al.*, An improved nonchromatographic method for the purification of recombinant proteins using elastin-like polypeptide-tagged proteases. *Analytical Biochemistry* **415**, 200 (2011).
133. T. Christensen, K. Trabbic-Carlson, W. Liu, A. Chilkoti, Purification of recombinant proteins from Escherichia coli at low expression levels by inverse transition cycling. *Analytical Biochemistry* **360**, 166 (2007).
134. J. Y. Kim, S. O'Malley, A. Mulchandani, W. Chen, Genetically engineered elastin-protein a fusion as a universal platform for homogeneous, phase-separation immunoassay. *Analytical Chemistry* **77**, 2318 (2005).
135. J. Kostal, A. Mulchandani, W. Chen, Tunable biopolymers for heavy metal removal. *Macromolecules* **34**, 2257 (2001).
136. J. Kostal, A. Mulchandani, W. Chen, Affinity purification of plasmid DNA by temperature-triggered precipitation. *Biotechnology and Bioengineering* **85**, 293 (2004).
137. D. W. Urry, T. M. Parker, M. C. Reid, D. C. Gowda, Biocompatibility of the Bioelastic Materials, Poly(GVGVP) and Its γ-Irradiation Cross-Linked Matrix: Summary of Generic Biological Test Results. *Journal of Bioactive and Compatible Polymers* **6**, 263 (1991).
138. D. Topcic *et al.*, An Activation-Specific Platelet Inhibitor That Can Be Turned On/Off by Medically Used Hypothermia. *Arteriosclerosis, Thrombosis, and Vascular Biology* **31**, 2015 (2011).
139. W. Liu *et al.*, Injectable intratumoral depot of thermally responsive polypeptide–radionuclide conjugates delays tumor progression in a mouse model. *Journal of Controlled Release* **144**, 2 (2010).
140. M. F. Shamji *et al.*, An Injectable and In Situ-Gelling Biopolymer for Sustained Drug Release Following Perineural Administration. *Spine* **33**, 748 (2008).
141. M. F. Shamji *et al.*, Development and characterization of a fusion protein between thermally responsive elastin-like polypeptide and interleukin-1 receptor antagonist: Sustained release of a local antiinflammatory therapeutic. *Arthritis & Rheumatism* **56**, 3650 (2007).
142. M. F. Shamji *et al.*, Synthesis and characterization of a thermally-responsive tumor necrosis factor antagonist. *Journal of Controlled Release* **129**, 179 (2008).
143. D. E. Meyer, B. C. Shin, G. A. Kong, M. W. Dewhirst, A. Chilkoti, Drug targeting using thermally responsive polymers and local hyperthermia. *Journal of Controlled Release* **74**, 213 (2001).
144. A. J. MacKay *et al.*, Self-assembling chimeric polypeptide-doxorubicin conjugate nanoparticles that abolish tumours after a single injection. *Nat Mater* **8**, 993 (2009).
145. R. E. Sallach *et al.*, Micelle Density Regulated by a Reversible Switch of Protein Secondary Structure. *Journal of the American Chemical Society* **128**, 12014 (2006).
146. W. Kim, J. Thévenot, E. Ibarboure, S. Lecommandoux, E. L. Chaikof, Self-Assembly of Thermally Responsive Amphiphilic Diblock Copolypeptides into Spherical Micellar Nanoparticles. *Angewandte Chemie International Edition* **49**, 4257 (2010).
147. T. A. T. Lee, A. Cooper, R. P. Apkarian, V. P. Conticello, Thermo-Reversible Self-Assembly of Nanoparticles Derived from Elastin-Mimetic Polypeptides. *Adv. Mater.* **12**, 1105 (2000).
148. Y. Fujita, M. Mie, E. Kobatake, Construction of nanoscale protein particle using temperature-sensitive elastin-like peptide and polyaspartic acid chain. *Biomaterials* **30**, 3450 (2009).

149. M. R. Dreher *et al.*, Temperature Triggered Self-Assembly of Polypeptides into Multivalent Spherical Micelles. *Journal of the American Chemical Society* **130**, 687 (2007).
150. D. J. Callahan *et al.*, Triple Stimulus-Responsive Polypeptide Nanoparticles That Enhance Intratumoral Spatial Distribution. *Nano Lett.* **12**, 2165 (2012).
151. A. J. Simnick *et al.*, In vivo tumor targeting by a NGR-decorated micelle of a recombinant diblock copolypeptide. *Journal of Controlled Release* **155**, 144 (2011).
152. S. R. MacEwan, A. Chilkoti, Digital Switching of Local Arginine Density in a Genetically Encoded Self-Assembled Polypeptide Nanoparticle Controls Cellular Uptake. *Nano Lett.* **12**, 3322 (2012).
153. G. Sun, P.-Y. Hsueh, S. M. Janib, S. Hamm-Alvarez, J. Andrew MacKay, Design and cellular internalization of genetically engineered polypeptide nanoparticles displaying adenovirus knob domain. *Journal of Controlled Release* **155**, 218 (2011).
154. P. Koria *et al.*, Self-assembling elastin-like peptides growth factor chimeric nanoparticles for the treatment of chronic wounds. *Proceedings of the National Academy of Sciences* **108**, 1034 (2011).
155. W. Hassouneh *et al.*, Unexpected Multivalent Display of Proteins by Temperature Triggered Self-Assembly of Elastin-like Polypeptide Block Copolymers. *Biomacromolecules* **13**, 1598 (2012).
156. H. Betre, L. A. Setton, D. E. Meyer, A. Chilkoti, Characterization of a Genetically Engineered Elastin-like Polypeptide for Cartilaginous Tissue Repair. *Biomacromolecules* **3**, 910 (2002).
157. E. R. Wright, R. A. McMillan, A. Cooper, R. P. Apkarian, V. P. Conticello, Thermoplastic Elastomer Hydrogels via Self-Assembly of an Elastin-Mimetic Triblock Polypeptide. *Adv. Funct. Mater.* **12**, 149 (2002).
158. R. E. Sallach *et al.*, Elastin-mimetic protein polymers capable of physical and chemical crosslinking. *Biomaterials* **30**, 409 (2009).
159. X. Wu, R. E. Sallach, J. M. Caves, V. P. Conticello, E. L. Chaikof, Deformation Responses of a Physically Cross-Linked High Molecular Weight Elastin-Like Protein Polymer. *Biomacromolecules* **9**, 1787 (2008).
160. M. Mie, Y. Mizushima, E. Kobatake, Novel extracellular matrix for cell sheet recovery using genetically engineered elastin-like protein. *J. Biomed. Mater. Res. Part B* **86B**, 283 (2008).
161. H. A. Currie, O. Deschaume, R. R. Naik, C. C. Perry, D. L. Kaplan, Genetically Engineered Chimeric Silk–Silver Binding Proteins. *Adv. Funct. Mater.* **21**, 2889 (2011).
162. J. Huang, C. Wong, A. George, D. L. Kaplan, The effect of genetically engineered spider silk-dentin matrix protein 1 chimeric protein on hydroxyapatite nucleation. *Biomaterials* **28**, 2358 (2007).
163. L. F. Drummy *et al.*, Repeat sequence proteins as matrices for nanocomposites. *Materials Science and Engineering: C* **29**, 1266 (2009).
164. R. Alvarez-Rodriguez, M. Alonso, A. Girotti, V. Reboto, J. C. Rodriguez-Cabello, One-pot synthesis of pH and temperature sensitive gold clusters mediated by a recombinant elastin-like polymer. *European Polymer Journal* **46**, 643 (2010).
165. N. Nath, A. Chilkoti, Interfacial Phase Transition of an Environmentally Responsive Elastin Biopolymer Adsorbed on Functionalized Gold Nanoparticles Studied by Colloidal Surface Plasmon Resonance. *Journal of the American Chemical Society* **123**, 8197 (2001).

166. H.-C. Huang, A. Nanda, K. Rege, Investigation of Phase Separation Behavior and Formation of Plasmonic Nanocomposites from Polypeptide-Gold Nanorod Nanoassemblies. *Langmuir* **28**, 6645 (2012).
167. K. M. Morin, S. Arcidiacono, R. Beckwitt, C. M. Mello, Recombinant expression of indolicidin concatamers in Escherichia coli. *Appl. Microbiol. Biotechnol.* **70**, 698 (2006).
168. X. Rao *et al.*, Design and expression of peptide antibiotic hPAB-β as tandem multimers in Escherichia coli. *Peptides* **26**, 721 (2005).
169. T. Kempe *et al.*, Multiple-copy genes: production and modification of monomeric peptides from large multimeric fusion proteins. *Gene* **39**, 239 (1985).
170. X. Ma *et al.*, Poly-GLP-1, a novel long-lasting glucagon-like peptide-1 polymer, ameliorates hyperglycaemia by improving insulin sensitivity and increasing pancreatic beta-cell proliferation. *Diabetes, Obesity and Metabolism* **11**, 953 (2009).
171. R. A. McMillan, T. A. T. Lee, V. P. Conticello, Rapid assembly of synthetic genes encoding protein polymers. *Macromolecules* **32**, 3643 (1999).
172. R. V. Lewis, M. Hinman, S. Kothakota, M. J. Fournier, Expression and purification of a spider silk protein: A new strategy for producing repetitive proteins. *Protein Expr. Purif.* **7**, 400 (1996).
173. J. H. Lee, P. M. Skowron, S. M. Rutkowska, S. S. Hong, S. C. Kim, Sequential amplification of cloned DNA as tandem multimers using class-IIS restriction enzymes. *Genetic Analysis-Biomolecular Engineering* **13**, 139 (1996).
174. J. I. Won, A. E. Barron, A new cloning method for the preparation of long repetitive polypeptides without a sequence requirement. *Macromolecules* **35**, 8281 (2002).
175. D. E. Meyer, A. Chilkoti, Genetically encoded synthesis of protein-based polymers with precisely specified molecular weight and sequence by recursive directional ligation: Examples from the elastin-like polypeptide system. *Biomacromolecules* **3**, 357 (2002).
176. A. Junger, D. Kaufmann, T. Scheibel, R. Weberskirch, Biosynthesis of an elastin-mimetic polypeptide with two different chemical functional groups within the repetitive elastin fragment. *Macromol. Biosci.* **5**, 494 (2005).
177. J. L. Hartley, T. J. Gregori, Cloning multiple copies of a DNA segment. *Gene* **13**, 347 (1981).
178. E. Blachinsky, I. Marbach, R. Cohen, M. R. Grably, D. Engelberg, Procedure for controlling number of repeats, orientation, and order during cloning of oligonucleotides. *Biotechniques* **36**, 933 (2004).
179. N. I. Topilina *et al.*, Bilayer fibril formation by genetically engineered polypeptides: Preparation and characterization. *Biomacromolecules* **7**, 1104 (2006).
180. M. Amiram, F. G. Quiroz, D. J. Callahan, A. Chilkoti, A highly parallel method for synthesizing DNA repeats enables the discovery of 'smart' protein polymers. *Nat Mater* **10**, 141 (2011).
181. L. X. Mi, Molecular cloning of protein-based polymers. *Biomacromolecules* **7**, 2099 (2006).
182. J. R. McDaniel, J. A. MacKay, F. G. a. Quiroz, A. Chilkoti, Recursive Directional Ligation by Plasmid Reconstruction Allows Rapid and Seamless Cloning of Oligomeric Genes. *Biomacromolecules* **11**, 944 (2010).
183. M. Radlinska, C. E. Drabik, W. S. Tong, L. C. Lutter, Generating tandem repeats by cloning with double initiator fragments. *Biotechniques* **31**, 340 (2001).
184. W. J. Crookes *et al.*, Reflectins: The unusual proteins of squid reflective tissues. *Science* **303**, 235 (2004).

185. K. D. Tartoff, C. A. Hobbs. (Bethesda Research Labs Focus, 1987), vol. 9, pp. 12.
186. J. W. C. Dunlop, P. Fratzl, Biological Composites. *Annual Review of Materials Research* **40**, 1 (2010).
187. H. S. Gupta *et al.*, Nanoscale deformation mechanisms in bone. *Nano Lett.* **5**, 2108 (2005).
188. B. Ji, H. Gao, Mechanical Principles of Biological Nanocomposites. *Annual Review of Materials Research* **40**, 77 (2010).
189. P. Fratzl, Biomimetic materials research: what can we really learn from nature's structural materials? *Journal of The Royal Society Interface* **4**, 637 (2007).
190. X. Li, W.-C. Chang, Y. J. Chao, R. Wang, M. Chang, Nanoscale Structural and Mechanical Characterization of a Natural Nanocomposite Material: The Shell of Red Abalone. *Nano Lett.* **4**, 613 (2004).
191. S. Weiner, H. D. Wagner, The material bone: Structure mechanical function relations. *Annual Review of Materials Science* **28**, 271 (1998).
192. H. Chai, J. J.-W. Lee, P. J. Constantino, P. W. Lucas, B. R. Lawn, Remarkable resilience of teeth. *Proceedings of the National Academy of Sciences of the United States of America* **106**, 7289 (2009).
193. H. D. Espinosa *et al.*, Tablet-level origin of toughening in abalone shells and translation to synthetic composite materials. *Nat Commun* **2**, 173 (2011).
194. C. Sachs, H. Fabritius, D. Raabe, Influence of microstructure on deformation anisotropy of mineralized cuticle from the lobster Homarus americanus. *J Struct Biol* **161**, 120 (2008).
195. G. Mayer, Rigid biological systems as models for synthetic composites. *Science* **310**, 1144 (2005).
196. P. Podsiadlo, Z. Liu, D. Paterson, P. B. Messersmith, N. A. Kotov, Fusion of Seashell Nacre and Marine Bioadhesive Analogs: High-Strength Nanocomposite by Layer-by-Layer Assembly of Clay and 3,4-Dihydroxyphenylalanine Polymer. *Adv. Mater.* **19**, 949 (2007).
197. Z. Y. Tang, N. A. Kotov, S. Magonov, B. Ozturk, Nanostructured artificial nacre. *Nat. Mater.* **2**, 413 (2003).
198. E. Munch *et al.*, Tough, Bio-Inspired Hybrid Materials. *Science* **322**, 1516 (2008).
199. J. Aizenberg *et al.*, Skeleton of Euplectella sp.: Structural hierarchy from the nanoscale to the macroscale. *Science* **309**, 275 (2005).
200. P. Fratzl, R. Weinkamer, Nature's hierarchical materials. *Progress in Materials Science* **52**, 1263 (2007).
201. J.-Y. Rho, L. Kuhn-Spearing, P. Zioupos, Mechanical properties and the hierarchical structure of bone. *Medical Engineering & Physics* **20**, 92 (1998).
202. L. J. Bonderer, A. R. Studart, L. J. Gauckler, Bioinspired Design and Assembly of Platelet Reinforced Polymer Films. *Science* **319**, 1069 (2008).
203. A. S. Deshpande, E. Beniash, Bioinspired Synthesis of Mineralized Collagen Fibrils. *Crystal Growth & Design* **8**, 3084 (2008).
204. P. A. Price, D. Toroian, J. E. Lim, Mineralization by Inhibitor Exclusion The Calcification of Collagen with Fetuin. *Journal of Biological Chemistry* **284**, 17092 (2009).
205. F. Nudelman *et al.*, The role of collagen in bone apatite formation in the presence of hydroxyapatite nucleation inhibitors. *Nat Mater* **9**, 1004).

206. M. J. Olszta *et al.*, Bone structure and formation: A new perspective. *Materials Science and Engineering: R: Reports* **58**, 77 (2007).
207. A. M. Belcher *et al.*, Control of crystal phase switching and orientation by soluble mollusc-shell proteins. *Nature* **381**, 56 (1996).
208. B. L. Smith *et al.*, Molecular mechanistic origin of the toughness of natural adhesives, fibres and composites. *Nature* **399**, 761 (1999).
209. G. E. Fantner *et al.*, Sacrificial bonds and hidden length dissipate energy as mineralized fibrils separate during bone fracture. *Nat. Mater.* **4**, 612 (2005).
210. G. E. Fantner *et al.*, Nanoscale Ion Mediated Networks in Bone: Osteopontin Can Repeatedly Dissipate Large Amounts of Energy. *Nano Lett.* **7**, 2491 (2007).
211. P. K. Hansma, P. J. Turner, R. S. Ruoff, Optimized adhesives for strong, lightweight, damage-resistant, nanocomposite materials: new insights from natural materials. *Nanotechnology* **18**, 044026 (2007).
212. R. Wang, H. S. Gupta, in *Annual Review of Materials Research, Vol 41,* D. R. F. P. Clarke, Ed. (2011), vol. 41, pp. 41-73.
213. E. Wang, S.-W. Lee, F. Bronner, M. C. Farach-Carson, H. I. Roach, Eds. (Springer London, 2010), vol. 6, pp. 201-214.
214. S. Dorozhkin, Calcium orthophosphate cements for biomedical application. *Journal of Materials Science* **43**, 3028 (2008).
215. H. H. K. Xu, J. B. Quinn, S. Takagi, L. C. Chow, Processing and Properties of Strong and Non-rigid Calcium Phosphate Cement. *Journal of Dental Research* **81**, 219 (2002).
216. C. D. Friedman, P. D. Costantino, S. Takagi, L. C. Chow, BoneSource™ hydroxyapatite cement: A novel biomaterial for craniofacial skeletal tissue engineering and reconstruction. *Journal of biomedical materials research* **43**, 428 (1998).
217. B. Stevens, Y. Yang, A. Mohandas, B. Stucker, K. T. Nguyen, A review of materials, fabrication methods, and strategies used to enhance bone regeneration in engineered bone tissues. *Journal of Biomedical Materials Research Part B: Applied Biomaterials* **85B**, 573 (2008).
218. K. Miyazaki, T. Horibe, J. M. Antonucci, S. Takagi, L. C. Chow, Polymeric calcium phosphate cements: analysis of reaction products and properties. *Dental Materials* **9**, 41 (1993).
219. R. A. Mickiewicz, A. M. Mayes, D. Knaack, Polymer–calcium phosphate cement composites for bone substitutes. *Journal of biomedical materials research* **61**, 581 (2002).
220. Z. H. Pan, P. P. Jiang, Q. Y. Fan, B. Ma, H. P. Cai, Mechanical and biocompatible influences of chitosan fiber and gelatin on calcium phosphate cement. *J. Biomed. Mater. Res. Part B* **82B**, 246 (2007).
221. M. B. Murphy, J. D. Hartgerink, A. Goepferich, A. G. Mikos, Synthesis and in Vitro Hydroxyapatite Binding of Peptides Conjugated to Calcium-Binding Moieties. *Biomacromolecules* **8**, 2237 (2007).
222. D. Denhardt, X. Guo, Osteopontin: a protein with diverse functions. *The FASEB Journal* **7**, 1475 (1993).
223. J. Benesch, J. o. F. Mano, R. L. Reis, Proteins and Their Peptide Motifs in Acellular Apatite Mineralization of Scaffolds for Tissue Engineering. *Tissue Engineering Part B: Reviews* **14**, 433 (2008).

224. P. Papagerakis *et al.*, Investigation of osteocalcin, osteonectin, and dentin sialophosphoprotein in developing human teeth. *Bone* **30**, 377 (2002).
225. K. Yokogawa *et al.*, Selective Delivery of Estradiol to Bone by Aspartic Acid Oligopeptide and Its Effects on Ovariectomized Mice. *Endocrinology* **142**, 1228 (2001).
226. M. J. Harrington, A. Masic, N. Holten-Andersen, J. H. Waite, P. Fratzl, Iron-Clad Fibers: A Metal-Based Biological Strategy for Hard Flexible Coatings. *Science* **328**, 216 (2010).
227. M. J. Gorbunoff, The interaction of proteins with hydroxyapatite : II. Role of acidic and basic groups. *Analytical Biochemistry* **136**, 433 (1984).
228. R. Goobes *et al.*, Thermodynamic Roles of Basic Amino Acids in Statherin Recognition of Hydroxyapatiteâ€ *Biochemistry* **46**, 4725 (2007).
229. M. D. Roy, S. K. Stanley, E. J. Amis, M. L. Becker, Identification of a Highly Specific Hydroxyapatite-binding Peptide using Phage Display. *Adv. Mater.* **20**, 1830 (2008).
230. S. Segvich, S. Biswas, U. Becker, D. H. Kohn, Identification of Peptides with Targeted Adhesion to Bone-Like Mineral via Phage Display and Computational Modeling. *Cells Tissues Organs* **189**, 245 (2009).
231. M. Gilbert *et al.*, Chimeric Peptides of Statherin and Osteopontin That Bind Hydroxyapatite and Mediate Cell Adhesion. *Journal of Biological Chemistry* **275**, 16213 (2000).
232. A. Courvoisier, F. Isel, J. FranÃ§ois, M. Maaloum, End-Adsorbed Telechelic Polymer Chains at Surfaces: Bridging and Elasticity. *Langmuir* **14**, 3727 (1998).
233. N. Wadcharawadee, K. S. Jack, D. Martin, M. Trau, Understanding the roles of nanoparticle dispersion and polymer crystallinity in controlling the mechanical properties of HA/PHBV nanocomposites. *Biomedical Materials* **4**, 015003 (2009).
234. V. Lemieux, P. H. H. M. Adams, J. C. M. van Hest, Elastin-based stimuli-responsive gold nanoparticles. *Chemical Communications* **46**, 3071 (2010).
235. Q. Wang *et al.*, High-water-content mouldable hydrogels by mixing clay and a dendritic molecular binder. *Nature* **463**, 339 (2010).
236. W. E. Brown, L. C. Chow, in *Cements Research Progress 1986,* P. W. Brown, Ed. (American Ceramic Society, Ohio, 1987), pp. 352-379.
237. J. E. Barralet, M. Hofmann, L. M. Grover, U. Gbureck, High-Strength Apatitic Cement by Modification with α-Hydroxy Acid Salts. *Adv. Mater.* **15**, 2091 (2003).
238. E. Fernández *et al.*, High-strength apatitic cement by modification with superplasticizers. *Biomaterials* **26**, 2289 (2005).
239. S. Hesaraki, R. Nemati, Cephalexin-loaded injectable macroporous calcium phosphate bone cement. *Journal of Biomedical Materials Research Part B: Applied Biomaterials* **89B**, 342 (2009).
240. R. A. Metzler, G. A. Tribello, M. Parrinello, P. U. P. A. Gilbert, Asprich Peptides Are Occluded in Calcite and Permanently Disorder Biomineral Crystals. *Journal of the American Chemical Society* **132**, 11585 (2010).
241. Y.-Y. Kim *et al.*, Bio-Inspired Synthesis and Mechanical Properties of Calcite–Polymer Particle Composites. *Adv. Mater.* **22**, 2082 (2010).
242. B. Pokroy, J. P. Quintana, E. a. N. Caspi, A. Berner, E. Zolotoyabko, Anisotropic lattice distortions in biogenic aragonite. *Nat Mater* **3**, 900 (2004).

243. S. M. Kenny, M. Buggy, Bone cements and fillers: A review. *Journal of Materials Science: Materials in Medicine* **14**, 923 (2003).
244. Y. Matsuya, J. M. Antonucci, S. Matsuya, S. Takagi, L. C. Chow, Polymeric calcium phosphate cements derived from poly(methyl vinyl ether-maleic acid). *Dental Materials* **12**, 2 (1996).
245. L. A. Dos Santos *et al.*, Influence of polymeric additives on the mechanical properties of [alpha]-tricalcium phosphate cement. *Bone* **25**, 99S (1999).
246. J. L. Moreau, M. D. Weir, H. H. K. Xu, Self-setting collagen-calcium phosphate bone cement: Mechanical and cellular properties. *Journal of Biomedical Materials Research Part A* **91A**, 605 (2009).
247. E. F. Burguera, H. H. K. Xu, L. Sun, Injectable calcium phosphate cement: Effects of powder-to-liquid ratio and needle size. *Journal of Biomedical Materials Research Part B: Applied Biomaterials* **84B**, 493 (2008).
248. X. Wang, L. Chen, H. Xiang, J. Ye, Influence of anti-washout agents on the rheological properties and injectability of a calcium phosphate cement. *Journal of Biomedical Materials Research Part B: Applied Biomaterials* **81B**, 410 (2007).
249. W. Shen, J. A. Kornfield, D. A. Tirrell, Dynamic Properties of Artificial Protein Hydrogels Assembled through Aggregation of Leucine Zipper Peptide Domains. *Macromolecules* **40**, 689 (2007).
250. S. Lv *et al.*, Designed biomaterials to mimic the mechanical properties of muscles. *Nature* **465**, 69 (2010).
251. X. Wu *et al.*, Alterations in Physical Cross-Linking Modulate Mechanical Properties of Two-Phase Protein Polymer Networks. *Biomacromolecules* **6**, 3037 (2005).
252. K. S. Straley, S. C. Heilshorn, Dynamic, 3D-Pattern Formation Within Enzyme-Responsive Hydrogels. *Adv. Mater.* **21**, 4148 (2009).
253. G. Liu *et al.*, Three-Dimensional Biomimetic Mineralization of Dense Hydrogel Templates. *Journal of the American Chemical Society* **131**, 9937 (2009).
254. K. S. Straley, S. C. Heilshorn, Independent tuning of multiple biomaterial properties using protein engineering. *Soft Matter* **5**, 114 (2009).
255. B. A. Fong, W.-Y. Wu, D. W. Wood, Optimization of ELP-intein mediated protein purification by salt substitution. *Protein Expr. Purif.* **66**, 198 (2009).
256. A. C. Tas, Monetite (CaHPO4) Synthesis in Ethanol at Room Temperature. *Journal of the American Ceramic Society* **92**, 2907 (2009).
257. R. Mohr *et al.*, Initiation of shape-memory effect by inductive heating of magnetic nanoparticles in thermoplastic polymers. *Proceedings of the National Academy of Sciences of the United States of America* **103**, 3540 (2006).
258. J. Liu *et al.*, Synthesis, Characterization, and Multilayer Assembly of pH Sensitive Graphene-Polymer Nanocomposites. *Langmuir* **26**, 10068 (2010).
259. E. Boisselier, D. Astruc, Gold nanoparticles in nanomedicine: preparations, imaging, diagnostics, therapies and toxicity. *Chemical Society Reviews* **38**, 1759 (2009).
260. C. Lee, X. Wei, J. W. Kysar, J. Hone, Measurement of the Elastic Properties and Intrinsic Strength of Monolayer Graphene. *Science* **321**, 385 (2008).

261. A. A. Balandin *et al.*, Superior Thermal Conductivity of Single-Layer Graphene. *Nano Lett.* **8**, 902 (2008).
262. A. K. Geim, K. S. Novoselov, The rise of graphene. *Nat Mater* **6**, 183 (2007).
263. R. R. Nair *et al.*, Fine Structure Constant Defines Visual Transparency of Graphene. *Science* **320**, 1308 (2008).
264. Y. Hernandez *et al.*, High-yield production of graphene by liquid-phase exfoliation of graphite. *Nat Nano* **3**, 563 (2008).
265. A. Reina *et al.*, Large Area, Few-Layer Graphene Films on Arbitrary Substrates by Chemical Vapor Deposition. *Nano Lett.* **9**, 30 (2008).
266. W. S. Hummers, R. E. Offeman, Preparation of Graphitic Oxide. *Journal of the American Chemical Society* **80**, 1339 (1958).
267. S. Stankovich *et al.*, Synthesis of graphene-based nanosheets via chemical reduction of exfoliated graphite oxide. *Carbon* **45**, 1558 (2007).
268. S. Park, R. S. Ruoff, Chemical methods for the production of graphenes. *Nat Nano* **4**, 217 (2009).
269. Y. Zhu *et al.*, Graphene and Graphene Oxide: Synthesis, Properties, and Applications. *Adv. Mater.* **22**, 3906 (2010).
270. J. T. Robinson, F. K. Perkins, E. S. Snow, Z. Wei, P. E. Sheehan, Reduced Graphene Oxide Molecular Sensors. *Nano Lett.* **8**, 3137 (2008).
271. G. Eda, G. Fanchini, M. Chhowalla, Large-area ultrathin films of reduced graphene oxide as a transparent and flexible electronic material. *Nat Nano* **3**, 270 (2008).
272. D. R. Dreyer, H.-P. Jia, C. W. Bielawski, Graphene Oxide: A Convenient Carbocatalyst for Facilitating Oxidation and Hydration Reactions. *Angewandte Chemie International Edition* **49**, 6813 (2010).
273. S. Stankovich *et al.*, Graphene-based composite materials. *Nature* **442**, 282 (2006).
274. X. Sun *et al.*, Nano-graphene oxide for cellular imaging and drug delivery. *Nano Research* **1**, 203 (2008).
275. J. H. Jung, D. S. Cheon, F. Liu, K. B. Lee, T. S. Seo, A Graphene Oxide Based Immuno-biosensor for Pathogen Detection. *Angewandte Chemie International Edition* **49**, 5708 (2010).
276. A. J. Patil, J. L. Vickery, T. B. Scott, S. Mann, Aqueous Stabilization and Self-Assembly of Graphene Sheets into Layered Bio-Nanocomposites using DNA. *Adv. Mater.* **21**, 3159 (2009).
277. S. Park, J. An, J. W. Suk, R. S. Ruoff, Graphene-Based Actuators. *Small* **6**, 210 (2010).
278. J. Liang *et al.*, Electromechanical Actuator with Controllable Motion, Fast Response Rate, and High-Frequency Resonance Based on Graphene and Polydiacetylene. *ACS Nano* **6**, 4508 (2012).
279. S.-E. Zhu *et al.*, Graphene-Based Bimorph Microactuators. *Nano Lett.* **11**, 977 (2011).
280. J. T. Robinson *et al.*, Ultrasmall Reduced Graphene Oxide with High Near-Infrared Absorbance for Photothermal Therapy. *Journal of the American Chemical Society* **133**, 6825 (2011).
281. J. Liang *et al.*, Infrared-Triggered Actuators from Graphene-Based Nanocomposites. *The Journal of Physical Chemistry C* **113**, 9921 (2009).

282. C. Wu *et al.*, Large-area graphene realizing ultrasensitive photothermal actuator with high transparency: new prototype robotic motions under infrared-light stimuli. *Journal of Materials Chemistry* **21**, 18584 (2011).
283. C.-W. Lo, D. Zhu, H. Jiang, An infrared-light responsive graphene-oxide incorporated poly(N-isopropylacrylamide) hydrogel nanocomposite. *Soft Matter* **7**, 5604 (2011).
284. C.-H. Zhu, Y. Lu, J. Peng, J.-F. Chen, S.-H. Yu, Photothermally Sensitive Poly(N-isopropylacrylamide)/Graphene Oxide Nanocomposite Hydrogels as Remote Light-Controlled Liquid Microvalves. *Adv. Funct. Mater.*, n/a (2012).
285. D. Li, M. B. Muller, S. Gilje, R. B. Kaner, G. G. Wallace, Processable aqueous dispersions of graphene nanosheets. *Nat Nano* **3**, 101 (2008).
286. B. J. Hong, O. C. Compton, Z. An, I. Eryazici, S. T. Nguyen, Successful Stabilization of Graphene Oxide in Electrolyte Solutions: Enhancement of Biofunctionalization and Cellular Uptake. *ACS Nano*, (2011).
287. J. I. Paredes, S. Villar-Rodil, A. Martínez-Alonso, J. M. D. Tascón, Graphene Oxide Dispersions in Organic Solvents. *Langmuir* **24**, 10560 (2008).
288. S. Park *et al.*, Colloidal Suspensions of Highly Reduced Graphene Oxide in a Wide Variety of Organic Solvents. *Nano Lett.* **9**, 1593 (2009).
289. Y. Si, E. T. Samulski, Synthesis of Water Soluble Graphene. *Nano Lett.* **8**, 1679 (2008).
290. S. Stankovich, R. D. Piner, S. T. Nguyen, R. S. Ruoff, Synthesis and exfoliation of isocyanate-treated graphene oxide nanoplatelets. *Carbon* **44**, 3342 (2006).
291. S. Park *et al.*, Biocompatible, Robust Free-Standing Paper Composed of a TWEEN/Graphene Composite. *Adv. Mater.* **22**, 1736 (2010).
292. H. J. Salavagione, G. Martínez, G. Ellis, Recent Advances in the Covalent Modification of Graphene With Polymers. *Macromolecular Rapid Communications* **32**, 1771 (2011).
293. S.-Z. Zu, B.-H. Han, Aqueous Dispersion of Graphene Sheets Stabilized by Pluronic Copolymers: Formation of Supramolecular Hydrogel. *The Journal of Physical Chemistry C* **113**, 13651 (2009).
294. E.-Y. Choi *et al.*, Noncovalent functionalization of graphene with end-functional polymers. *Journal of Materials Chemistry* **20**, 1907 (2010).
295. M. Fang, J. Long, W. Zhao, L. Wang, G. Chen, pH-Responsive Chitosan-Mediated Graphene Dispersions. *Langmuir* **26**, 16771 (2010).
296. Q. Su *et al.*, Composites of Graphene with Large Aromatic Molecules. *Adv. Mater.* **21**, 3191 (2009).
297. J. Gao *et al.*, Environment-Friendly Method To Produce Graphene That Employs Vitamin C and Amino Acid. *Chemistry of Materials* **22**, 2213 (2010).
298. T. Fujigaya, T. Morimoto, Y. Niidome, N. Nakashima, NIR Laser-Driven Reversible Volume Phase Transition of Single-Walled Carbon Nanotube/Poly(N-isopropylacrylamide) Composite Gels. *Adv. Mater.* **20**, 3610 (2008).
299. C. Guo, B. Book-Newell, J. Irudayaraj, Protein-directed reduction of graphene oxide and intracellular imaging. *Chemical Communications* **47**, 12658 (2011).
300. P. Laaksonen *et al.*, Interfacial Engineering by Proteins: Exfoliation and Functionalization of Graphene by Hydrophobins. *Angewandte Chemie International Edition* **49**, 4946 (2010).

301. J. Liu, S. Fu, B. Yuan, Y. Li, Z. Deng, Toward a Universal "Adhesive Nanosheet" for the Assembly of Multiple Nanoparticles Based on a Protein-Induced Reduction/Decoration of Graphene Oxide. *Journal of the American Chemical Society* **132**, 7279 (2010).
302. Y. Xu, H. Bai, G. Lu, C. Li, G. Shi, Flexible Graphene Films via the Filtration of Water-Soluble Noncovalent Functionalized Graphene Sheets. *Journal of the American Chemical Society* **130**, 5856 (2008).
303. P. Laaksonen *et al.,* Interfacial Engineering by Proteins: Exfoliation and Functionalization of Graphene by Hydrophobins. *Angewandte Chemie* **122**, 5066 (2010).
304. C. Li, J. Adamcik, R. Mezzenga, Biodegradable nanocomposites of amyloid fibrils and graphene with shape-memory and enzyme-sensing properties. *Nat Nano* **7**, 421 (2012).
305. J. R. Potts, D. R. Dreyer, C. W. Bielawski, R. S. Ruoff, Graphene-based polymer nanocomposites. *Polymer* **52**, 5 (2011).
306. C. K. Y. Lau, Masters, Massachusetts Institute of Technology (2004).
307. Y. Cui *et al.,* Chemical Functionalization of Graphene Enabled by Phage Displayed Peptides. *Nano Lett.* **10**, 4559 (2010).
308. S. N. Kim *et al.,* Preferential Binding of Peptides to Graphene Edges and Planes. *Journal of the American Chemical Society* **133**, 14480 (2011).
309. J. Liu *et al.,* Thermosensitive graphene nanocomposites formed using pyrene-terminal polymers made by RAFT polymerization. *Journal of Polymer Science Part A: Polymer Chemistry* **48**, 425 (2010).
310. C. R. So *et al.,* Controlling Self-Assembly of Engineered Peptides on Graphite by Rational Mutation. *ACS Nano* **6**, 1648 (2012).
311. J. A. Mann, J. Rodríguez-López, H. D. Abruña, W. R. Dichtel, Multivalent Binding Motifs for the Noncovalent Functionalization of Graphene. *Journal of the American Chemical Society* **133**, 17614 (2011).
312. Y. Xu, Q. Wu, Y. Sun, H. Bai, G. Shi, Three-Dimensional Self-Assembly of Graphene Oxide and DNA into Multifunctional Hydrogels. *ACS Nano* **4**, 7358 (2010).
313. F. Yang, Y. Liu, L. Gao, J. Sun, pH-Sensitive Highly Dispersed Reduced Graphene Oxide Solution Using Lysozyme via an in Situ Reduction Method. *The Journal of Physical Chemistry C* **114**, 22085 (2010).
314. W. Zhang *et al.,* Synergistic effect of chemo-photothermal therapy using PEGylated graphene oxide. *Biomaterials* **32**, 8555 (2011).
315. Y. Yang *et al.,* Synthesis of PNIPAM polymer brushes on reduced graphene oxide based on click chemistry and RAFT polymerization. *Journal of Polymer Science Part A: Polymer Chemistry* **50**, 329 (2012).
316. T. Shiraki *et al.,* Heat and light dual switching of a single-walled carbon nanotube/thermo-responsive helical polysaccharide complex: a new responsive system applicable to photodynamic therapy. *Chemical Communications* **47**, 7065 (2011).
317. J. R. McDaniel, D. J. Callahan, A. Chilkoti, Drug delivery to solid tumors by elastin-like polypeptides. *Advanced Drug Delivery Reviews* **62**, 1456 (2010).
318. X. Shi *et al.,* Regulating Cellular Behavior on Few-Layer Reduced Graphene Oxide Films with Well-Controlled Reduction States. *Adv. Funct. Mater.* **22**, 751 (2012).

319. K. Trabbic-Carlson, L. A. Setton, A. Chilkoti, Swelling and Mechanical Behaviors of Chemically Cross-Linked Hydrogels of Elastin-like Polypeptides. *Biomacromolecules* **4**, 572 (2003).
320. D. W. Lim, D. L. Nettles, L. A. Setton, A. Chilkoti, Rapid Cross-Linking of Elastin-like Polypeptides with (Hydroxymethyl)phosphines in Aqueous Solution. *Biomacromolecules* **8**, 1463 (2007).
321. M. Malkoch *et al.*, Synthesis of well-defined hydrogel networks using Click chemistry. *Chemical Communications*, 2774 (2006).
322. T. Tanaka, D. J. Fillmore, Kinetics of swelling of gels. *The Journal of Chemical Physics* **70**, 1214 (1979).
323. A. B. Imran, T. Seki, Y. Takeoka, Recent advances in hydrogels in terms of fast stimuli responsiveness and superior mechanical performance. *Polym J* **42**, 839 (2010).
324. X.-Z. Zhang, Y.-Y. Yang, T.-S. Chung, Effect of Mixed Solvents on Characteristics of Poly(N-isopropylacrylamide) Gels. *Langmuir* **18**, 2538 (2002).
325. H. Yamauchi, Y. Maeda, LCST and UCST Behavior of Poly(N-isopropylacrylamide) in DMSO/Water Mixed Solvents Studied by IR and Micro-Raman Spectroscopy. *The Journal of Physical Chemistry B* **111**, 12964 (2007).
326. P. J. Nowatzki, D. A. Tirrell, Physical properties of artificial extracellular matrix protein films prepared by isocyanate crosslinking. *Biomaterials* **25**, 1261 (2004).
327. N. Bassik, B. T. Abebe, K. E. Laflin, D. H. Gracias, Photolithographically patterned smart hydrogel based bilayer actuators. *Polymer* **51**, 6093 (2010).
328. G. Stoychev, N. Puretskiy, L. Ionov, Self-folding all-polymer thermoresponsive microcapsules. *Soft Matter* **7**, 3277 (2011).
329. M. Jamal, A. M. Zarafshar, D. H. Gracias, Differentially photo-crosslinked polymers enable self-assembling microfluidics. *Nat Commun* **2**, 527 (2011).
330. J. Kim, J. A. Hanna, M. Byun, C. D. Santangelo, R. C. Hayward, Designing Responsive Buckled Surfaces by Halftone Gel Lithography. *Science* **335**, 1201 (2012).
331. X. Zhang *et al.*, Optically- and Thermally-Responsive Programmable Materials Based on Carbon Nanotube-Hydrogel Polymer Composites. *Nano Lett.* **11**, 3239 (2011).
332. J. Ryu *et al.*, Photo-origami---Bending and folding polymers with light. *Applied Physics Letters* **100**, 161908 (2012).
333. L. Dong, H. Jiang, Autonomous microfluidics with stimuli-responsive hydrogels. *Soft Matter* **3**, 1223 (2007).
334. A. Pelah, T. M. Jovin, Polymeric Actuators for Biological Applications. *ChemPhysChem* **8**, 1757 (2007).
335. J.-i. Edahiro *et al.*, In Situ Control of Cell Adhesion Using Photoresponsive Culture Surface. *Biomacromolecules* **6**, 970 (2005).
336. J. Yoon, P. Bian, J. Kim, T. J. McCarthy, R. C. Hayward, Local Switching of Chemical Patterns through Light-Triggered Unfolding of Creased Hydrogel Surfaces. *Angewandte Chemie International Edition* **51**, 7146 (2012).
337. K. Yamaki, I. Harada, M. Goto, C.-S. Cho, T. Akaike, Regulation of cellular morphology using temperature-responsive hydrogel for integrin-mediated mechanical force stimulation. *Biomaterials* **30**, 1421 (2009).

338. M. J. Fernández-Merino *et al.*, Vitamin C Is an Ideal Substitute for Hydrazine in the Reduction of Graphene Oxide Suspensions. *The Journal of Physical Chemistry C* **114**, 6426 (2010).
339. A. E. Carpenter *et al.*, CellProfiler: image analysis software for identifying and quantifying cell phenotypes. *Genome biology* **7**, R100 (2006).

Appendix

```
   1 TTTTGAATTC CTCGAGTACA TATGACGGTC TCAGGACTCC TACGCCTGGG ACGCCAACTC CTGGTACCCC
  71 CTTACCAGGC ACGCCCACAC CTGGAACACC TACGCCCGGC ACGCCCACGC CAGGCACACC AACACCCGGA
 141 ACTCCTTTAC CGGGCACTCC TACACCTGGC ACGCCTACGC CAGGCACGCC GACCCCAGGT ACGCCAACAC
 211 CCGGGACGCC TTTACCAGGC ACACCGACAC CAGGTACACC AACCCCTGGA ACGCCCACCC CAGGAACACC
 281 AACGCCCGGA ACACCTTTAC CCGGGACTCC GACGCCCGGA ACCCCGACGC CCGGGACACC CACGCCCGGC
 351 ACTCCAACAC CCGGCACCCC TTTTCCCGGC ACCCCGACTC CCGGAACACC GACCCCGGGG ACTTGTCTTC
 421 GCATATGTGA AGGATCCGAA TTCCCCCGAC GAGCTTCATG CCGTTAGTCG CACTGCAAGG GGTGTTATGA
 491 GCCATATTCA GGTATAAATG GGCTCGCGAT AATGTTCAGA ATTGGTTAAT TGGTTGTAAC ACTGACCCCT
 561 ATTTGTTTAT TTTTCTAAAT ACATTCAAAT ATGTATCCGC TCATGAGACA ATAACCCTGA TAAATGCTTC
 631 AATAATATTG AAAAAGGAAG AATATGAGTA TTCAACATTT CCGTGTCGCC CTTATTCCCT TTTTTGCGGC
 701 ATTTTGCCTT CCTGTTTTTG CTCACCCAGA AACGCTGGTG AAAGTAAAAG ATGCTGAAGA TCAGTTGGGT
 771 GCACGAGTGG GTTACATCGA ACTGGATCTC AACAGCGGTA AGATCCTTGA GAGTTTTCGC CCCGAAGAAC
 841 GTTTTCCAAT GATGAGCACT TTTAAAGTTC TGCTATGTGG CGCGGTATTA TCCCGTATTG ACGCCGGGCA
 911 AGAGCAACTC GGTCGCCGCA TACACTATTC TCAGAATGAC TTGGTTGAGT ACTCACCAGT CACAGAAAAG
 981 CATCTTACGG ATGGCATGAC AGTAAGAGAA TTATGCAGTG CTGCCATAAC CATGAGTGAT AACACTGCGG
1051 CCAACTTACT TCTGACAACG ATCGGAGGAC CGAAGGAGCT AACCGCTTTT TTGCACAACA TGGGGGATCA
1121 TGTAACTCGC CTTGATCGTT GGGAACCGGA GCTGAATGAA GCCATACCAA ACGACGAGCG TGACACCACG
1191 ATGCCTGTAG CGATGGCAAC AACGTTGCGC AAACTATTAA CTGGCGAACT ACTTACTCTA GCTTCCCGGC
1261 AACAATTAAT AGACTGGATG GAGGCGGATA AAGTTGCAGG ACCACTTCTG CGCTCGGCCC TTCCGGCTGG
1331 CTGGTTTATT GCTGATAAAT CCGGAGCCGG TGAGCGTGGT TCTCGCGGTA TCATCGCAGC GCTGGGGCCA
1401 GATGGTAAGC CCTCCCGTAT CGTAGTTATC TACACGACGG GGAGTCAGGC AACTATGGAT GAACGAAATA
1471 GACAGATCGC TGAGATAGGT GCCTCACTGA TTAAGCATTG GTAAGCAGAG CATTACGCTG ACTTGACGGG
1541 ACGGCGCAAG CTCATGACCA AAATCCCTTA ACGTGAGTTA CGCGCGCGTC GTTCCACTGA GCGTCAGACC
1611 CCGTAGAAAA GATCAAAGGA TCTTCTTGAG ATCCTTTTTT TCTGCGCGTA ATCTGCTGCT TGCAAACAAA
1681 AAAACCACCG CTACCAGCGG TGGTTTGTTT GCCGGATCAA GAGCTACCAA CTCTTTTTCC GAAGGTAACT
1751 GGCTTCAGCA GAGCGCAGAT ACCAAATACT GTTCTTCTAG TGTAGCCGTA GTTAGCCCAC CACTTCAAGA
1821 ACTCTGTAGC ACCGCCTACA TACCTCGCTC TGCTAATCCT GTTACCAGTG GCTGCTGCCA GTGGCGATAA
1891 GTCGTGTCTT ACCGGGTTGG ACTCAAGACG ATAGTTACCG GATAAGGCGC AGCGGTCGGG CTGAACGGGG
1961 GGTTCGTGCA CACAGCCCAG CTTGGAGCGA ACGACCTACA CCGAACTGAG ATACCTACAG CGTGAGCTAT
2031 GAGAAAGCGC CACGCTTCCC GAAGGGAGAA AGGCGGACAG GTATCCGGTA AGCGGCAGGG TCGGAACAGG
2101 AGAGCGCACG AGGGAGCTTC CAGGGGGAAA CGCCTGGTAT CTTTATAGTC CTGTCGGGTT TCGCCACCTC
2171 TGACTTGAGC GTCGATTTTT GTGATGCTCG TCAGGGGGGC GGAGCCTATG GAAAAACGCC AGCAACGCGG
2241 CCTTTTTACG GTTCCTGGCC TTTTGCTGGC CTTTTGCTCA CATGTTCTTT CCTGCGTTAT CCCCTGATTC
2311 TGTGGATAAC CGTATTACCG CCTTTGAGTG AGCTGATACC GCTCGCCGCA GCCGAACGAC CGAGCGCAGC
2381 GAGTCAGTGA GCGAGGAAGC GGAAGGCGAG AGTAGGGAAC TGCCAGGCAT CAAACTAAGC AGAAGGCCCC
2451 TGACGGATGG CCTTTTTGCG TTTCTACAAA CTCTTTCTGT GTTGTAAAAC GACGGCCAGT CTTAAGCTCG
2521 GGCCCC
```

Features:

```
ELP-K25 5-443
AmpR 654-1511
pUC Ori 1551-2392
ELPSeqR 499-518
ELPSeqF 2408-2427
```

Restriction Sites:

```
XhoI C^TCGAG     11
Eco31I GGTCTCN^  27
BpiI GAAGACNN^  415
BamHI G^GATCC   432
```

Figure A-1. Full sequence of K25 vector received from DNA 2.0 (Chapter 2).

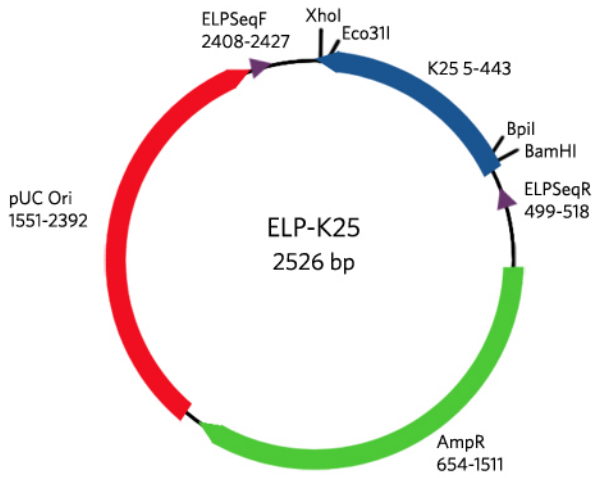

Figure A-2. Plasmid map of K25 vector received from DNA 2.0 (Chapter 2).

Table A-1. List of oligonucleotides used to synthesize the V*n*, E*n*, and K*n* series of genes.

Oligo	**Oligo Sequence (5′ to 3′)**
V5L-F	GATCCTTCACATATGCGAAGACAAGTCCCAGGTGTGGGCG TACCG
V5L-R	CACCAACGCCCGGTACGCCCACACCTGGGACTTGTCTTCGC ATATGTGAAG
V5R-F	GGCGTTGGTGTTCCTGGTGTCGGCGTGCCGGGCGTGGGTG TTCCGGGCGTAGGT
V5R-R	GGACACCTACGCCCGGAACACCCACGCCCGGCACGCCGAC ACCAGGAA
X5L1-F	GTCCCAGGTGTGGGCGTACCGGGCGTTGGTGTTCCT
X5R1-R	GGACACCTACGCCCGGAACACCCACGCCCGGCACG
X5L2-F	GTCCCGGGTGTTGGCGTACCAGGCGTGGGTGTGCCG
X5R2-R	GGACGCCCACACCCGGTACGCCAACGCCAGGAACA
E5L1-R	CCTTCACCAGGAACACCAACGCCCGGTACGCCCACACCTG
E5R1-F	GGTGAAGGCGTGCCGGGCGTGGGTGTTCCGGGCGTAGGT
E5L2-R	CCTTCACCCGGCACACCCACGCCTGGTACGCCAACACCCG
E5R2-F	GGTGAAGGTGTTCCTGGCGTTGGCGTACCGGGTGTGGGC
K5L1-R	CCTTTACCAGGAACACCAACGCCCGGTACGCCCACACCTG
K5R1-F	GGTAAAGGCGTGCCGGGCGTGGGTGTTCCGGGCGTAGGT
K5L2-R	CCTTTACCCGGCACACCCACGCCTGGTACGCCAACACCCG
K5L2-F	GGTAAAGGTGTTCCTGGCGTTGGCGTACCGGGTGTGGGC

Cloning Protocols

Plasmid Prep
Grow 5 mL of bacteria overnight in appropriate antibiotic
For pet28b (Kan)-based plasmids pellet 2.5 mL of Overnight Culture
For pJ54 (Amp)-based plasmids pellet 1.5 mL of Overnight Culture
Skip optional PB step
Elute in 40 uL of EB

Restriction Digestion (For Cloning)
X uL of purified plasmid (See Table)
3.2 uL of Enzyme Buffer
3 uL of Enzymes Total (1.5 uL each for double digest)
3.2 uL of 10X BSA (if needed)
Y uL of H20
32 uL total

For use as:	Plasmid Type	X uL
Vector	pet28b (Kan)-based	**16**-18
Vector	pJ54 (Amp)-based	**8**-10
Insert	pJ54 (Amp)-based	12-14

37 °C for 3-5hrs
65 °C for 20min
4 °C forever

For Vectors add 3.7uL of 10X Antarctic Phosphatase Buffer and 1.2uL of Antarctic Phosphatase
37° C for 30-1hr
65 °C for 1hr
4 °C forever

Gel Purification
Use 0.6-0.7% Agarose Gel
Run at 120 V
Run for ~40 minutes (If gel purifying an ELP gene of 125 pentapeptides then use a 1% gel and run for a longer time, if necessary post stain in solution of SYBR Green)
Run dissolved agarose through the spin column twice
Elute with 30 uL of EB

Ligation
X uL of vector (See Table)
Y uL of insert (See Table)
0.5 uL of 10X Ligase Buffer
0.5 uL of T4 DNA Ligase
Z uL of H20
5 uL total

RXN	Vector	X uL	Insert	Y uL
1	pet28b (Kan)-based	2.5	Annealed Oligos	1 of 0.15 uM
2	pet28b (Kan)-based	1	ELP-gene	2-3 GelPure
3	pJ54 (Amp)-based	0.5	Annealed Oligos for Concatenation	0.75 of 2:1:1 mix*
4	pJ54 (Amp)-based	0.5	ELP-gene	2 GelPure

* 2uL of A1 or B1 w/ 1uL each of A2 & B2

Control RXNs have no insert
Add everything but the ligase buffer and ligase first
Heat to 37 °C for ~1 min then bring to 4 °C in thermocycler
Add Ligase Buffer and Ligase and mix

For RXN 2,4 1-3 hours at RT is fine
For RXN 1,3 better to do overnight at 16 °C (Optionally due cycling between 24 and 16 °C first
PROGRAM: LIGCYCLE 24 °C 2min → 16 °C 15 sec Repeated 60X before going to 16 °C for 15 hours
Heat inactivate ligase at 65 °C for 10 minutes

Transformation
Transform 1.5 uL of ligation reaction into 40 uL of XL-1 Blue Electrocompetent Cells
Generally sufficient to plate 30 uL